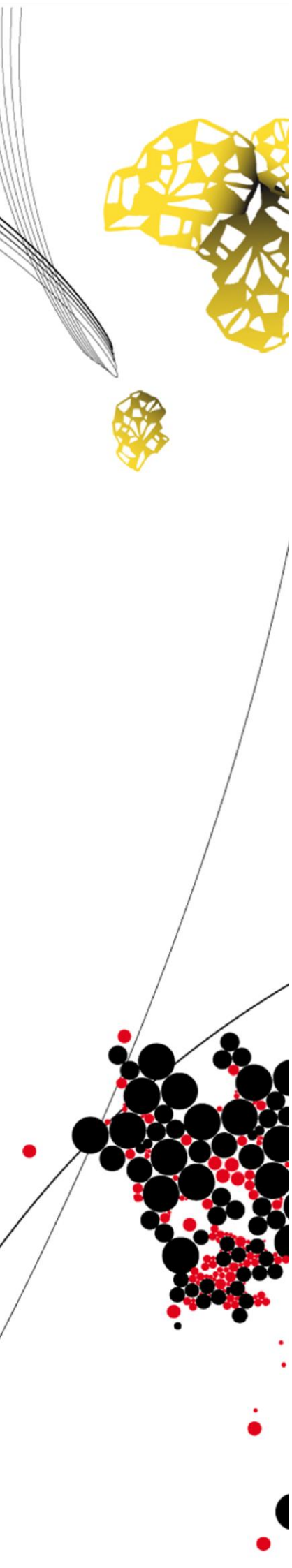

UNIVERSITY OF TWENTE.

Faculty of Engineering Technology,
Design & Manufacturing

Maximizing energy absorption properties of 3D printed programmed auxetic metamaterials

Jonne F. Postmes

Thesis for the degree of
Master of Science in Mechanical Engineering

Supervisor: dr. ir. M. Mehrpouya
Chair: dr.ir. T.H.J. Vaneker
External member: dr. habil. C. Soyarslan
External member: dr. V. Kalpathy Venkiteswaran

Faculty of Engineering Technology (ET),
University of Twente
P.O. Box 217
7500 AE Enschede The Netherlands

Date of graduation: 10 November 2022
Registration number: DPM 1977

Abstract

Key words

Mechanical Metamaterials, Programmable Materials, Auxetics, Sandwich, Energy absorption, Compression, Multi-material, Chiral.

Research of mechanical metamaterials has become more accessible in recent years, in part due to the advances in 3D printing technologies. Allowing for easy access to the rapid prototyping of complex multi-material structures. This thesis has furthered the research of metamaterials. Specifically on a chiral based auxetic shape and how multi-material designs can program this structures behaviour, as this combination is not yet researched extensively.

A literary research has been conducted on the following subjects, in order: How metamaterials are defined and classified; Examples of programmed metamaterials; Different auxetic structures and their beneficial properties; The definition of energy absorption within the context of this thesis; How a 3D printer functions; The effects of printing parameters.

Models were created using SolidWorks, samples were created with an Ultimaker 3 and made from PLA, C8, TPC-91a, and PCL100. They were printed with a 0.4mm nozzle, at a 0.2mm layerheight. Samples were additively manufactured with dimensions of 50x50x15mm after which they were compressed by a Zwick Z5.0 mechanical tester and its 2.5kN loadcell.

This thesis was concluded with three experiments to determine the most optimal shape, material and multi-material respectively. Testing eight different shapes, four different materials and four different multi-material configurations. The shapes and materials were experimented to find the best combination of energy absorption properties. These were used within multi-material configurations, which were programmed to show different behaviours during compression.

The best performing structure was a symmetrical chiral based structure with four connections between cells, named Chiral N4. This shape showed double the energy absorption performance compared to most other shapes, and is suited for multi-material design. PLA and PCL were selected as hard and soft materials respectively. Both showed both good energy absorption properties, and good adhesion with each other. Four different multi-material variants were designed, with the Chiral N4 shape, using PLA and PCL. The models were tested, and showed clear differences in compressive behaviour, with consistent results. Showing that it is possible to use chiral based shapes to create programmed metamaterials.

This research has shown the possibility to program different compressive behaviours in the Chiral N4 shape. Resulting in difference responses based on how the cellular structure was divided in hard and soft materials.

Acknowledgements

I have learned much from my time at the University of Twente. Both within classroom walls, and beyond. My student era will come to an end, with the completion of this thesis. But I could not have done this all alone.

I wish to show my appreciation to my research supervisor, dr.ir. Mehrshad Mehrpouya. This thesis could not have been completed without his help. I would like to thank him for his guidance throughout the project. His patience when I needed a bit more time to understand directions and his enthusiasm for my work.

The assistance provided by lab managers ing. Quint Meinders and ing. Bert Vos was greatly appreciated. Thank you for helping with the practical side, with 3D printing problems and performing experiments.

I would like to thank my parents, family, and friends. For supporting me throughout, and for lending their ears when times were tough. For letting me rattle on, and distracting me from yesterday's little worries. You have all been invaluable.

Jonne Postmes,
October 2022, Enschede, The Netherlands

Contents

Chapter 1

Introduction

This chapter will introduce this thesis. First the broader contexts will be explained, followed by the context of this research within the University of Twente. Then, the scope and purpose of this study will be stated. The introduction will conclude with the main research question and sub-questions which will guide the direction of this thesis.

1.1 Statement of the Problem

There is always a need for new materials which are lighter, and that can perform better under different loading conditions.

Sandwich structures are lightweight materials with excellent out-of-plane stiffness when combined with, for example, a honeycomb pattern. When compressed in plane, these panels show great energy absorption properties. When such a sandwich panel is compressed, kinetic energy is converted and absorbed, as the structure deforms plasticly.

Generic sandwich panels with the purpose of absorbing energy from forces in plane can be improved. The cellular core in-between the places can be changed for an auxetic pattern. Structures made from these shapes have a negative Poisson's ratio. This causes the structure to contract towards a point of impact, rather than flow away from it. This enhances the energy absorption properties of the sandwich panel. 3D printing allows for the rapid prototyping of small intricate structures, which is excellent for auxetic sandwich structures.

Furthermore, the cellular nature of auxetic structures make it possible to program the response of these sandwich structures. By selectively placing cells made from soft materials in between cells from hard materials, different compressive behaviours can be programmed into the structure. These multi-material structures introduce another dimension to creating optimized metamaterials for specific applications.

This thesis will investigate which auxetic shapes excel at energy absorption. Before experimenting with designing multi-material structures with their own compressive behavioural responses.

1.2 Background

The background literature related to the topic given the problem as stated above, indicates that the following areas are of interest to research further.

1.2.1 Introduction to related literature

To move forward with the problem introduced in section 1.1. three main topics are of interest. These are: metamaterials, auxetics structures and energy absorption. Other areas which are of interest for the literary research are the effects of 3D printing parameters on part strength of 3D

printed parts. The type of materials which are used in experiments combined with how these experiments are performed will be investigated. Finally, studies will be investigated which also focus on comparable multi-material auxetic structures under compression.

1.2.2 Academic Environment

The research will be carried out on the University of Twente, Faculty of Engineering Technology (ET), and under the supervision of dr. ir. Mehrshad Mehrpouya. The student has access to a workplace at the university, the rapid prototyping lab, and the mechanical lab WH125. The rapid prototyping lab has two Ultimaker 3 machines and two Ultimaker 2+ machines available. The mechanical lab of the university has a Zwick Z005 testmachine available for compression cycle testing.

1.3 Scope of the Study

This thesis focuses on literary and practical research. The study provides a broad basis which future studies could use to guide their design choices. This thesis is not aimed at producing a final design other than the structures which were used for testing purposes. Finally the project delivers a proof of concept for multi-material designs.

The number of different structures, and the number of variations on these structures can become very large. The quantity of tests must be limited for reasons of time constraints. This narrowing of the scope of the project is discussed by the student and the supervisor in bi-weekly meetings during the project.

1.4 Purpose of the Study

This study provides a review of the existing literature, focusing on energy absorption, auxetics, the effects of printing parameters, materials choice, and the effects of strain rate on the compression of polymers.

This study delivers a design of an auxetic metamaterial with good energy absorption properties. For this purpose, first a series of different auxetic structures will be selected, tested, and compared to each other. A single shape will be selected for the second part, where structures with the chosen shape are created using different materials. The design principles learned during parts one and two will be used to create multi-material structures. By selectively utilizing soft or hard materials, the behaviour of the structures under compression will be programmed to behave in ways distinct from one another.

Thereafter, the study will be rounded off with the conclusion, discussion, and recommendations for future works.

1.5 Research Questions

The main research question and sub-questions guide the project throughout until its completion. The answers to these questions can be found in the conclusion of this report. The main research question for the thesis is:

- How to maximize energy absorption of multimaterial auxetic metamaterials during compression?

The Sub-questions to guide the project towards this main question are:

- Which beneficial properties do auxetic structures exhibit?

- How do process parameters during 3D printing affect the functionality of the structure.
- Which auxetic shape has the best energy absorption properties?
- Which materials have the best energy absorption properties, when using FDM 3D printing?
- How can the chosen shape and materials be combined to create multimaterial auxetic metamaterials?

Chapter 2

Review of the Literature

The literary review started with a general look at metamaterials. Investigating which classifications exist and what their general working principles are. This is followed by a more in-depth research on programmed metamaterials, which are studied under compressive loading conditions. These are structures which can exhibit different behaviours, based on how the internal structure was designed. Auxetics are a commonly used type of metamaterial, their classification and beneficial properties will be investigated. The ways in which structures absorb energy will be explained, and the definitions used within this thesis will be summarized. Lastly, the 3D printer which was used for the creation of samples will be explained, together with the impact of certain printing parameters on part strength.

2.1 Metamaterials

Metamaterials were first described in 1968 within the field of electrodynamics as artificial materials with properties which are not found in nature [23]. Most research has been conducted on optical and electromagnet metamaterials.

More recently, research has been made on mechanical metamaterials as well. These materials are defined differently. Cui et al (2010) defined mechanical metamaterials as ''a material which gains its properties from its structure rather than directly from its composition'' [43]. This definition is in line with other studies [22]. Some studies state that metamaterials must be manmade with properties not found in nature [38]. Other studies do include examples from nature. The blue wings from morpho butterflies derive their colour from nanostructures which only reflect light of certain colours [20]. This is an example which could be classified as a metamaterial.

Metamaterials are an interesting field of research, as they can be used to create a large number of innovative designs. For example, metamaterials can be used to create shoe soles which are specifically designed for individual needs [1]. Metamaterials have found their way in biomedical applications [57] and other general purposes as energy absorbers, improving airplanes crashworthiness, or packaging of sensitive goods [38]. It is possible to finetune a structure to generate specific behaviour [24]. Metamaterials can be used to create structures that can act as actuators, activated by changes in their environment. This can be done by utilizing the shape memory effect of polymers. This area was studied extensively for this thesis, but was later determined not to be in line with the experiments which were performed. The literary research on this subject can be found in Appendix K. Another example of a metamaterial is the combination of different materials, to create a new material with its own new unique properties [50]. This method of creating new materials and structures has become more accessible in recent years with the increased availability of 3D printing.

2.1.1 Classification of mechanical metamaterials

There are different methods of classifying mechanical metamaterials. Bertoldi et al. (2017) focussed on mechanical behaviour and functionalities [62]. Categorizing linear-based metamaterials, mechanism-based metamaterials, Instability-based metamaterials, and topological metamaterials.

Linear-based metamaterials can show nonuniform stresses and deformations, that allow for new properties and the creation of metamaterials. Auxetics and extremal materials are given as examples which deform locally at hinges, such that the global response of these materials becomes different from the bulk material. Auxetic materials are materials with a negative Poisson's ratio. This means that material flows inwards instead of outwards when an auxetic structure is compressed. Extremal materials are materials which are very stiff in most modes of deformation, but compliant in other modes. Extremal materials may have large values for eigenvalues of the elasticity tensor, indicating stiffness, or small values indicating lower resistance. Further categorizations could be made on their number of very small eigenvalues. For example, Pentamode metamaterials have small eigenvalues for five out of six principal directions.

Mechanism-based metamaterials are characterized by flexible hinges which connect a series of rigid elements together, to form a design that allows for zero-energy, free motion. This includes rotating squares and origami based structures such as Miura-Ori designs. Both are examples of auxetic structures, see Figure 2.1a. Kirigami are another type of sheet-based metamaterial, that is made by making many small cuts in a thin sheet of material. By placing these cuts in specific patterns, the elastic properties of the material can be controlled with large strains and shape changes as a result.

Instability-based metamaterials are divided into three categories. Buckling, which can occur in slender beams. This can lead to precisely designed non-linear behaviour under loading conditions. When a metamaterial is composed of an array or elastic beams, buckling may occur in a reversible homogeneous pattern. A basic example of a buckling induced auxetic structure can be seen in Figure 2.1b. Where the principle of the mechanism based on rotating squares is combined with the buckling behaviour of the beams which connect these elements. Bi-stalbe materials utilize a snap-through like behaviour, by snapping between two different stable configurations. These mechanisms keep their deformed state after unloading, allowing them to lock in energy which was used during loading. This mechanism can be used to create reusable energy-traping metamaterials. Lastly, frustrated metamaterials are materials where the underling structures do not deform cooperatively. Interactions within the structure caused by frustrations cause a complex energy landscape which can obstruct the original functionality. One example of a frustrated metamaterial can be seen in Figure 2.1c, where a lattice defect was placed in a flexible origami sheet. This method can be used to program the stiffness of the structure.

Topological metamaterials metamaterials exhibit topologically protected properties. These materials are unaffected by small amounts of disorder or smooth deformations, making them more robust. An example of a topological mechanism can be seen in Figure 2.1d. This structure is created by several rigid rotors, which are connected by rigid beams. Motions within the beam can travel from the right edge to the left edge, but not in the other direction. As small motions near the right edge of the beam remain localized.

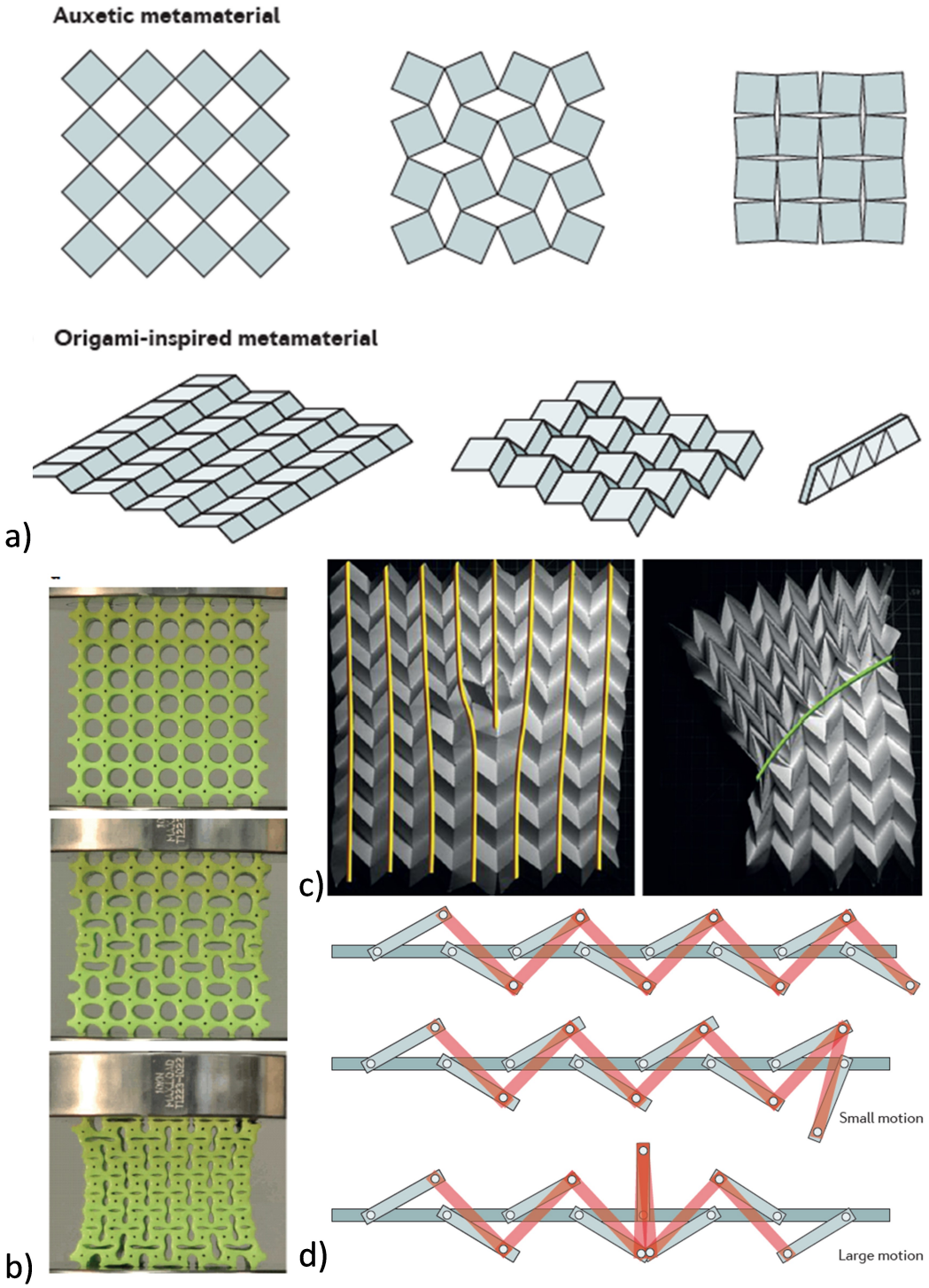

Figure 2.1: a) Two examples of mechanism-based metamaterials. Above a sheet with precise cuts, creating an arrangement of rotating squares with auxetic properties. Below a foldable origami-based metamaterial, using the Miura-Ori pattern. b) An example of an instability-based metamaterial, a rubber sheet with circular holes undergoes buckling instability. c) Lattice defect within a Miura-Ori pattern. One point within the fold pattern has been 'popped through', creating a dislocation. Leading to a different compressive modulus and a change in the compressive behaviour. d) Elastic springs in red, connecting rigid bars in grey create a topological metamaterial. When balanced, the system is on the verge of mechanical instability. However, their boundary modes are insensitive to small motions. Causing small impulses not to propagate to the left of the bar, whereas larger motions do.

2.1.2 Other classifications

A different method of categorizing mechanical metamaterials was used by Zadpoor et al. (2016) [62]. Their research focused on materials with unusual elastic mechanical properties. Focusing on the linear elastic behaviour which is described by the elasticity tensor and non-linear deformation behaviour with large strains.

Their first category consists of extremal materials. Which are given a category on their own, instead of being part of linear-based materials. Auxetic materials fall under the subset of extremal materials.

Their second category consists of negative metamaterials, these are materials with negative moduli. For example, materials with a negative bulk modulus, which expand when placed under uniform compression. Or materials with a negative stiffness. Materials which are designed to deform in a direction counter opposite to an applied force, thus working with the deformation instead of against it.

Snapp-through like behaviour, or a simple beam which buckles under compression. Ultra-property metamaterials are mentioned, as ideal materials with two or more of the properties: high stiffness, high strength, high toughness, and low mass density. These properties are difficult to combine in a single material, due to their conflicting nature.

Lastly, origami-based metamaterials are mentioned as an emerging area. Using the same Miura-ori origami metamaterials as an example

2.2 Studies on programmed sandwich structures

One area of mechanical metamaterials which has become the topic of more recent studies are structures with a programmed response. A number of advancements have been made on ways to program a specific behaviour in sandwich structures during compression. This does not include the act of changing the material, for example changing the material from steel to aluminum. In order to program a metamaterial, the cellular design of the structure is changed, or multiple materials ‘are introduced in specific areas.

2.2.1 Mono-material programmed metamaterials

Most mechanical metamaterials which are created with a single material rely on auxetic cellular patterns. These studies can focus on a single cell structure, and study the impact of geometric parameters on their behaviour. Dong et al. (2021) [6] studied an auxetic sinusoidal pattern within a sandwich structure. Their study created several similar structures, but with different geometrical angles, see Figure 2.2-1). It was found that greater angles result in more uniform buckling behaviour. As well as their impact on the Poisson’s ratio of the structure. Which benefited from greater angles, up to a point, where studs would come in contact with each other during the compressive deformation behaviour.

Studies are not limited to two dimensional structures. A three dimensional version of the sinusoidal based structure has also been investigated [58]. This study was conducted with a similar goals of investigating the optimal geometric parameters for this structure to function. Showing how minor changes in the geometric angle can increase the effective Young’s modulus and energy absorption properties. Their model found a good comparison with numerical simulations.

Another example of a study which investigated an auxetic structure with a single material was performed by Kochmann et al. (2017) [22]. Their study showed that some structures can show auxetic properties when exposed to compressive forces in one direction. But showed non-auxetic deformation patterns when subjected to forces in different directions. The effective properties of the structure were controlled by limiting the amount of instability within the structure, see Figure 2.2-2.

Even more unique was a cylindrical tube, with wall made from a chiral based auxetic pattern by Geng et al. (2019) [11], see Figure 2.2-3. They investigated the impact of different geometrical angles within the cellular structure, as well as the number of cells present. These cylinders were axially compressed, until buckling occurred. Their models were created using SLS additive manufacturing, instead of more common FDM techniques.

It is not necessary to use auxetic patterns to create metamaterials. A programmed response during compression can also be achieved by systematically changing wall thicknesses within certain cells [3], see Figure 2.2-4. This effect is occurs because changing the wall thickness changes leads to a change in the local stiffness of the cells. Four different behaviours were shown to be programmed within a structure with this method.

Another method of non-auxetic metamaterials with a single material can be found by using material properties in innovative ways. Bodaghi et al. (2016) [4] used the shape memory effect from polymers to create an actuator which could be activated by heating the element. The cellular structure was created in such a way as to allow the shape recovery mechanism to act as an actuator force. Which makes this an example of a metamaterial.

2.2.2 Multi-material programmed metamaterials

Bodaghi et al. (2020) [5] have continued their research on metamaterials, and investigated multimaterial auxetic structures. Their research covered different patterns of hard and soft plastics which formed layers within a honeycomb re-entrant structure, see Figure 2.3-1. The impact of these changes was investigated, with a focus on how these impact the energy absorption properties of the structure. Hard materials increase the amount of energy which gets dissipated, whereas utilizing more flexible materials increases the relative amount of energy that gets absorbed. The implementation of materials with different stiffness has an effect which is comparable to the changes in wall thickness from Figure 2.3-4. Locally changing the stiffness and elasticity of cells. Their work also continued investigation of the effect of shape memory polymers. This was used to show that the structure could be restored to its original shape after deformation. Khatri et al. (2021) [21] has performed a similar study, where a hard and soft material were combined in different layers to investigate their impact on the structure. This was done with the aim of creating a structure with increased synergistic performances. Adding softer TPU to a structure made from ABS to the compressive behaviour of the structure, see Figure 2.3-2. This was done to tune the moment where stress peaks occur, thus demonstrating the feasibility of constructing multi-material lattice systems.

Another way to make use of different material properties within a sandwich structure, is to exploit different glass transition temperatures. This can cause different parts of a structure to become structurally dominant, depending on the external temperature. One study showed how the same honeycomb based structure can be altered by selectively placing materials with a different T_G. In Figure 2.3-3, two models are shown. The green and black materials have a similar Young's modulus at room temperature, causing the two structures to behave near identical in this situation. However, the green material has a lower T_G than the black material. Causing the underling black structure to become dominant at higher environmental temperatures. This causes the two structures to exhibit different programmed responses to compression. In this example either a layered response, or auxetic behaviour.

Instead of a single structure which can behave in two different modes, it is also possible to use the principle of different glass transition temperatures to create a single structure with multiple compressive stages. Triggered by changes in ambient temperature, see Figure 2.3-4. This structure is made out of two materials, with a different T_G and different Young's moduli at all temperatures. Initial compression at room temperature deforms a structure into a certain shape where the most flexible material deforms primarily. At higher temperatures, the previously stiff materials reach their T_G, reversing the relative stiffness of the two polymers. This causes the deformed structure to change shape within the confines of the original compression.

Another method of introducing multi-material designs to auxetic structures, is to alter selective parts of a single cell. Changing the material at locations with the highest stress concentrations is most common in literature [18] [56]. These are often the corners or hinges where structures experience the greatest deformation. This can prevent structural failure and has shown to be favourable for the Poisson's ratio and maximum volume reduction up to a point.

2.3 Auxetics

The Poisson's ratio is a measure for the deformation of a material in the direction tangent to an applied force, see Figure 2.4a. For a material which experiences deformations in only two directions, the Poisson's ratio is defined as in Equation 2.1. The ratio is equal to the negative value of the transverse strain divided by the strain in the axial direction. The negative value of this ratio was used in the definition because most materials expand when they are compressed and narrow when elongated. The first time auxetics were described in a scientific paper was in 1987 [25]. Auxetics behave different to normal materials, expanding when elongated and contracting when compressed see Figure 2.4b. Auxetics are most commonly used as repeating shapes inside sandwich panels. Plates on the outside of these panels allow for an even distribution of forces over several cells at once.

$$\nu = -\frac{d\varepsilon_{trans}}{d\varepsilon_{axial}} = -\frac{d\varepsilon_y}{d\varepsilon_x} \tag{2.1}$$

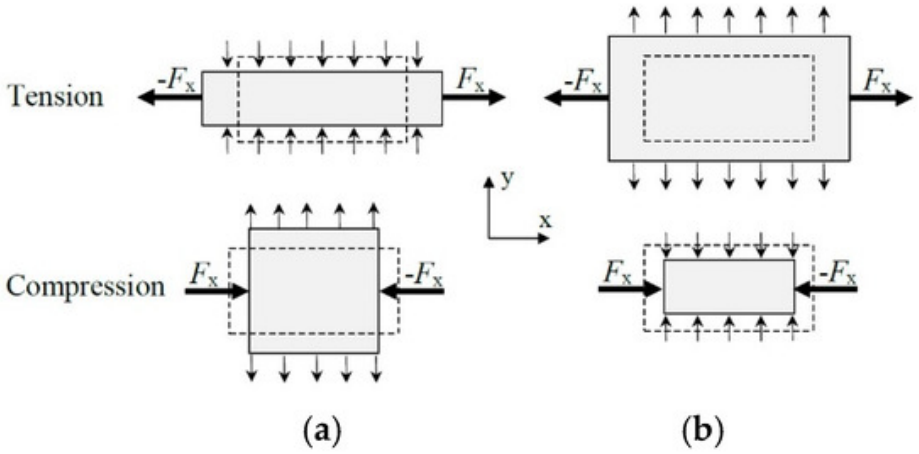

Figure 2.4: Non-auxetic (a) and auxetic (b) behaviour [9].

The force-displacement diagram when compressing auxetic structures has 3 distinct stages [65]. The elastic stage where elastic deformation takes place. The plateau stage, where plastic deformation takes place. Followed by the final stage where the force climbs rapidly, and the densified structure gets crushed.

In normal use, materials which undergo plastic deformation remain deformed permanently. This means that if an auxetic structure would be used, as for example a shock damper, it would be a single use product. Bodaghi et al. (2020) [5] has shown that it is possible to restore such sandwich structures back to their original shape after plastic deformation. This would allow for both the first and second compressive stages to be used and re-used for energy absorption purposes. This was achieved by utilizing the shape memory effect of polymers. Polymers with shape memory properties operate by the dual-state mechanism. Amorphous thermoplastics have different states, depending on temperature. A glassy state at lower temperatures, and a rubbery state at higher temperatures. Within the polymer are different segments. Hard

segments composed of chain entanglements or covalent bonds, and soft segments made up out of the free ends of polymer chains. When a structure of this material is deformed plasticly without fractures, the soft segments deform. Where the hard segments provide rigidity and do not deform. At this point, the polymer can be heated to above the glass transition point of the material. This allows the free chain ends to vibrate, and start to move and roll over one another. This allows the crosslinks to pull the material back to its original shape.

This subject has been investigated further. However, it has not been utilized effectively within this project. Extensive research on shape memory properties requires water tanks where the temperature can be accurately controlled. This equipment was not available on the university for this project. Combined with time restraints and the possibility to research other areas meant that this subject was not used within experiments. Further literary research on this subject can be found in Appendix K.

2.3.1 Classifications of auxetic structures

Auxetic materials can be broadly classified into natural materials and synthetic materials. Some of the more well-known natural materials are listed in Figure 2.5, however the focus of this report lies on two-dimensional synthetic auxetics. This was done because the focus of this project lies on creating duo-material structures. Restricting the material to a two-dimensional shape removed unneeded complexity for this thesis [8], [31].

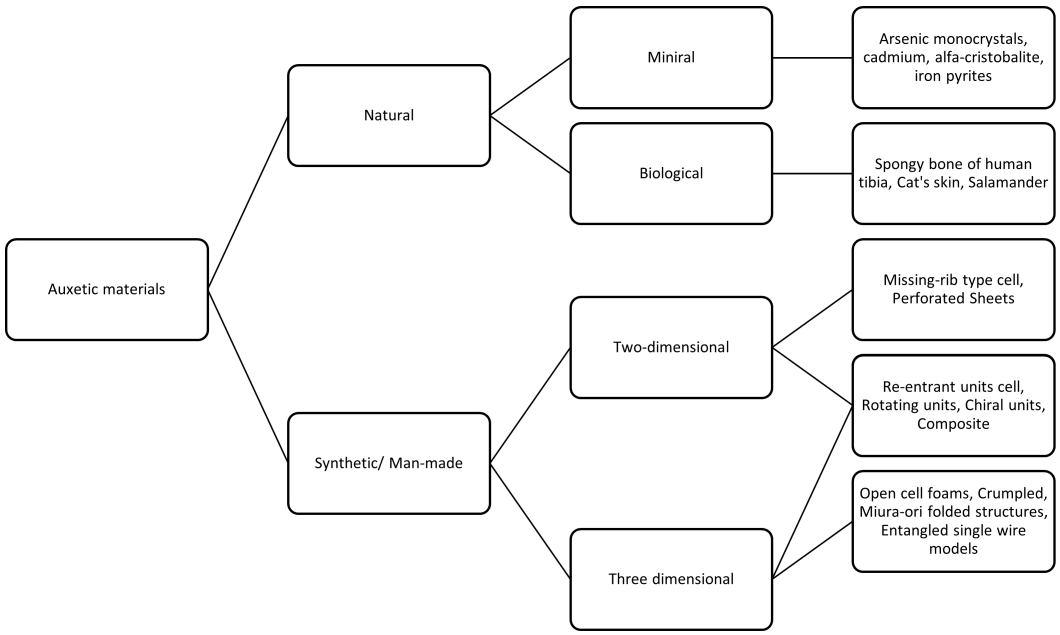

Figure 2.5: Classification of auxetic materials, based on a figure by A V Mazaev et al [31].

There are two shape-types which have no three-dimensional counterpart. First are perforated plates, which imitate rotating square units. Other shapes such as rhombuses' or triangles are also possible.

Secondly are missing-rib type models. This shape is created by taking two identical ribs, and fastening them perpendicularly at their midpoint. These shapes are then connected to each other, perpendicularly to their ends. This creates an unfinished square, called a missing-rib type structure.

Next are four shapes which have two dimensional and 3 dimensional variants. First are re-

entrant based shapes. Re-entrant means an angle pointing inwards. The first re-entrant structure was derived from hexagonal honeycombs, but with two opposing angles pointing inwards instead of outwards [28]. All shapes which fold inwards due to inwards facing corners are classified as re-entrant based shapes. The re-entrant shape is auxetic both in tension and when compressed. The honeycomb based re-entrant shape has been studied the most in literature, but there are many other auxetic re-entrant based shapes.

Secondly, rotating units. This shape is similar to the perforated sheets above, but is not created out of a single sheet. Due to the rotation of the solid shapes, the Poisson's ratio is almost equal to -1 [14]. Other shapes such as rectangles, rhombuses or triangles are also possible. These shapes do not require additive manufacturing technologies for production, which made them less interesting for this study.

Thirdly, chiral units. Auxetic behaviour stems from the rotational movement of the nodes. As a node rotates, the ribs between the nodes will wind up onto the nodes. Thus pulling the nodes together when under a compression or tensile load.

Fourth, composites which make use of auxetic fibers. These fibers can be made from a single or multiple materials and often use mechanisms illustrated in Figure 2.6f and Figure 2.6g.

Lastly, there are three dimensional auxetics which have no two dimensional counterpart. The first three categories are open cell foams, crumpled sheets and entangled single wire models. These structures are not suited for additive manufacturing techniques and are not further investigated.

The last category are Miura-Ori folded structures. These are structures which follow a zig-zag pattern, perpendicular to the plane. When this plane is compressed, the structure folds inwards based on these zig-zag patterns. When bend, this structure deforms into a saddle shape. Based on the configuration of the structure, different properties can be created [47].

(a) Perforated sheet

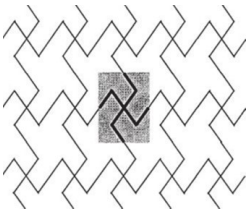

(b) Missing-rib unit

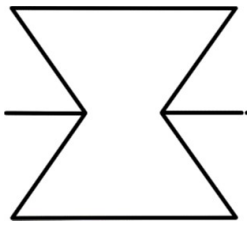

(c) Re-entrant unit

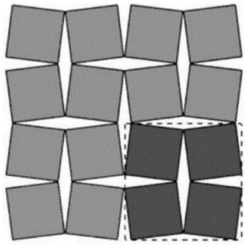

(d) Rotating unit

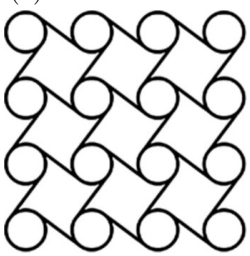

(e) Chiral unit

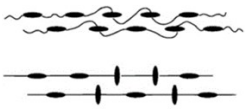

(f) Mono material auxetic fibre [8]

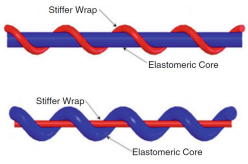

(g) Duo material auxetic fibre[19]

Figure 2.6: Different auxetic units. Figures were taken from [31] unless stated otherwise.

2.3.2 Beneficial properties of auxetics

Auxetic structures have properties most other materials do not have. The rotating square based designs have a variable permeability, depending on their stretched state. Furthermore, auxetics have a relatively high shear stiffness, indentation resistance and facture toughness [8], [65], [46], [54].

The shear modulus and indentation resistance can be described mathematically for homogeneous isotropic linear elastic materials with Equation 2.2 and Equation 2.3.

$$G = \frac{E}{2(1+\nu)} \tag{2.2}$$

$$H \propto (\frac{E}{1-\nu^2})^{\gamma} \tag{2.3}$$

Here the Shear modulus (G) is defined in terms of Young's modulus (E) and Poison's ratio (ν). For G, it can be seen that as ν approaches -1, G will tend towards infinity. Auxetic materials are anisotropic materials with non-linear behaviour, so this will not happen in practice. However, it indicates that auxetic materials can exhibit a relatively high shear resistance. It is worth noting that ν of a structure is a function of strain, and therefore not constant. As strain increases, ν will move closer to zero as there are limits to how dense the internal structure can ultimately become.

The Indentation resistance (H) is proportional to E, ν, and γ. The value of γ depends on the method of indentation. γ is equal to 1 for uniform pressure and equal to 2/3 for Hertzian indentation, or indentation using a sphere. As ν gets smaller, H will tend towards infinity. This equation alone does not reveal the behaviour of auxetic structures. When auxetic materials experience a local impact force, material is drawn towards the area of impact. This is illustrated in Figure 2.7.

The negative Poisson's ratio has a relationship with compressive strength. Under similar relative densities, greater negative values will increase the compressive strength [59].

A factor which complicates calculations with Poisson's ratios, is their strain dependency. There is a limit to how much material can be pulled together, when this limit is reached, densification starts. At this point, the Poisson's ratio goes to zero or even positive values. Different shapes behave differently when compressed [34].

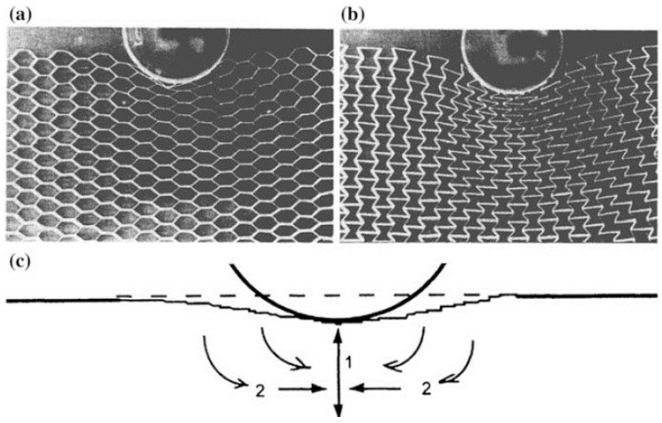

Figure 2.7: Densification of auxetic material, compared to a non-auxetic structure [28].

2.4 Energy absorption

One goal of this thesis is to maximize energy absorption within sandwich structures. It is therefore important to know how energy is absorbed when these structures are compressed. Then, a formula is defined which will be used to compare the energy absorption performance of different experiments later in this thesis. Finally, the beneficial properties of auxetic structures with regards to energy absorption are investigated briefly.

2.4.1 Methods of energy absorption

One goal of this thesis is to maximize energy absorption within sandwich structures. It is therefore important to know how energy is absorbed when these structures are compressed. Then, a formula is defined which will be used to compare the energy absorption performance of different experiments later in this thesis. Finally, the beneficial properties of auxetic structures with regards to energy absorption are investigated briefly.

Elastic deformation

Elastic deformation is a temporary deformation which takes place in the elastic region of a material. Small deformations caused by external forces allow the material to return to its original shape, when the forces are removed. Linear elastic deformation is governed by Hooke's law, see Equation 2.4. Here σ is the stress in [N/m2], E is the elastic modulus or Young's modulus in [N/m], and ε is the strain in [m]. Hooke's law only holds for deformation in the elastic range of a material, if greater forces are applied, the yield strength of the material will be exceeded, and the material will start to deform plastic.

$$\sigma = E \cdot \varepsilon \tag{2.4}$$

Plastic deformation

Unlike elastic deformation, plastic deformation cannot be undone by removing the force which caused the deformation. Removing the force from an object which has undergone plastic deformation will let the object return partially to its original shape, but not fully. Soft thermoplastics have a relatively large plastic deformation range, when compared to harder materials. For example, plastics with a crystalline structure, or acrylic plates, have relatively smaller plastic deformation ranges.

Figure 2.8 shows a typical tensile test. Plastic deformation occurs when the applied force exceeds the yield strength. At which point strain hardening will occur. During strain hardening, atoms become dislocated. This not only permanently deforms the material, but depending on the material, also hardens the material. Increasing forces even further, will lead to a maximum strength, or ultimate strength. Beyond this point, stress will no longer increase with increased strain, and will lead to material failure or fracture.

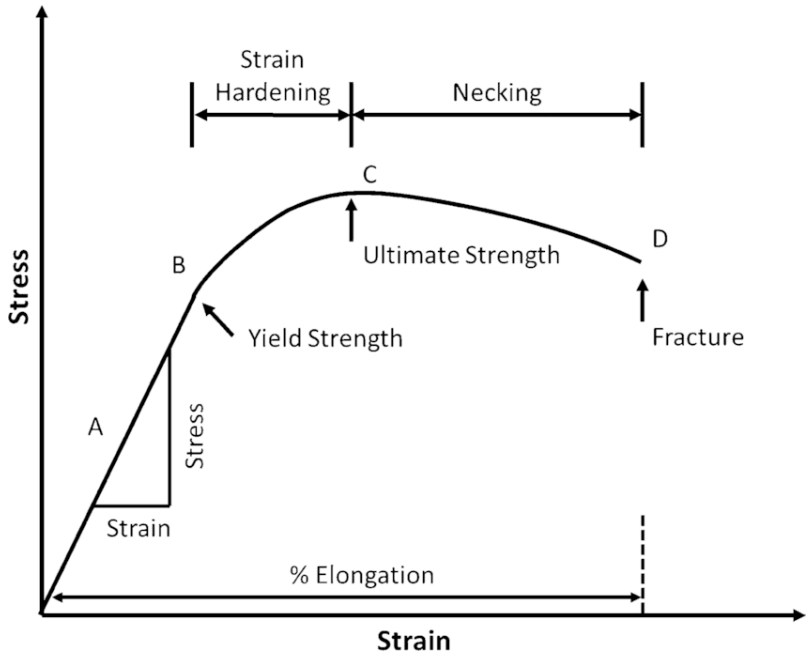

Figure 2.8: Typical stress strain curve for a tensile test of a polymer [27]

2.4.2 Defining energy absorption within this thesis

This study will compare the energy absorption performance of different shapes and different materials. Absolute values of energy absorption and dissipation are not suited for this purpose. Therefore, the dissipated energy divided by the absorbed energy will be used as the primary method for comparing different structures. This same metric was used by Bodaghi [5] for similar comparisons. To keep in line with the work of Bodaghi, energy absorption will be defined by Equation 2.5 and Figure 2.9. Furthermore, the same parameter used by Bodaghi, energy absorption as percentage of total energy experienced, will be used when comparing experimental results. Other papers have also mentioned the same metric when analyzing experimental results [40].

Figure 2.9 shows, a sandwich structure which is compressed in a cycle. First an structure is compressed to 20mm, after which the structure is allowed to spring back. The area underneath the curve is defined as dissipated energy and absorbed energy respectively.

$$E_{Absorption\ \%\ of E_{total}} = \frac{E_{absorbed}}{E_{dissipated} + E_{absorbed}} \cdot 100\% = \frac{\int_{\varepsilon(F=0)}^{\varepsilon_{max}} F(\varepsilon)\, d\varepsilon}{\int_{0}^{\varepsilon_{max}} F(\varepsilon)\, d\varepsilon} \cdot 100\% \tag{2.5}$$

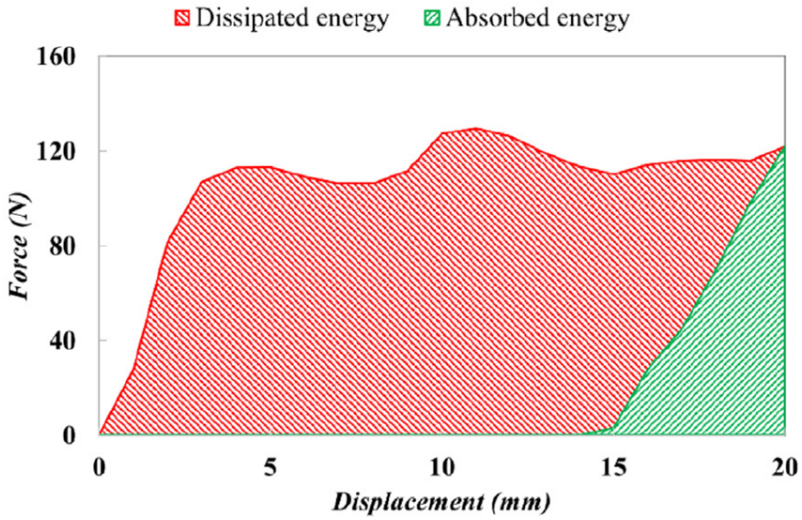

Figure 2.9: Graph illustrating the difference between dissipated energy and absorbed energy [5]

2.4.3 Energy absorption of auxetics

The general compression behaviour of auxetic structures can be described by three distinct stages [7] [65].

At first the elastic stage, where elastic deformation takes place with a mostly constant young's modulus. Second, the plateau stage. In this stage, plastic deformation and buckling behaviour are dominant. Most auxetic structures experience constant stress level on average while being compressed. But the specific behaviour is design dependent. Lastly, the strain hardening stage or densification stage. This stage starts when all buckling behaviour that could occur during compression has transpired. More and more plastic is compressed and packed denser and denser until a material of solid plastic remains. This stage is characterized by a sharp increase in stress levels. These stages are visualized in Figure 2.10.

The same study also studied failure modes for honeycomb re-entrant structures. Five different modes were found, with wall thickness as the main parameter which influences the failure mode of a structure.

Beneficial properties of auxetics

Several papers have mentions of auxetic structures and their enhanced energy absorption properties [8], [65], [48], [30], [49], [63], [64]. However, of the literature found during this literature study, not many papers focus on energy absorption and dissipation. Of the literature investigated for this report, only two papers were found to make a clear distinction between energy absorption and energy dissipation [5] [48].

This means that auxetics are listed as having increased energy absorption properties. However, the previously defined parameter, in subsection 2.4.2, of dividing the dissipated energy by the absorbed energy for comparing the performance of different structures, is a relatively novel method. Nevertheless, this parameter was chosen in consultation with the supervisor to be used during this project. In part because this thesis was to be an extension of the work done by Bogadhi [5].

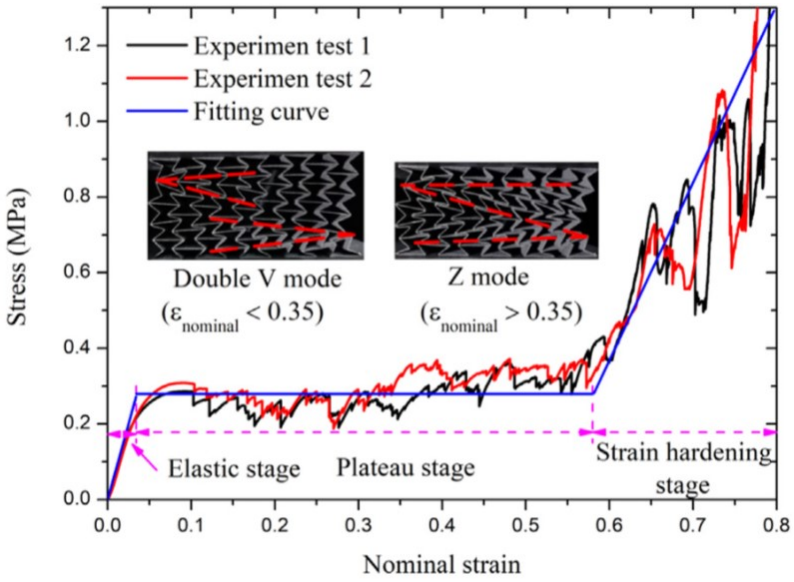

Figure 2.10: Three stages of compression, figure taken from [7].

2.5 3D printing

3D printing is a form of additive manufacturing. In contrast to traditional production methods such as a lathe or mill, material is added to a part instead of removed. All additive manufacturing techniques create a product by adding one layer at a time. Creating a free-form fabrication process with, depending on the technique used, relatively little limitations to shape complexity. Additive manufacturing has an emphasis on quickly creating a single product, often used as a prototype. 3D printing is often used for rapid prototyping. It is often more expensive and time-consuming for a craftsman to create prototype parts. Especially as the complexity of the prototype increases and more iterative stages would be required for an alternative manufacturing process. 3D printing is not suited for large scale production, the manufacturing process itself takes a considerable amount of time per product. However, the time between iterations is reduced with additive manufacturing techniques. The amount of work preparation is limited for 3D printing. No specialized molds or tools are required, and short production runs are possible [12].

2.5.1 Fused deposition modelling

Many different additive manufacturing methods exist. Some examples are electron beam melting which can create parts from metal powders. Stereolithography (SLA) which uses a laser, or other light source, to selectively harden a resin. Selective laser melting (SLM), which uses a heat source to melt powders within a print bed. Of all additive manufacturing techniques, FDM or fused deposition modelling is the most widespread. The machines are relatively cheap, starting as hobbyist machines below 100€. They require relatively inexpensive plastic filament to operate and do not produce toxic or foul-smelling fumes. Depending on the type of plastics used.

Figure 2.11a Shows the most important parts of an FDM style 3D printer. The plastic which is used to create parts starts as filament on a spool to the side of the machine. This filament has a constant diameter and is guided towards the extrusion head. Here, small drive wheels pull on the filament coming from the spool, and push it towards the nozzle. Around the nozzle are heating elements, surrounding an area where plastic gets liquified. As plastic keeps being pushed through, it moves outwards through the narrow opening of the extrusion nozzle. Plastics have a melting zone, and are not fully melted within the nozzle. They instead

remain viscous and semi-solid. A constant pressure within the nozzle results in a constant flow of plastic. As material flows out of the nozzle, the extrusion head moves around in the XYZ directions. Leaving some molten plastic behind, which bonds to previously placed plastic and cools down to create a coherent solid structure. The movement follows a pre-programmed path, in a controlled manner. Plastics should cool down quickly, so they do not deform after they are printed. The previous layer must be solidified before a new layer can be printed on top of the old layer.

The printer used for this thesis is an Ultimaker 3, see Figure 2.11b. This printer has two nozzles, allowing for two different materials to be used simultaneously within the same print job. The drive wheels within this machine are located at the back, in a Bowden style setup. This removes weight from the extruder head but requires the filament to be guided towards the nozzles. These guiding tubes can introduce slack withing the feeding system which can result in lower surface quality prints. But removing the weight from the printhead allows for this part to move faster with greater accuracy.

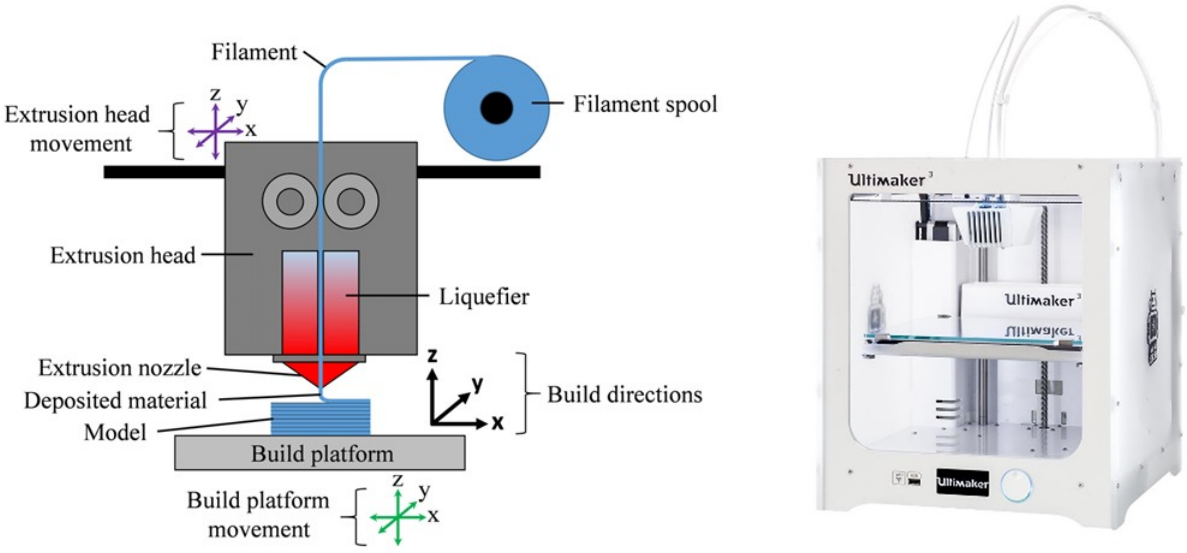

(a) (b)

Figure 2.11: Left, a schematic overview of the basic components of an FDM style 3D printer [13]. Right, a picture of an Ultimaker 3, which was used for this project.

2.5.2 General production process

3D printed models must start with a software model which describes the geometry. This model can be made in software such as SolidWorks. Within the CAD software, the model is saved as an STL file. This file type only saves the external closed surfaces of the original model. The STL file is loaded into a slicer. The software used for this project was Cura 4.11.0. This program can perform some minor manipulations to the model, such as rotation and scaling. The slicer also allows to control the printing parameters, or build parameters. Settings such as temperature, layer height, and speed are set within the slicer. Then the slicer slices the model. This means that the model is cut into thin horizontal slices, which will form the layers which will be filled in by the printer. This step is needed, as 3D printing is a layer by layer process. Once the operator is ready, the slicer can create G-code. This is a list of XYZ locations, combined with acceleration, extrusion and other command which act as instructions for the 3D printer to follow. The building part is automated, once the printer is finished the operator can retrieve the printed part from the buildplate. Depending on the model and slicer settings, some post-processing steps need to be taken. Support material needs to be removed or surfaces may

need to be cleaned before the printed part is ready for use.

2.5.3 Effect of printing parameters on part strength

Literature indicates three main printing parameters which impact part strength. These are layer thickness, infill percentage, extrusion temperature, and Build orientation [53].

Layer thickness impacts the ultimate tensile strength, compressive strength, and impact loading strength. Lowering the layer thickness increases ultimate tensile strength. This effect occurs due to the fabrication method. When molten plastic is extruded, it is compressed between the nozzle and the previous layer. This changes the shape of the printed layer into an oval shape. The flatter this oval, the larger the relative contact area becomes. Therefore creating a better fusion to the underlying layer.

Infill percentage has an obvious relation to part strength. Hollow parts have lower tensile strengths and compressive strengths, compared to solid parts. Infill patterns have a notable impact on strength, but at 100% infill, infill patterns lose their distinctiveness.

Extrusion temperature, or nozzle temperature has a limited impact on part strength. Increasing the extrusion temperature increases tensile strengths up to a point. For PLA for example, 175°C results in less strength than 185°C. However, there is no difference in tensile strength, yield strength, or Elastic modulus when printing at 185°C or 205°C.

Build orientation, or printing direction is another method of influencing part strength. FDM printing creates anisotropic parts. This means that applying forces in the direction of the printed layers results in higher tensile strength when compared to forces perpendicular to this direction. This happens because delamination can not occur in the printing direction, but it is possible in other directions.

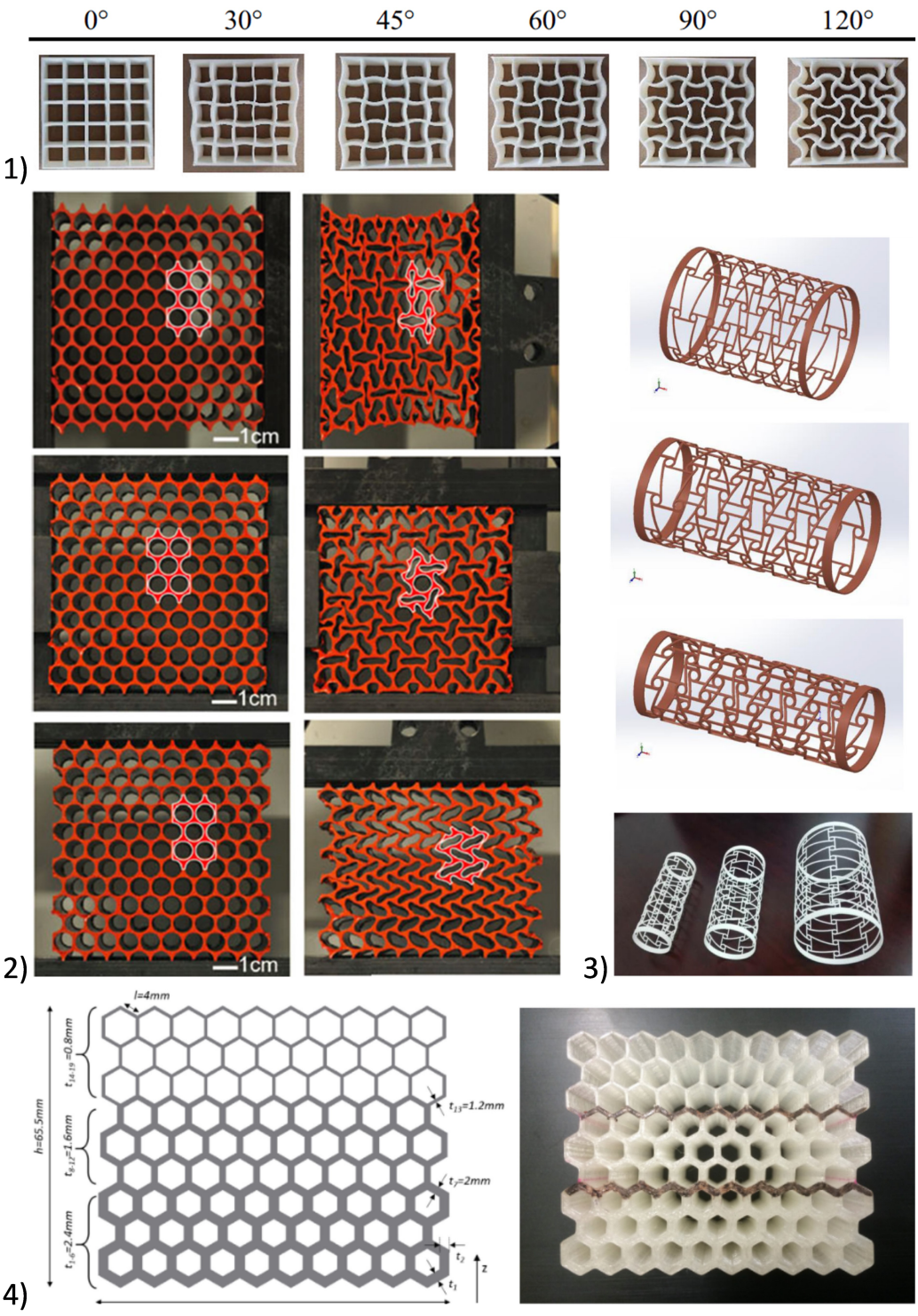

Figure 2.2: 1) Auxetic sandwich structure of a sinusoidal pattern with different geometric angles. 2) Different failure modes of the same structure, depending on the direction of the applied force, showing auxetic behaviour in one direction. 3) Cylinders used in buckling experiments. The pattern of the cylinder is a symmetrical chiral based pattern. 4) A honeycomb based structure, with thin walls at the top, and thick walls at the bottom. Creating different sections with their own effective Young's modulus.

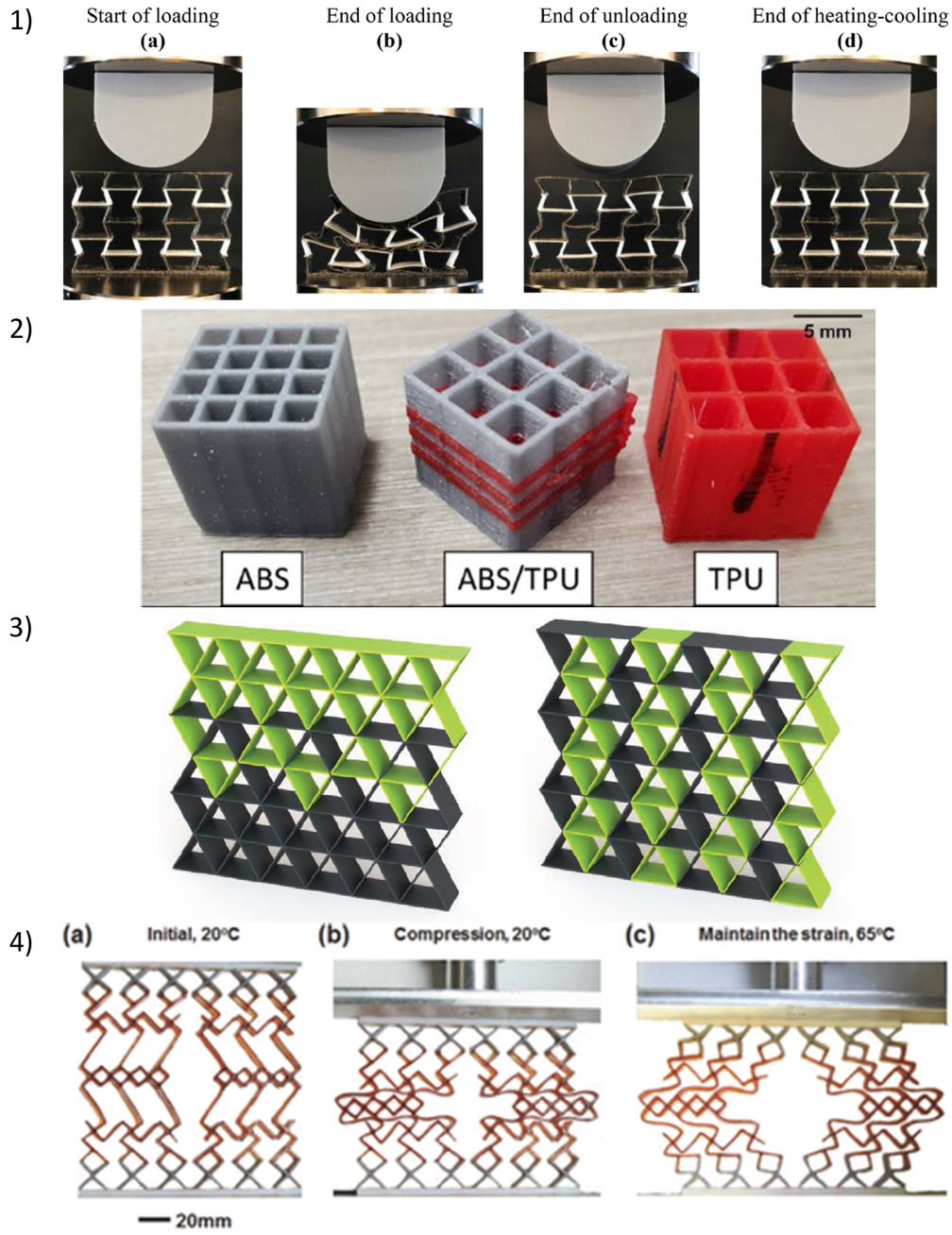

Figure 2.3: 5) A honeycomb re-entrant model with different layers of hard PLA (black) and elastic (white) material. Step c) and d) show the shape memory effect. 6) Cubes with made with different materials. These were created with differing patterns and ratios of hard-to-soft materials. 7) Using a honeycomb base, the green polymer softens at a lower temperature than the black polymer. Resulting in identical behaviour at room temperature. Where the shape of the black polymer becomes dominant at higher temperatures, left a layered response and right an auxetic response. 8) The grey polymer has a lower T_G, than the red part. Increasing the temperature, changes the ratio between the forces applied by the two materials. Causing the red sections to push outwards.

Chapter 3

Materials and method

3.1 Polymer Selection

In order to create programmed meta-material structures, one hard and one soft polymer is required. The hard material has as function to provide strength, and rigidity. It must not break under deformation. The soft material will provide the bulk of the energy absorption properties. Furthermore, both materials must be printable with a FDM stile 3D printer, and be available as filament. The two selected materials must adhere well to each other. A structure which falls apart after printing is of no use after all. The materials must exhibit shape memory properties if they undergo plastic deformation when compressed during tests.

For the purpose of this study, four different materials were used. These are two hard plastics, PLA and Filican C8, and two soft plastics, Filican PCL100 and TPC-91a. PLA is the industry standard material and is likely used the most out of all materials in FDM 3D printing. C8 is a material based on PLA, but with additions which improve the properties of the plastic. Resulting in higher impact strength, better layer adhesion, and better surface quality when compared to PLA according to the manufacturer. C8 is made with between 60% and 70PCL100 is one of many variations on polycaprolactone. It is a soft and flexible material, but lies somewhere between hard PLA and flexible rubber like materials. PCL100 is a shape memory polymer with a unusual low melting point of 60C. PCL has properties which are beneficial for biomedical applications [39], and has been used in biomedical applications because of the shape memory properties of PCL [55]. TPC is a very flexible and elastic rubber like material, and will provide excellent energy absorption properties.

3.1.1 Polymer properties

Four different polymers materials were selected based on their properties, availability and relevance to other research performed at the university. The mechanical properties and most important printing parameters can be seen in Table 3.1. One pair of hard polymers and one pair of soft polymers were chosen, these were PLA and C8, and PCL100 and TPC-91a respectively.

The flexible materials required some fine tuning of printing parameters before samples of good quality were created. The lessons learned during this process are summarized in Appendix F, and can support future students who will work with these materials.

	PLA	Facilan™ C8	Facilan™ PCL 100	TPC-91a
Chemical composition	Polylactic Acid	Polylactide resin (60%-70% by weight)	2-oxepanone, homopolymer (>99% by weight)	Thermoplastic copolyester (TPE-E) with a shore hardness rating of 91A
Density	1,24 g/cm³	1.4 g/cm³	1.1 g/cm3	1.22 g/cm³
Tensile strength at yield	66 MPa	45 MPa	45 MPa	17.7 MPa
Elongation at yield	8% - 6%*	4%	15 %	>500%
Youngs (E) modulus	3027 MPa	3000 MPa	350 MPa	67 MPa
Glass transition temperature	57°C	-	-60°C	-
Melting temperature	145 – 160°C	-	58°C – 60°C	160°C
Decomposition temp	-	-	200 °C	-

Table 3.1: Material properties, data was taken from www.3d4makers.com and www.matterhackers.com

3.1.2 Biodegradability of PLA

PLA is the most commonly used polymer for FDM 3D printing, due to low prices, ease of use and availability. Research which makes use of PLA often cites how PLA is made from corn starch, and how PLA is biodegradable. The latter is deceptive.

The European norm EN13432 defines the properties of a biodegradable polymer. Living organisms must be able to decompose a material of predefined sizes into CO2, water, minerals and non-toxic biomass within 12 weeks. With restrictions to the size limits of the leftovers at the end of this period. Microbes are able to degrade PLA within this norm. However, this only happens under specific laboratory conditions [41].

PLA is a very durable material within soil at ambient temperatures. Microbes required to decompose the polymer are not normally present within soil in the same concentrations as within laboratories [61]. PLA placed in household compost bins will not biodegrade within a reasonable time frame. Without specific waste separation and waste treatments, PLA will not act as a biodegradable polymer in practice. Further literary research on the biodegradability of PLA was performed and can be seen in Appendix K.

3.2 3D printing setup

An Ultimaker 3 was used to 3D print samples for this project. Samples created together as much as possible, see Figure 3.1 and Figure 3.2. Some tools were used to aid the printing process, spray adhesive and blue masking tape to provide better bed adhesion where needed. Plyers and a spatula to remove parts from the printbed. 3D models were created with Solidworks. G-code for the Ultimaker was created with the slicer Cura, version 4.11.0.

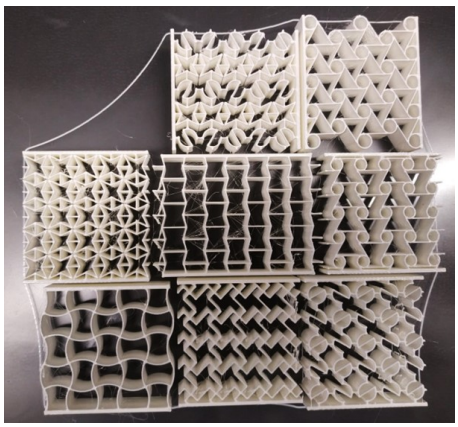

Figure 3.1: Several models for the first experiment, printed at the same time.

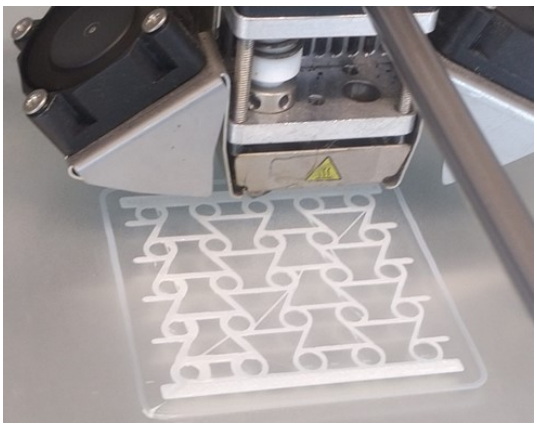

Figure 3.2: A ChiralN4 sample being printed.

3.3 3D printing parameters

While printing, small adjustments were made continually in attempts to improve the print quality. The final settings for the most important parameters per polymer can be seen in Table 3.2. In general, the nozzle speed and temperature were being set according to the recommendations from the manufacturers. In the case that a range was given, initial tests started with the average value of this range. These settings were iterated upon during the creation process. Qualities such as bed adhesion, print quality and stringing were also looked into. Other interesting settings and options within Cura which will be discussed are line width, layer height, and mesh overlap.

Printing temperature	200°C	200°C	130°C (- 170°C)	(230 -) 270 °C
Bed temperature	60°C	60°C	30°C	60°C
Print speed	40mm/s	40 - 50mm/s	10 - 30 mm/s	40mm/s

Table 3.2: The main 3D printing parameters used to create samples. Values between brackets indicate temperature ranges suggested by manufacturers.

3.3.1 Line width

Linde width is the width of a single line. The value of the line width is generally equal to the width of the nozzle. However, Cure normally slightly reduces this value from 0.4mm to 0.35mm This is done to improve print quality.

However, for this project, the line width was set at 0.4mm. This was done because samples are composed of segments which are mainly one wall thick. Surface quality is not important for these parts, therefore the slight under extrusion suggested by Cure was removed. Additionally, thicker walls result in stronger parts.

When Solidworks creates an STL file of a curved wall, the wall is turned into a wall made up of several straight edges. This method slightly undercuts the curved wall. When Cura 4.11.0 tries to place a line with a thickness of 0.4mm, Cure will not be able to place a line when there is no room for it. Reversly, when the STL file made a wall 0.5mm thick, Cure will fill this wall with a line 0.4mm thick. These two software quirks required the wall thickness in Solidworks to be slightly larger (0.1mm) compared to an ideal workflow. Starting at Cura 5.0, the software handles thin walls differently. For simplicity only Cura 4.11.0 was used for this project.

3.3.2 Layer height

Increasing the layer height results in several different property changes. First, a worse surface quality. This property is not important for this study as only the functionality will be investigated. Second, lower print times. This is a much desired outcome, as a large amount of parts will be printed for this project. Third, increasing the layer height will reduce the tensile strength of the printed part. This effect is undesired, however, the only strength requirement of the printed parts is to not fail during compression tests. Lastly, changing the layer height impacts the shape memory behavior of the printed part. Increasing layer height will reduce recovery time and response time, but will increase the recovery ratio.

It was decided to set the layer height at 0.2mm for this project. This provides a middle ground between print speed, part strength, and properties related to the shape memory properties, recovery time and recovery ratio.

3.3.3 Mesh Overlap

One way to improve the adhesion between two different materials, on the same layer during printing, is the setting mesh overlap. This setting can be used when two different STL models

are adjacent. The effect of this setting is visualised in Figure 3.3. As the endpoints of the two different lines of plastic overlap more, a stronger bond is created between the two different plastics. This function was useful to bond thin walls head to head. However, it was found that different settings for mesh overlap would be ideal when models overlap differently, such as along the broad side of two parallel walls. This meant that during the iterative design process, a maximum of 0.4mm for mesh overlap was found.

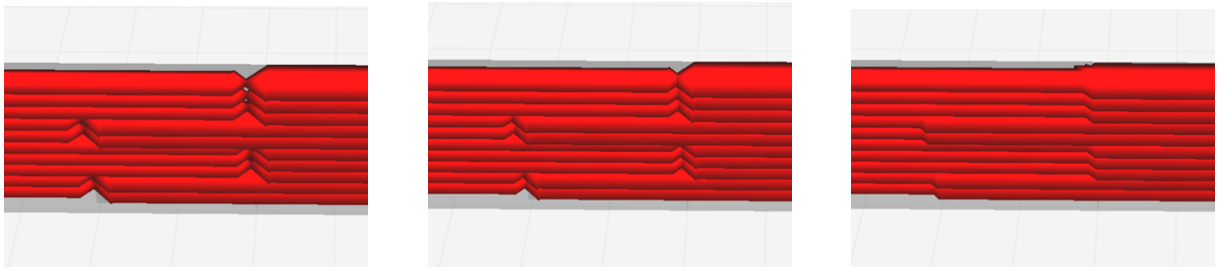

(a) 0mm Mesh-overlap (b) 0.1mm meshoverlap (c) 0.4mm meshoverlap

Figure 3.3: Merged meshes overlap setting in Cura. For visual clarity, the flow of the right model was increased.

3.4 Compression tests

To perform compression tests, the Zwick Z5.0 mechanical tester was used, shown in Figure 3.4. This machine can perform both tensile tests and compression tests. For experiment, the machine was configured with a push-block extension combined with a loose steel plate to evenly distribute the compressive force onto the test samples. This configuration can be seen in Figure 3.5. A light source, camera fixture and mobile phone were used to collect pictures and video material during testing.

3.4.1 Test setup

To perform the compression tests, a single program was configured in the software Zwick/Roell. This made sure all compression tests were performed in the same way. The main settings are listed in Table 3.3. To perform a test, the machine is first equipped with the appropriate tools and calibrated. The sample which will be tested is placed on the base, with a steel plate on top which covers the entire surface area of the top of the sample. Next, the machine is brought to its starting position and the program is run until it is completed and the sample can be removed.

All experiments were performed in triplicate. Three identical samples were used and average values were used in calculations. This is done to check the consistency of these experiments. To check if one sample shows significantly different results compared to what was expected to be identical samples. If such a discrepancy would occur, it would be discussed with the supervisor and a probable cause would be investigated. 3D printed samples were subjected to a visual inspection, to verify the quality of the printed samples. When significant flaws were detected, the printing parameters were adjusted and new samples were created. Optimizing printing parameters was a larger task for flexible materials, compared to the hard plastics.

Figure 3.4: Zwick Z5.0 mechanical tester.

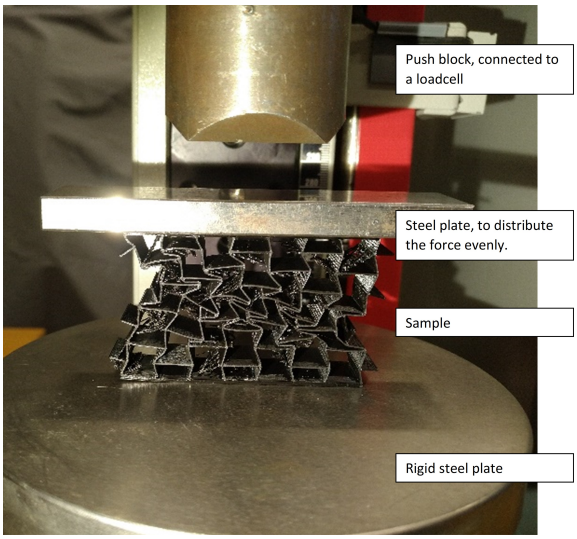

Figure 3.5: Compression test setup with sample.

Parameter	Value
Start position	2cm above the sample and steel plate
Pre-load	0.5N
Hold time at pre-load	1s
Number of cycles	1 cycle
Point of load application of the cycle (standard travel)	Changes per test
Speed, both compression and relaxation	8mm/min
Upper force limit	2000N
Lower force limit	0.4N
Travel save interval	10 micrometer
Time save interval	0.1s

Table 3.3: Settings used to configure compression tests.

3.5 Effect of Strain rate

Temperature and strain rate have a similar effect on polymers. Varying the temperature when performing impact tests, shows that polymers become stronger and stiffer at lower temperatures. However, their impact resistance will decrease at the same time. The inverse is also true, lowering the temperature will result in a higher impact resistance at the cost of strength and stiffness. There is a transition from brittle to ductile failure as temperature increases.

Strain rate has a very similar effect on the failure modes from polymers as temperature. A similar brittle to ductile transitions exists for strain rates. High strain rates, with relatively high elongations or compressions over a short amount of time, will favour the elastic properties of the material. Conversely, low strain rates favour the viscous or energy damping effects of the material. The viscous flow of a material is generally associated with the impact resistances or toughness of the material. A lower temperature and higher strain rates will result in brittle failures, higher temperatures and lower strain rates will result in ductile failures [17].

Because polymers behave as non-linear viscoelastic materials, the Young's modulus, shear modulus and Poisson's ratio all vary as the strain rate changes. The sensitivity of these elastic constants is the greatest around the glass transition temperature of the material, but is also

noticeable in other areas [26] [52].

At very high strain rates, the impact of inertial forces becomes dominant over other effect. Leading to the effects of wave propagation to determine the behavior during compression [65]. This effect only occurs at very high strain rates, well above the scope of this thesis.

Most studies which investigate the compressive behaviour from plastic structures use strain rates which create quasi static deformation. Normal strain rates in literature include 1mm/min [2] [5] [11] [45] [48], 2mm/min [15] [60], or 10mm/min [18] [37]. To investigate the impact of strain rate on the compressive behavior of an auxetic structure, an initial test was performed. Here, a honeycomb re-entrant structure was 3D printed four times, and compressed with two different speeds.

Three observations can be made on the results, seen in Figure 3.6. First, the peak force does not change significantly based on strain rate. Secondly, between 1mm and 6mm, it can be seen that higher strain rates result in a greater resistance against compression. Thirdly, the backstroke shows that the plastic behaves more elastically under higher strain rates, this will result in more energy absorption.

The compressive behaviour between 6mm and 15mm is subject to buckling, which results in more chaotic behaviour. The sample size of this test is not large enough to draw strong conclusions from this part of the experiment. However, higher strain rates seem to be correlated to a lower compressive force.

The same experiment was performed with a ChiralN6 structure. These results were unfortunately not conclusive and were thus left out of the main report. For completeness, the graph of this experiment has been included in Appendix E.

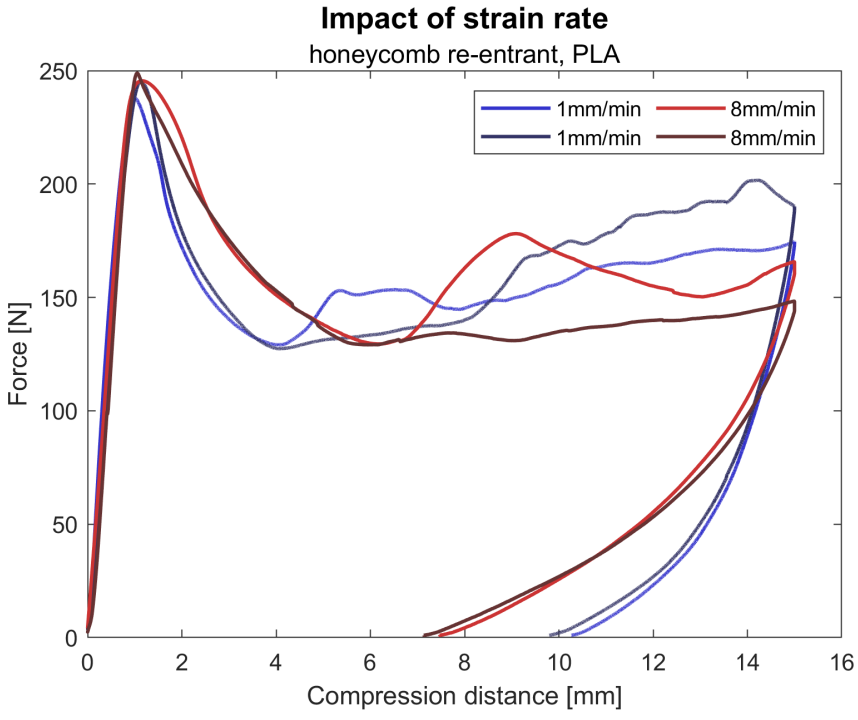

Figure 3.6: Impact of strain rates on a honeycomb re-entrant structure.

3.6 Structure selection

The first experiment will test eight different structures. The shape with the best performing energy absorption properties will be used in further experiments. It is important to limit the

selection, to reduce the scale of the experiment.

There exist a great number of auxetic shapes which can be used to create auxetic sandwich structures. Some have been investigated more than others. The honeycomb re-entrant is likely the most researched shape, where others are merely described in passing mention.

The largest problem with comparing different shapes based on literature, are the many minor variations between papers. Different materials, dimensions, or angles make it difficult to directly compare data points of different structures. Additionally, papers focus on specific areas and do not mention every possible variable. For example, a parameter such as specific energy absorption $[E/mm^3]$, cannot easily be compared if the volume of the tested sample is unknown.

Using a single source as primary way of comparing different shapes would solve this problem. This is why the paper by Elipe and Lantada [10] was used as primary source for structure selection. This paper has performed an extensive FEM study. Twenty-five different 2D auxetic structures were systematically compared based on a large amount of different properties. This research uses the naming conventions of these two studies. Similar structures are also known under different names. For example, the honeycomb re-entrant shape is also known as simply re-entrant.

The second structure selection was made based on the work by Meena and Singamneni [34] [33] [32]. Who designed a chiral based shape which divides stress evenly, with an interesting stress strain curve. Showing more linear incline behaviour compared to the buckling plateau behaviour seen with most other auxetic structures.

3.6.1 Auxetic structure selection

Eight different structures were chosen for experimentation with PLA, these can be seen in Figure 3.7. The dimensions of the repeating shapes have been designed to have a similar height and width of 10mm where possible. These shapes have been arranged in a 5x5 pattern, and use a wall thickness of 0.4mm. All models are 15mm wide. This is small enough that it reduces the printing time of models somewhat, and large enough to prevent buckling during testing. The technical drawings for all shapes can be found in Appendix C. Closeups from the appendix are also placed in Figure 3.8.

The dimensions of the repeating inner shapes has been used as deterministic for the structures dimensions. This has caused a minor difference in total height. Shapes a) and e)-h) are 50mm high, whereas shapes b)-c) are 53mm high. This difference is minor, and still allows for good comparison of results. This research uses the naming conventions of these two studies. Similar structures are also known under different names. For example, the honeycomb re-entrant shape is also known as simply re-entrant.

These structures were selected based on different reasons. The honeycomb re-entrant was selected based on its prevalence in literature. The hybrid S- and Star shape was selected as the best performing structure within one study. The two shapes which make up the hybrid were tested as well. The S-shape showed unique compressive behavior, which was very linear. The other four shapes were selected based on the study by the Elipe and Lantada [10]. Each shape outperformed the other shapes in one catagory. Chiral N6 showed the highest equivalent Young's modulus. Chiral N4 showed the highest area reduction in compression. The lozenge grid square also showed high area reduction. This shape also had connections with other studies on the university and was added as well. The sinusoidal shape was added as the shape with the lowest relative density, combined with a good equivalent Young's modulus.

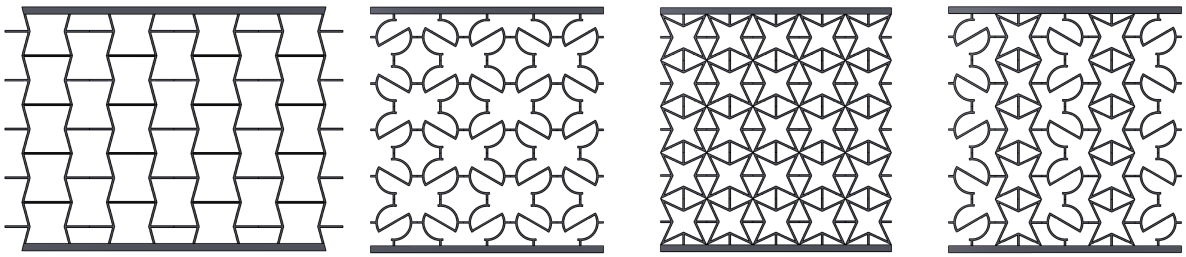

(a) Honeycomb Re-entrant (b) S-Shape (c) Star shape (d) Hybrid S- and Star shape

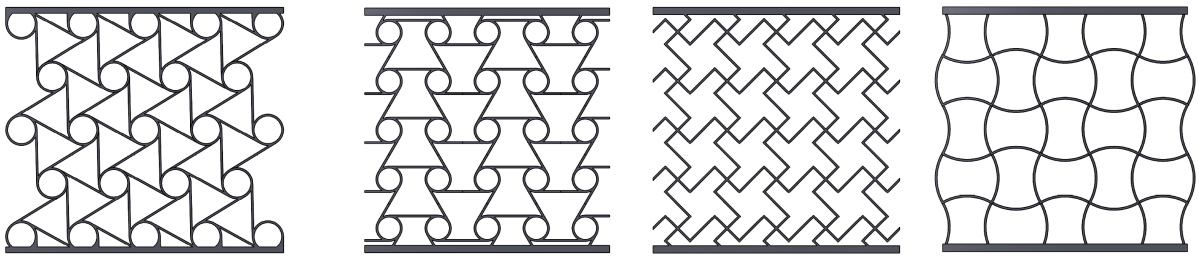

(e) Chiral N6 (f) Chiral N4 (g) Lozenge grid square (h) Sinusoidal

Figure 3.7: Auxetic structures used during experiments

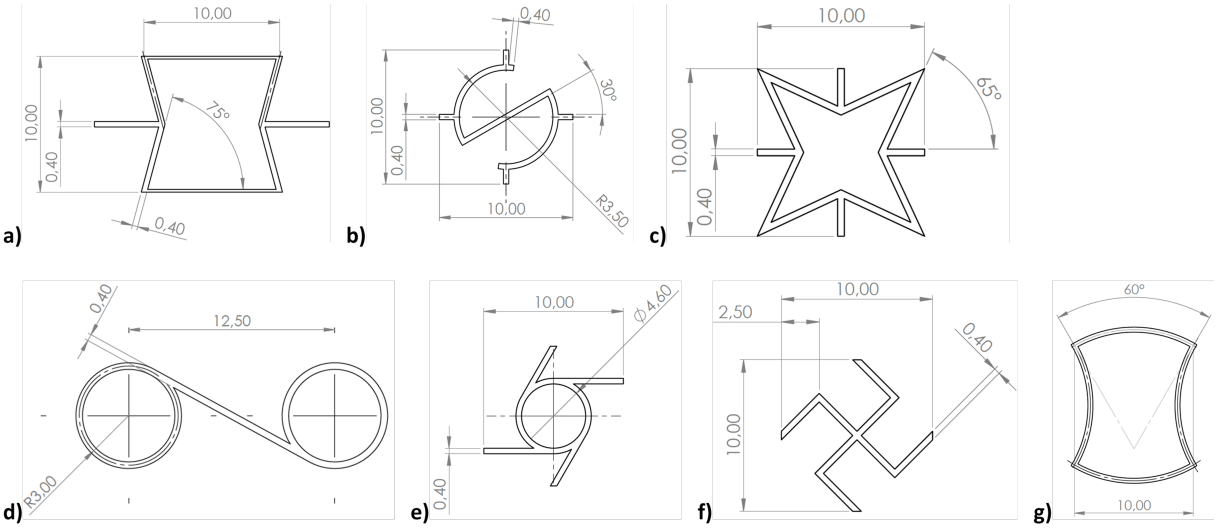

Figure 3.8: Dimensions of the cells which create the eight samples from Figure 3.7.

Honeycomb re-entrant

This shape has been studied the most in literature. For example, the mathematical theoretical Poisson's ratio and effective E-mod for small deformations have been investigated [51]. Failure modes have been investigated [7], and multi-material variations of this shape have also been experimented with [5]. This shape has a high and consistent initial young's modulus. During the plateau stage, the structures strength is slightly lower than the initial peak. This structure has a relatively high E_{eq}, and a decent NPR of -1,68 [10]. An optimal re-entrant angle found by [59] to be an angle of 75 degrees, as this increases the absolute value of the negative Poison's ratio.

S-shape

This chiral based shape has been designed to spread out internal stresses as much as possible. The NPR is relatively high at -2. Furthermore, compression experiments by this study show no signs of buckling with a very linear stress-strain relationship. Which makes for an interesting

comparison.

Star shape
This re-entrant based shape had poor performance according to [10]. A low NPR of -0.6, relatively little area reduction and a relatively low E_{eq}. This shape was selected to provide a point of comparison with other shapes, because it is incorporated within the next structure.

Hybrid star- and S-shape
Elipe and Lantada combined their S-shape variant with the star shape above. Out of four design iterations, this structure showed the best performance. With the highest nominal stress, a relatively high E_{eq}, and a decently long and NPR.

Chiral N6
This circular chiral based pattern has 6 symmetrically placed arm which connect neighbouring cells. Theoretical calculations of the NPR show a value of -1 [42], see Appendix E. Simulations however have shown a value of -0.628, and an average area reduction of 25.82% [10]. However, this shape does outperform others with an E_{eq} of 10.48MPa. Which is why this shape was selected for the first experiment.

Chiral N4
This pattern is also called 'chiral circular symmetric' or 'chiral tetrachiral and antitetrachiral hybrid metastructures' by other literature studies. To better differentiate between this and the previous pattern, the number of connections between cells has been used as main differentiator between the shapes. It showed a decent NPR of -1.18, but has a low E_{eq} of 0.11MPa. The chiral N4 pattern outperformed others in area reduction with 35.31%, which is why this shape was selected. Geometrical variations of this pattern have been studied in a cylindrical application [11].

Lozenge grid square
The mathematical NPR and E_{eq} of the Lozenge grid square have also been studied in literature [51]. This pattern has a high area reduction percentage, similar to the chiral N4 variant. However, both the NPR is closer to zero and the E_{eq} are lower. This shape was selected in part due to its relevance to other projects of the supervisor.

Sinusoidal
This pattern has some similarities to the honeycomb re-entrant, but uses curved walls. These guide the buckling behaviour and helps to divide stresses more evenly over the entire structure. This structure has an average NPR of -0.81, and average E_{eq}. The density of this structure is lower than most. The optimal geometry for this shape has been investigated in literature and found to circle segments with 60 degrees [6].

3.6.2 Determining compression distance

To prepare for the first experiment, it is first necessary to determine the compression distance of each structure. Different patterns will start densification at different lengths, so each patten must have their own setting during compression cycle tests.

To find the general length were densification will start, eight different structures were printed and compressed beyond the densification point. This was achieved by stopping the compression by limiting the maximum force on the loadcell, instead of setting a maximum compression distance. The upper force limit was set high enough to work with the PLA samples. The results of this initial experiment can be seen in Figure 3.9. This is the only compression test which did not use three separate structures and an average value.

Each structure was analysed to find the point of densification. Not every test sample will behave exactly the same. Small deviation during the manufacturing process can result in changes in the buckling behaviour, which results in different densification areas.

The values which were found can be seen in Table 3.4. The compression length used in future tests was set at 90% of the maximum values determined in this experiment.

One result from this initial test has impacted future experiments. The sample based on the Lorense grit square did not perform well during the test. Due to the nature of this shape, shear forces arise when the structure gets compressed. Pushing the top side of the part in the opposite direction of the bottom halve. During the test, the friction forces between the sample and the moving metal plates was not enough to keep the sample form slipping. Causing shape of the structure to change to a parallelogram. For this reason, the lozenge grit square design was not used in further experiments.

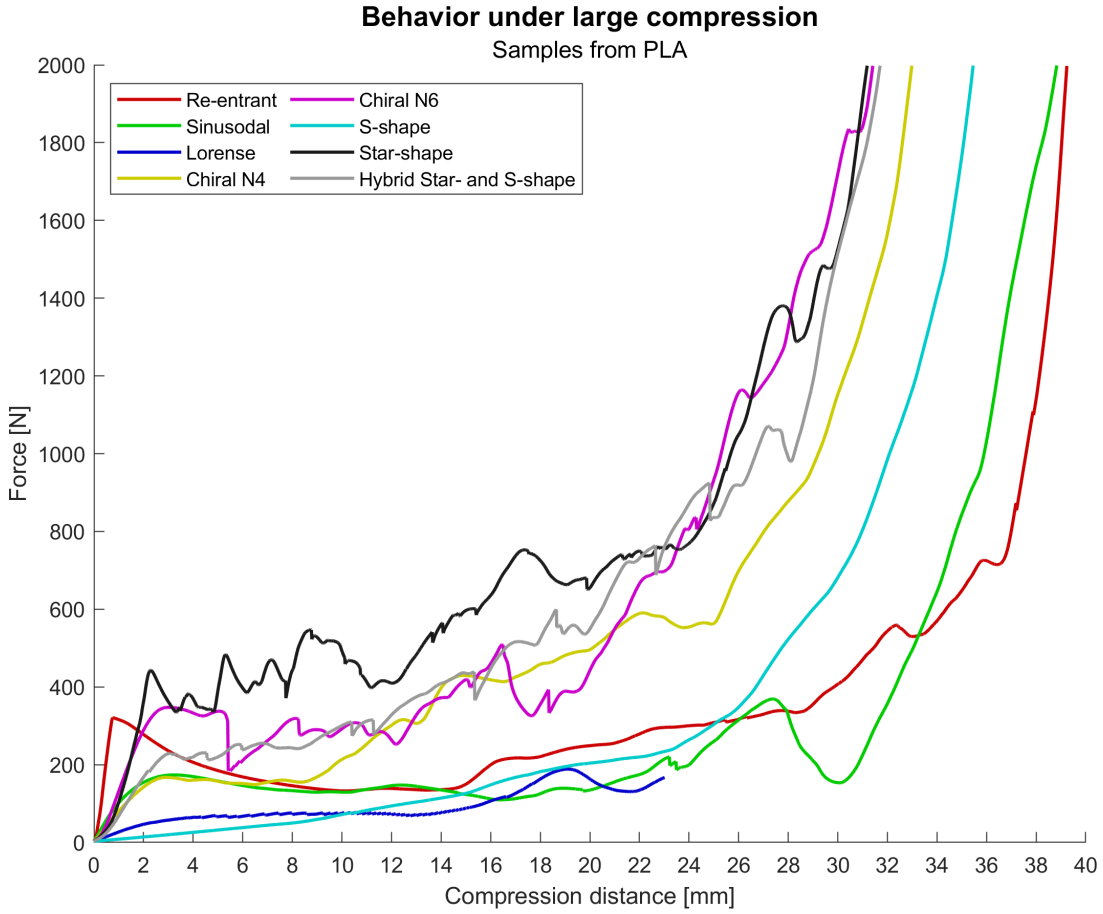

Figure 3.9: Compression tests, preformed to find an optimal compression distance

Shape	Point of densification [mm]	Compression distance with 10% margin [mm]
Honeycomb Re-entrant	28,5	25,65
S-Shape	23,4	21,06
Star shape	23,7	21,33
Hybrid S- and Star shape	19,8	17,82
Chiral N6	19,4	17,46
Chiral N4	13,0	11,7
Lozenge grid square	-	-
Sinusoidal	27,5	24,75

Table 3.4: Points of densification, with corresponding distances used for later experiments

Chapter 4

Results and Discussion

This project aims to create several multi-material auxetic sandwich structures which exhibit a different response when compressed. For this purpose, first a suitable structure must be found. From literature a list of eight different structures will be selected. They will be 3D printed in PLA and tested. Based on these test, one structure will be selected to continue this research with.

Secondly, at least one hard and one soft material are required to create multi-material structures. Therefore, two hard and two soft plastics will be used to create parts in the shape which was selected during the structure selection. All samples will be tested in the same manner and results will be compared to find the most optimal materials for multi-material designs.

Finally, the chosen shape can be combined with the two different materials to create multi-material structures. Combining two different materials together in the same printed part is challenging. The iterative design process will be highlighted. Then the results from the multi-material structures will be analysed and presented.

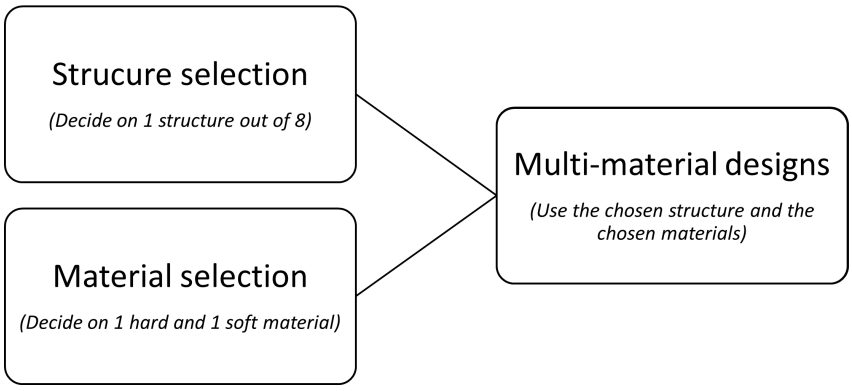

Figure 4.1: The structure of the experiments conducted in this thesis.

4.1 Structure selection

All force strain diagrams of the successful experiments of the first phase can be found in Figure 4.2. Thereafter, the energy absorption properties and elasticity of the experiments are shown in Figure 4.3. Red lines were used for the compressive behaviour and blue lines for the relaxation. Dark red lines correspond with dark blue lines, and vise-versa for light colored lines.

The honeycomb re-entrant samples that were tested showed a different compression and buckling behaviour compared to the previous samples which were used for the strain rate experiment. Material folded towards the side instead of folding inwards. The same model was used,

both in PLA with similar slicer settings. The reasons for this difference in behaviour is unclear.

The S-shape shows a steady increase in stress as strain increases, which mimics the behaviour shown by the designer. This behaviour is very distinct compared to other structures. Basic force-strain tests cannot easily be used to determine the locations of the elastic stage and the plateau stage. Almost no buckling behaviour is present and results are very consistent. Lastly, the structure can be compressed relatively far, and has good energy absorption properties.

The star-shape showed among the highest stress levels before densification. There was strong buckling behaviour present. This was amplified by dimples, creating rough walls which can hold the star point during compression. When a threshold is met, these parts can shoot loose, creating a sharp sudden drop in stress. This experiment failed to show clear auxetic behaviour, material had a tendency to flow sideways instead of folding inwards.

The hybrid S- and star-shape functioned differently then either shape separately. The guidance of the S-shape caused the star-shapes to fold properly, and auxetic behaviour was observed. However, this folding behaviour remained a bit inconsistent. The same final stress levels are reached as with the star-shape. Which is the highest out of all tests. The same jerk-like behaviour due to wall bumps can be observed, although it is less prominent.

The chiral N6 shape showed strong buckling behaviour. Additionally, the shape does not appear to rotate smoothly. Some beams connecting cylinders together buckled at two different locations within the same beam. This shows that the rotational behaviour did not work properly within this shape.

The chiral N4 shape shows a low, but steady plateau stage with minimal buckling behaviour. The shape behaves predictable and consistently. This shape is the second best performer with energy absorption.

The sinusoidal shape has a decreased plateau stage, compared to the elastic stage, similar to the honeycomb re-entrant. Spikes in stress correspond to moments where the walls fold inwards and make contact with each other. All three sinusoidal structures deformed asymmetrical. One side experienced more permanent deformation, where the other side was far more flexible. The reason for this uncertain.

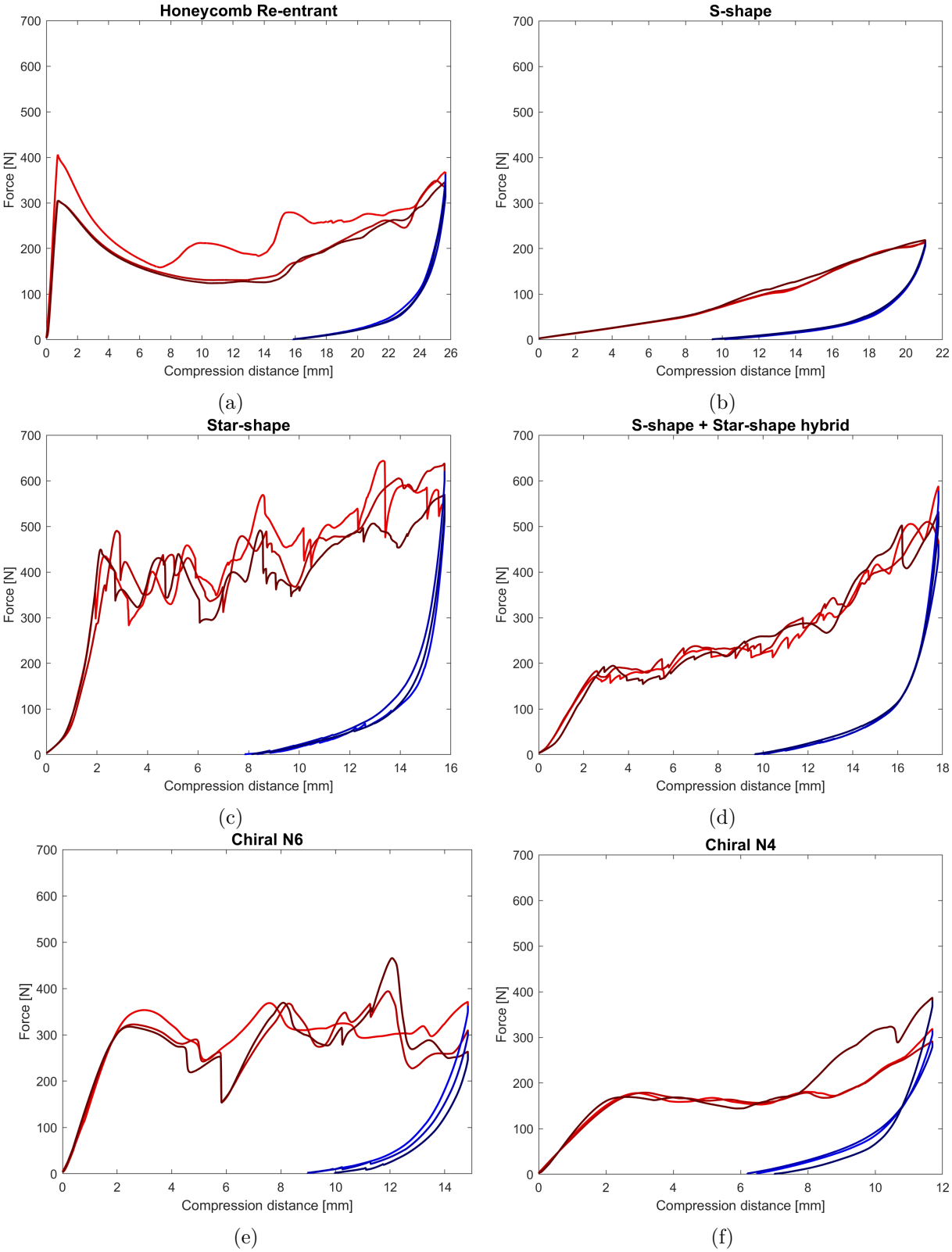

Figure 4.2: Force strain diagrams for different structure shapes

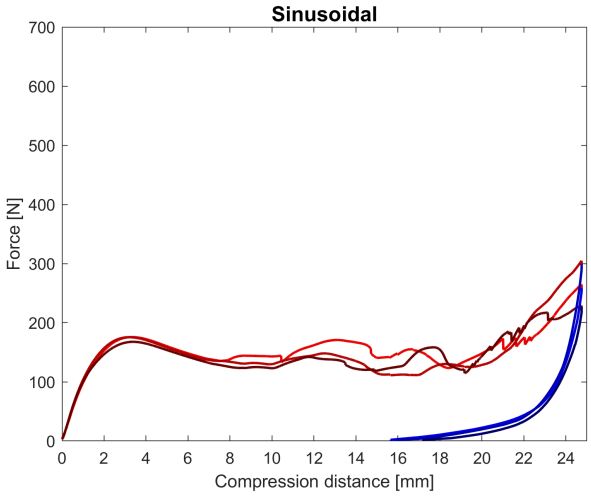

(g)

Figure 4.2: Force strain diagrams for different structure shapes

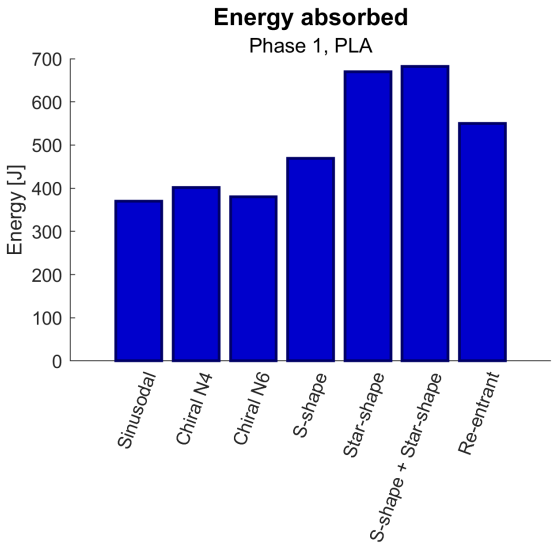

(a)

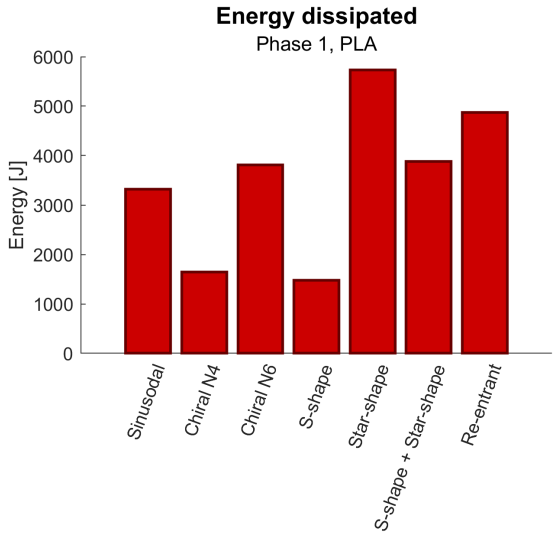

(b)

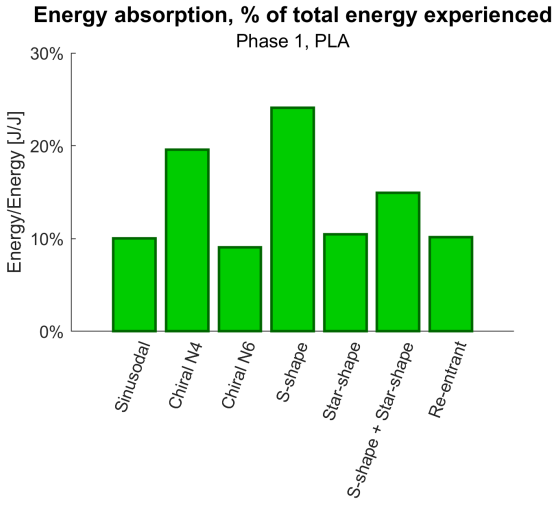

(c)

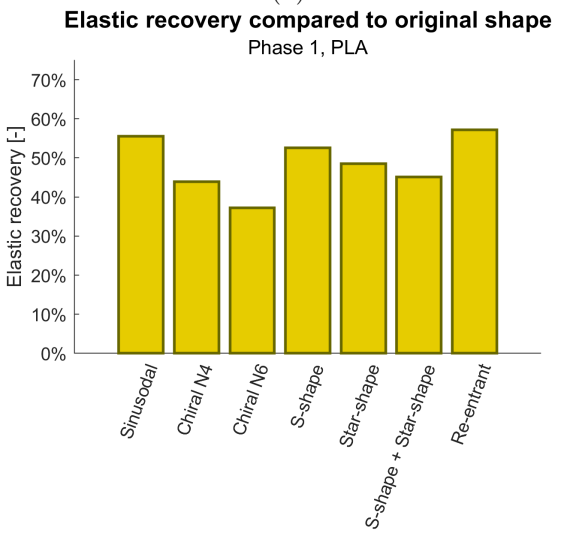

(d)

Figure 4.3: Results from phase 1, design selection

4.1.1 Conclusion on structure selection

In order to select a design to continue this research with, the focus was placed on energy absorption. Which is characterized by the energy absorption as a percentage of the total energy experienced. These results can be seen in Figure 4.3c. Based on this criteria, the S-shape variant performed the best out of all shapes. This structure was also very consistent and showed close to no buckling behaviour, see Figure 4.4. On closer inspection, it was found that this shape is more suited for mono-material design and not for multi-material design. There is no clear location for a cut where one polymer would transition to another. The beams which connect the circular areas together are too small. Lacking the space for strong end-to-end connections between different polymers. The S-shape itself is critical to the functioning of the structure, and must remain stiff enough to perform the rotational motion. Which is why this shape has not been selected for continued research. These issues became apparent after the experiment, otherwise different structures would have been selected.

The second best performing shape is the Chiral N4 shape. This design does lend itself to multi-material design. Furthermore, relatively little research has been performed on this exact shape. Continuing with the chiral N4 variant will add to the relevance of this research, and will therefore be used to continue this thesis.

Experiments showed good repeatability between experiments of the same structures. The three lines in each graph represent the three experiments performed for each shape. For example, peak values of stresses are often at similair strain values, but not always. These discrepancies are likely due to minor differences which arise in the manufacturing process. Samples of the same structure also show the same general behaviour, such as the rising equivalent Young's modulus within Figure 4.2d.

There were differences in elastic recovery between shapes, with a maximum of 57% for the honeycomb re-entrant and a maximum of 37% for the Chiral N6. There appears to be no correlation between elastic recovery and the energy absorption performance of the different structures. There is also no direct correlation between the compression distances and other results.

Some interesting patterns can be seen when comparing the structures ChiralN4 and sinusoidal. Both structures experienced a roughly equal force during the plateau stage of approximately 160N. However, the sinusoidal structure was compressed twice as far as the ChiralN4 samples, 24mm versus 12. This was done because the structures experience densification at different moments. This difference meant that the sinusoidal structure dissipated twice as much energy. In the relaxation part of the experiment, both structures performed very similairly. Absorbing 370 J and 401 J, for sinusoidal and ChiralN4 respectively. Therefore, when the energy absorption as a percentage of the total energy experienced was calculated, the ChiralN4 outperformed the sinusoidal with 19,6% over 10,0%.

This would change if shapes were not compressed until a point just before densification. If both shapes were to be compressed to 10mm, or 80% of their original length, both structures could perform near identical. Applications outside of academic studies set different use cases and requirements to products. For this study, the aforementioned energy absorption, combined with a compression until the point of densification were used for comparisons. In practice, the most optimal structure will differ based on application.

4.1.2 Discussion on structure selection

Four models gave unexpected results during the experiment, as illustrated in Figure 4.4.

The re-entrant models all showed a failure mode where material was pushed to one side, see Figure 4.4b and Figure 4.4c. This asymmetric deformation did not occur with the previous test in section 3.5, where an identical model with black coloured PLA of the same brand was used,

see figure Figure 4.4g. The cause for this change in results is unclear and would require further investigation. The impact of material thickness on the failure modes of honeycomb re-entrant structures was shown to be of importance [7]. It is possible that, as two different PLA colours were used, one material had aged more. Which could change the mechanical properties of the material, weakening the structure and leading to different failure modes.

The lozenge grid square model showed a sliding motion during compression, see Figure 4.4d. The behaviour could have been prevented by increasing the friction between the PLA structure and the metal plates. This realization came after the experiment had been completed, and further research was not conducted on this pattern.

The chiralN6 pattern showed heavy buckling behaviour of the beams which connect the cylinders together, see figure Figure 4.4e. This is unexpected, as the auxetic behaviour should stem from rotational behaviour. The cylinders were expected to wind the beams around themselves. Thereby pulling material inwards. This happened to some degree, but not as much as was expected. This means that geometrical dimensions of this shape were likely not optimal. Further research requires a closer investigation of the optimal cylinder radius and beam lengths.

Sinusoidal deformation was asymmetrical, see figure Figure 4.4f. The reason for the asymmetrical deformation within the sinusoidal shape is unknown. one reason why might be due to manufacturing errors during printing. Later experiments when printing flexible materials found that the printers had a tendency to extrude more material on the left side of the model. This might have had some impact here, but all eight models were printed simultaneously. There is no sign of this problem affecting the other structures. Which makes this explanation inconclusive.

During preparations, it was found that PLA can be compressed and used for testing. However, the material remains brittle. If the brittle nature becomes a problem, some steps could be taken. Selecting structures which distribute stresses and prevent high stress concentrations are beneficial to PLA. Alternatively, a lower compression speed could be used or the environment could be heated.

The print settings were not optimal. Stringing and little blobs of plastic were left on the models after printing. Further experiments will have a greater focus on optimizing the printing parameters before a model will be used for experiments. Stringing has no direct impact on the compressive behavior of samples. Little blobs can however introduce some stuttering effects. These are minor and did not impact the overall performance of the samples.

Lastly, The shape of the honeycomb re-entrant was incorrect. A 5x6 shape was created instead of a 5x5 shape, more similar to the sinusoidal shape. The project will not continue with the re-entrant shape, but this does make the direct comparison between results slightly less optimal.

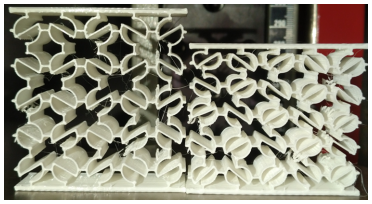

(a) Start and final position s-shape

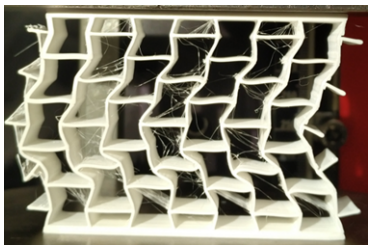

(b) Failure mode honeycomb re-entrant

(c) Failure mode honeycomb re-entrant

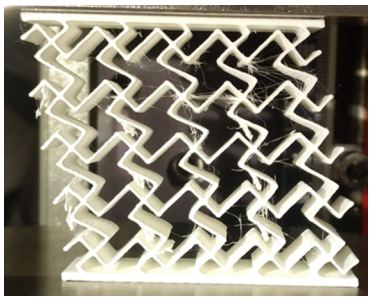

(d) Sliding of lozenge square grit

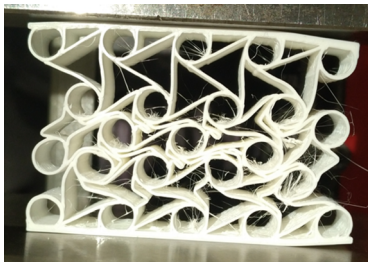

(e) buckling behavior of chiralN6

(f) Elastic left side after compression sinusoidal

(g) Failure mode re-entrant from strain rate experiment in section 3.5

Figure 4.4: Results from phase 1, design selection

4.2 Material selection

In the previous section, the ChiralN4 structure was selected for its energy absorption properties and multi-material design possibilities. In this chapter, the polymers for multi-material designs in the upcoming chapter will be selected. For this purpose, four materials will be investigated. Two hard materials and two flexible materials. The same shape which was chosen in the previous section will be used to create samples from the chosen materials. The samples will be tested, and the results will be analyzed. Finally, two materials will be selected to be used in the last experiments of this project.

4.2.1 Results of material selection

Figure 4.5 shows that PLA, C8 and PCL have the same phases of plastic deformation and plateau stage. The location where the plateau state starts differs for each material. Where C8 starts at around 1,8mm, PLA at 2,5mm and PLC much later at approximately 4mm.

PLA starts to show signs of densification near the end of the compression, whereas C8 and PCL do not appear to have reached this stage by this point. This is not necessarily a negative result. As densification occurs when the cylinders are being crushed and flattened. Which should be avoided.

PLA experiences higher stresses than C8 and has better energy absorption properties than C8. PLA and C8 are reported to have a similar Young's modulus. This result shows that the compressive behaviour of the structure is determined by more than just the Youngs modulus.

TPC experienced the lowest maximum stress. This was expected, as this is the most flexible material.

PLA showed the largest difference between samples. The samples made from PLA experienced an issue during experimentation, causing one sample to become unusable. To compensate for this, a third sample was created separately from the first batch. This sample was the light red line in Figure 4.2f, and showed behaviour that is slightly dissimilar compared to the other two samples. This could be caused by minor differences during the printing process, as the same model, slicing parameters, machine and filament source were used. All other materials showed good consistency within the same batch.

The TPC samples were also compressed to 25mm, this was done to showcase the elasticity of the material. These results can be found in Appendix G.

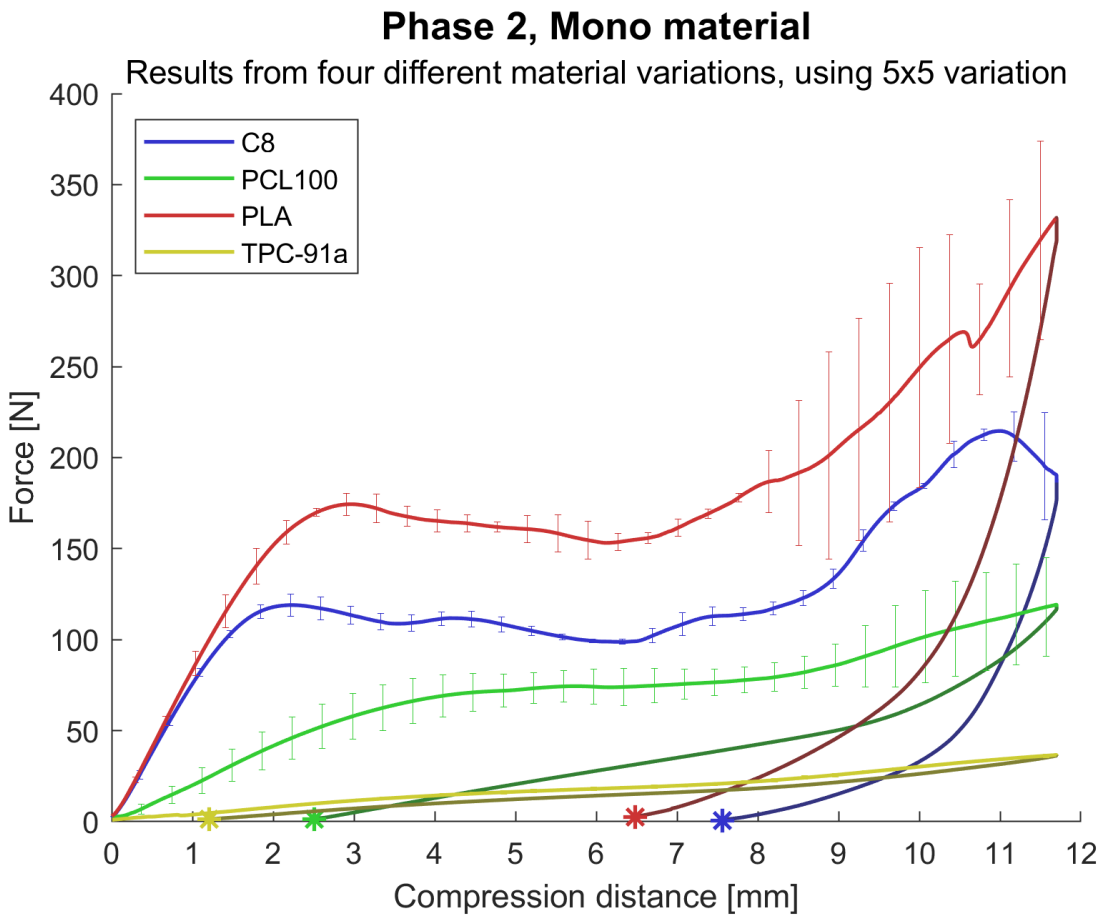

Figure 4.5: Force strain diagram for mono-material compression tests.

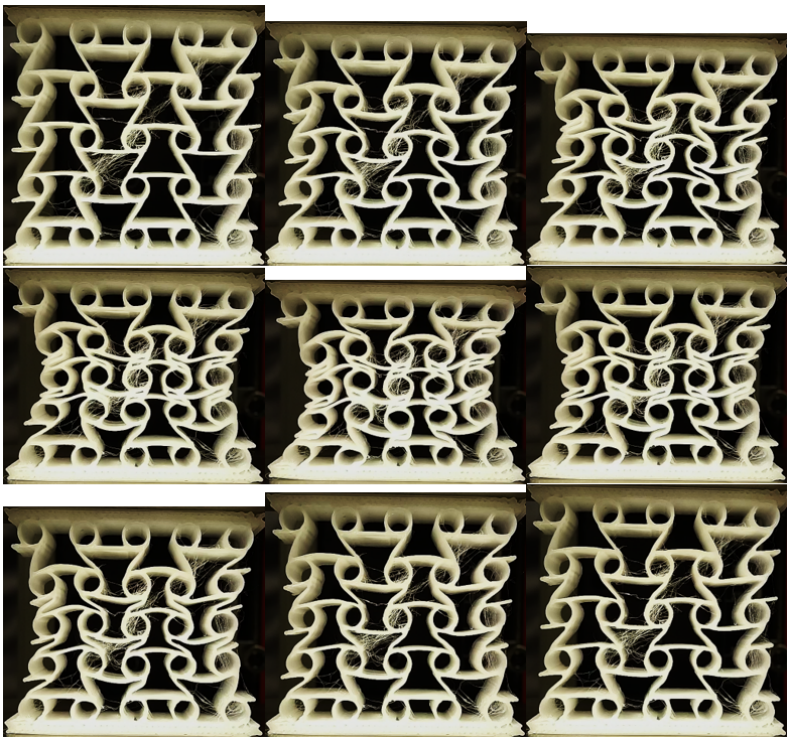

Figure 4.6: Compression test of TPC-91a, pictures taken with an 20 seconds interval.

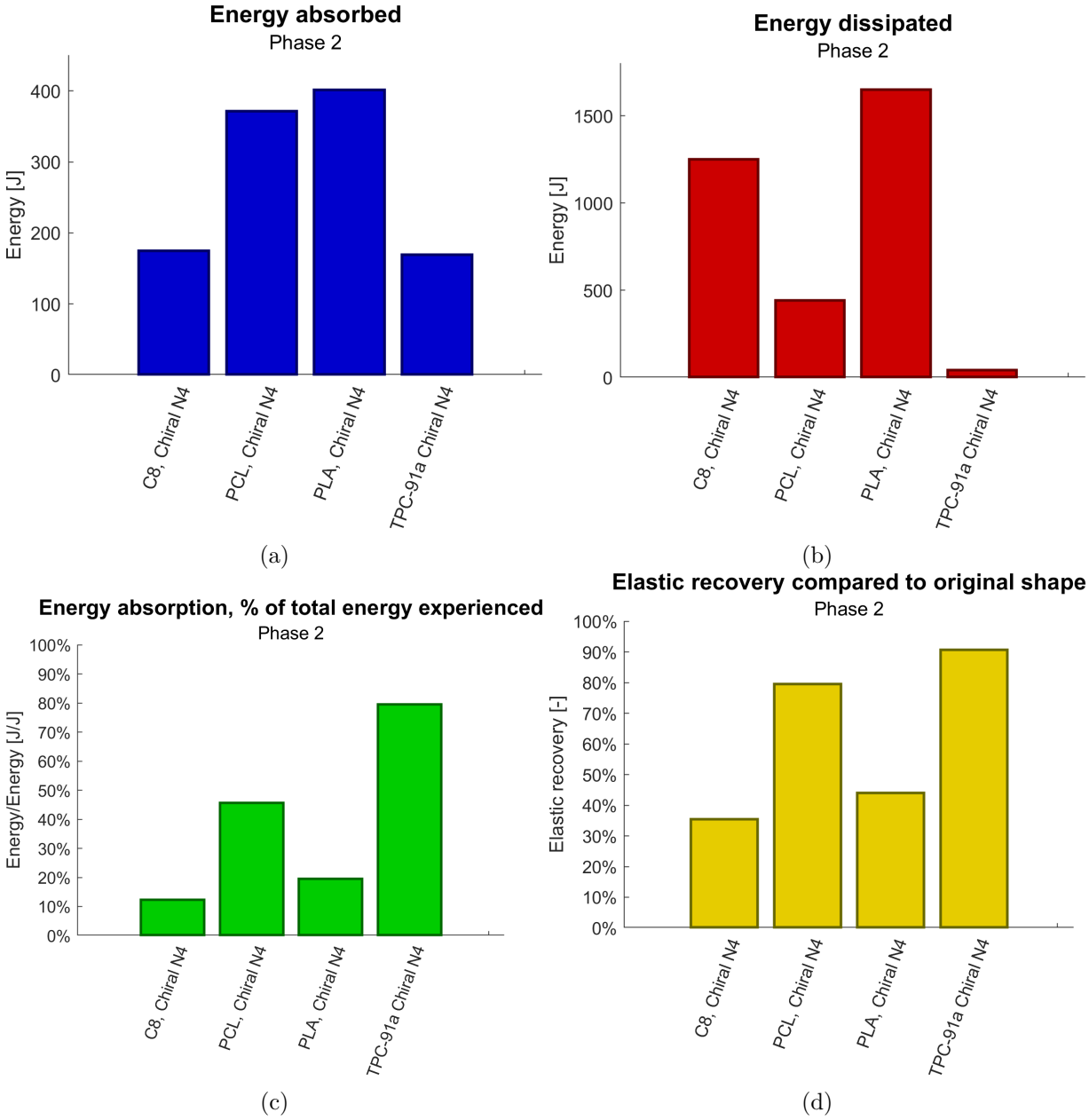

Figure 4.7: Results from phase 2, material selection

4.2.2 Conclusion on material selection

TPC was the material with the greatest energy absorption properties, with 79,5%, as shown in Figure 4.7c. With PCL performing second best, with 45,6%. Of the hard materials, PLA showed better energy absorption then C8. Absorbing 19,6% and 12,3% of the total energy dissipated respectively.

Therefore, PLA and TPC were selected for initial experimentations in multi-material design. Unfortunately, it was found that PLA and TPC do not adhere well to each other, early in the design process. As this is a critical function of the two materials, TPC was changed for PCL. PLA and PCL do adhere well to each other.

In practice, the model made from TPC recovered more than 90% of its original length. However, the testing machine was not sensitive enough to properly detect this part. A different machine might be required if more tests with this material will be conducted.

4.3 Multi-material structures

In the previous two sections, experiments were performed to find an auxetic shape and material with the best energy absorption properties suited for multi-material designs. In this chapter, these two results will be combined. First, some highlights of the design iteration process will be mentioned. Then all lessons which have been learned so far will be combined to create four multi-material designs. Selectively applying hard and soft polymers to create structures with distinct compressive behaviours from one another. Finally, the results of this experiment will be analyzed and discussed.

4.3.1 Multi-material design iteration

The previous experiment concluded that TPC showed better energy absorption behaviour over PCL. Therefore, some models were created with TPC and PLA to examine their feasibility. After it became clear that TPC did not bond well enough with PLA, PCL was used for all models. Next, some of the most important design iterations which improved the overall quality of the structures will be mentioned. Before the final multi-material designs will be presented.

Many steps were taken in the iterative design process before the final models were ready for experiments. TPC was selected as the best performing soft polymer, but showed poor adhesion with PLA. PCL performed better, but brought with it their own challenges to overcome. Several steps were required to find settings which provided good adhesion between polymers. Eventually, a method was found which provided good models without failure during compression and multi material designs could be made.

Adhesion tests with TPC

As mentioned in subsection 4.2.2, TPC and PLA were the first materials which were used for the multi-material design process. To gain an understanding of the strength of the bond between two materials, the test model of Figure 4.8a was created. This model allows tests of the strength of the most critical bond where two beams are joined end to end. Furthermore, it also tests the effectiveness of a serrated profile.

The serrated profile has proven to be an effective method of increasing the adhesion between two materials for this type of end-to-end joint. Initial tests with TPC were promising. Therefore, the two models as seen in Figure 4.8b and Figure 4.8c were created and printed with PLA and TPC. The adhesion which appeared to be present in the first test block, was not present in the auxetic structure. Small pushes were enough to separate the two materials. Models simmilair to Figure 4.8 using the serrated wall technique were created, and used for a compression test. These results showed that TPC was to flexible, as seen in Figure 4.9. The PLA could did not deform, there were no chiral motions, which meant that no auxetic behaviour was present. Furthermore, after this test, the sample was examined and showed structural failure. The two plastics were not bonded correctly and broke loose from each other. At this point, it was decided to use PCL instead for further testing.

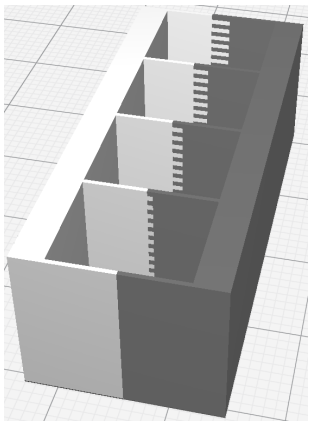

(a) Model for testing adhesion between two materials. The overlap between materials ranged between 0mm and 2mm, and was set at 2 layerheights high.

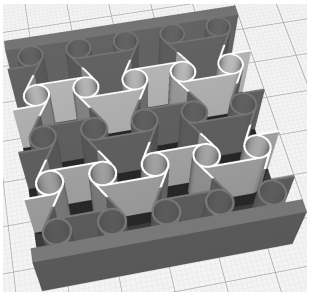

(b) Constant wall thickness, no serrated profile, TPC and PLA

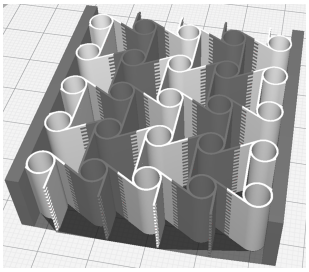

(c) Serrated profile for better adhesion between materials.

Figure 4.8: 3D prints with PLA and TPC.

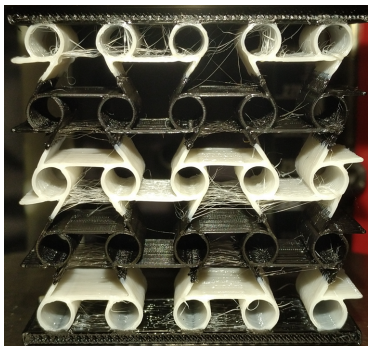

(a)

(b)

(c)

Figure 4.9: 3D prints with PLA and TPC. The TPC deformed under compression, but the PLA did not.

Multi material design iterations

The design process started with the same model as shown in Figure 4.9b, but using PCL instead of TPC. After some attempts at finding the optimal printing parameters, a different problem arose. This issue is highlighted in Figure 4.10.

This issue was caused by a combination of the PCL properties, and the nozzle toolpath. PCL has a low melting temperature, which means that the material needs a long time period to cool down. Cura has limited options for controlling the nozzle toolpath. The thin walls of this model caused the nozzle to re-trace the same lines. First placing a layer of PCL from a cylinder towards the black PLA parts, then following the same line back towards the PCL cylinder. This motion dragged the un-solidified PCL back to the cylinder, ruining the part.

Cura unfortunately does not provide enough options to change this tool pathing behaviour. Therefore, solutions with other methods were investigated.

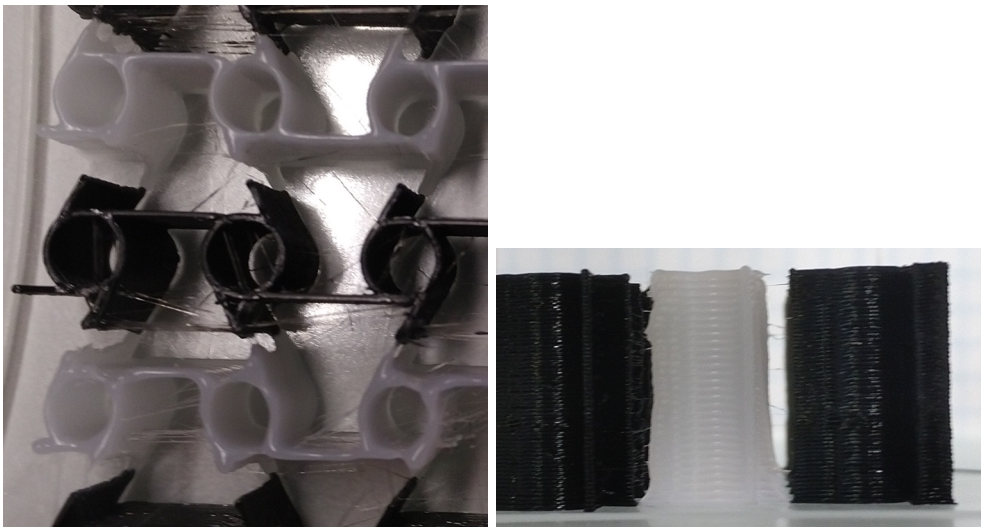

(a) Top down view. (b) sideways view.

Figure 4.10: The PLA and PCL parts were supposed to be connected and bonded together. This issue was created by toolpathing problems.

These solutions allowed the structure to be printed and to be strong enough for good experiments. Which is where a second problem forced a redesign. The PCL cylinders would deform and be crushed, before the PLA segments would properly rotate. This can be seen in Appendix H This caused these structures to fail under compression. The first attempt to prevent this behaviour from occurring was made by increasing the wall thickness of the cylinders, but leaving the connections between cylinders at a lower wall thickness. This did fix the problem. The results from this experiment can be seen in Appendix G, Figure H.10.

Next, a model was made where the cylinders were made from PLA, and the walls connecting them from PCL. See Figure 4.11a. This design was in part based on research by Wang [56] where flexible material was used in highly localized areas. This sample failed, because the attachment point between to two materials acted as loose hinges. The model could not provide the same amount of resistance and resilience as the previous models.

Models made from TPC failed, as cylinders buckled before they could rotate. This gave the idea that cylinders made from soft materials would need to be strengthened. This in order to not deform before the PLA could start the chiral motions. The design seen in Figure 4.11b was created. This model uses PLA top and bottom plates, an internal shell made from PCL, and PLA reinforcements with the PCL cylinders. This model could be printed and compressed without problems.

From initial experimental results, it was apparent that this model had less energy absorption properties than the 100% PCL model from phase 2. This is likely due to the inner PLA cylinders, that are less elastic and prohibit the cylinders from absorbing energy. At this time, another method for increasing energy absorption was investigated. Reducing the density within the sandwich structure can be beneficial to the energy absorption properties.

To test this, three new models were created. All three models have identical outer dimensions of 50x50x15mm, with the same cylinder radius as before. But the number of cylinders has been varied, thus changing the inner density of the structures. See Figure 4.11d, Figure 4.11e, and Figure 4.11f. This change required another design improvement, as seen in figure Figure 4.11c. When the PCL cylinders were imbedded within PLA plates, they adhere well. But in order to attach PCL beams in a near 90 degree angle to PLA plates, anchors were required. At this same time, a chamfer was added to the top and bottom plates. This prevent an elephant foot form forming, which could cause minor asymmetric pushing during the compression tests. The results of this experiment can be seen in Appendix I. A lower structure density results in better energy

absorption properties. It also allows for the structure to be compressed further, and results in greater elastic behaviour. After thirty iterations, the final designs were created.

The final multi-material designs will utilize a 4x4 chiral N4 structure shape. This increases the energy absorption properties, while still allowing for enough material to create multi-material designs. The outer dimensions of the structure were not enlarged. This could be done to increase the number of nodes, while keeping the same structure density. However, by keeping the same outer dimensions, the end results can be better compared with results of previous experiments.

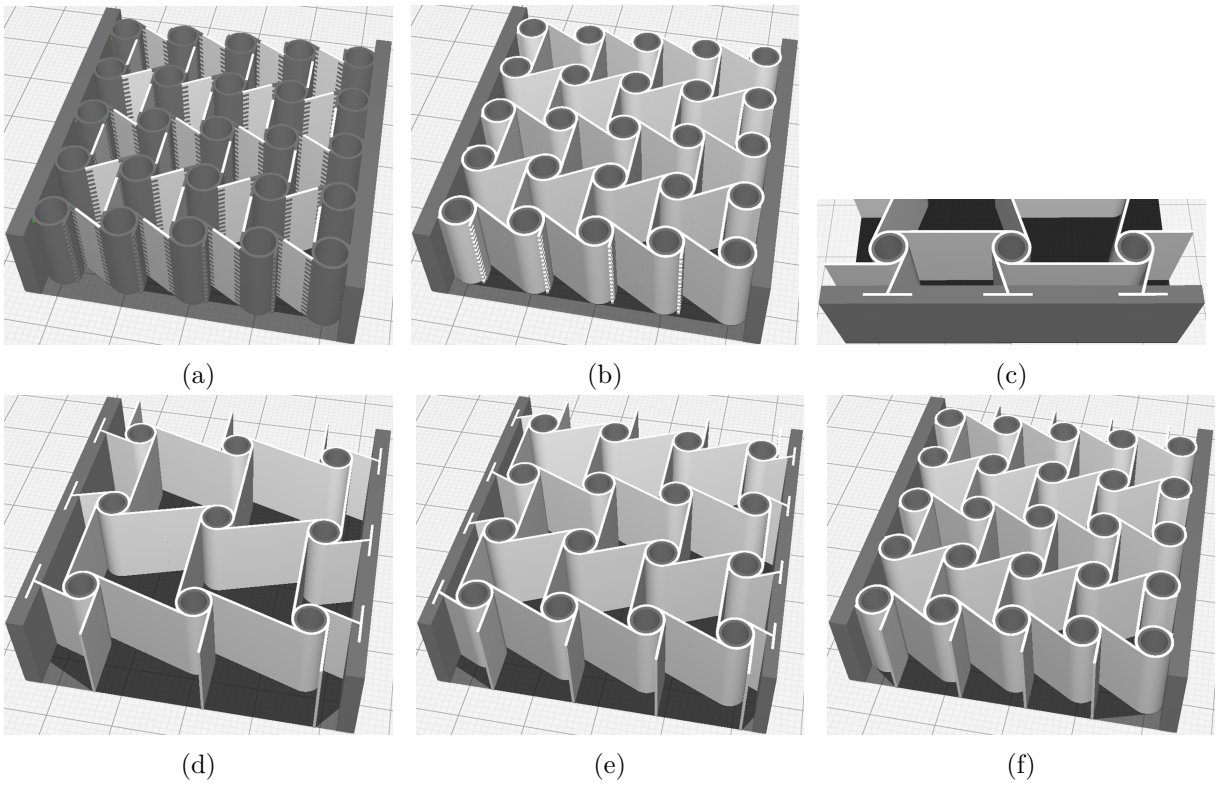

Figure 4.11: Design iteration highlights. a) PCL beams combined with PLA cylinders. b) PCL beams combined with PLA inner cylinders. c) Anchors used to improve the connection between PCL beams and PLA plates. d) A structure with 3x3 cells. e) A structure with 4x4 cells. f) A structure with 5x5 cells, structures d,e,and f all have the same 50x50mm surface area as other samples.

Chosen multi-material design variations

Out of many possible ways to divide the Chiral N4 structure with the selected materials, four designs were selected. Two methods were used to transition from PLA in black and PCL in white. First is an end-to-end transition which uses a serrated profile. The second method uses the PLA inner cylinders to connect half a cylinder of one material to half a cylinder of the other material. The four chosen design variations can be seen in Figure 4.12. First alternating layers HSH (black, white, black - Hard, Soft, Hard), the inverse SHS, Soft material on the outside of the structure (SOU), and a diagonal cut (DIA). These designs were chosen in consultation with the supervisor. The main criteria for these designs was a high likelihood of showing significant different and unique behaviour in force-displacement plot.

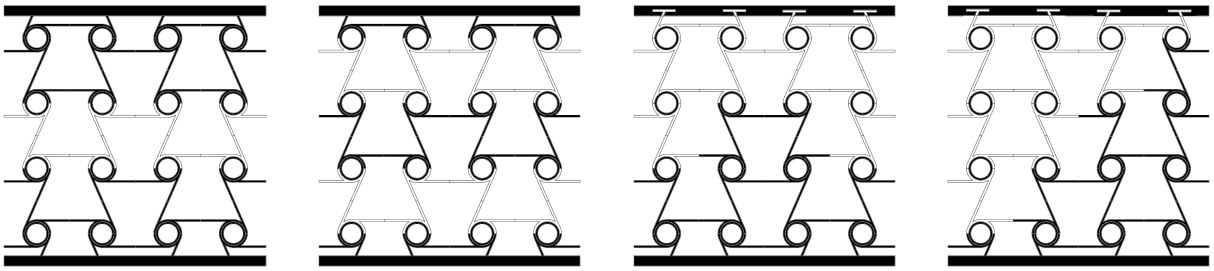

(a) HSH (b) SHS (c) FOU (d) DIA

Figure 4.12: The four multi-material designs, PLA in black and PCL in white.

4.3.2 Results of multi-material experiments

The results of the multi-material experiments can be seen in Figure 4.13 and Figure 4.14. The compression behaviour of all four structures can be seen in Figure 4.15, with an enlarged version in Appendix J. Pictures were taken at the start, midpoint, end, and the moments in between.

All samples have a roughly equal behaviour for the first 7mm. This is where all samples have at least one layer of PCL which experiences deformation before the PLA. The difference between the two top lines and two bottom lines in the first 7mm is likely due to where this PCL layer is located. Two samples have a PCL layer which connects directly to the top plates. This increases the flexibility of the upper row of cylinders. As the overall flexibility increases, the force required to deform a structure goes down.

Between approximately 7mm and 12mm, the second layer is compressed. Layers which require more of the hard PLA to be deformed show higher stress levels. Ending with the SHS sample, which shows similar stress levels as in the previous plateau as a second layer of PCL is compressed. The diagonal variant does show a step-wise rise in stress levels, but not as significant as expected. This is likely because the structure has a tendency to first deform the PCL, before the PLA. Once all available PCL has been deformed, the PLA starts to deform.

Between approximately 12mm and 16mm, behaviours differ per structure. A third layer can be compressed, or a gradual transition towards densification can start. Beyond 17mm, all structures have started the densification phase. This part can be located due to a sharp incline in the force strain plot, and larger error bars in the plot. As the exact distance at which densification starts can be influenced by minor differences.

The HSH and SHS variants have a near identical behaviour for the first 7mm of compression. In this phase, PCL is the main component which gets deformed. Some PLA is still deformed. The chiral motions causes some auxetic behaviour, which does deform the PLA, see Figure 4.15a-2.

At 7mm, all vertically placed PCL has been deformed. Between 7mm and 12mm, PLA and the horizontally placed PCL deform. This means that the ChiralN4 structure cannot first deform all of it's soft material, before deforming all hard material. Some transitional behaviour takes place.

Between 12mm and 16mm the third layer is deformed. The second and third layers have a tendency to deform together. This deformation pattern seeks the path of least resistance. First causing rotational behaviour in the eight middle cylinders. Before deforming the outer eight cylinders which are attached to the top and bottom plates. These attachments are relatively small, which lowers the available leverage, which increases the forces needed to deform the outer cylinders.

The SHS variant Shows the lowest forces of all variants. This was expected, as this model has two full layers of PCL. In contrast with the other variants, the SHS samples does not fold neatly inwards. This can be seen in Figure 4.15b. This is not beneficial for the auxetic behaviour. It

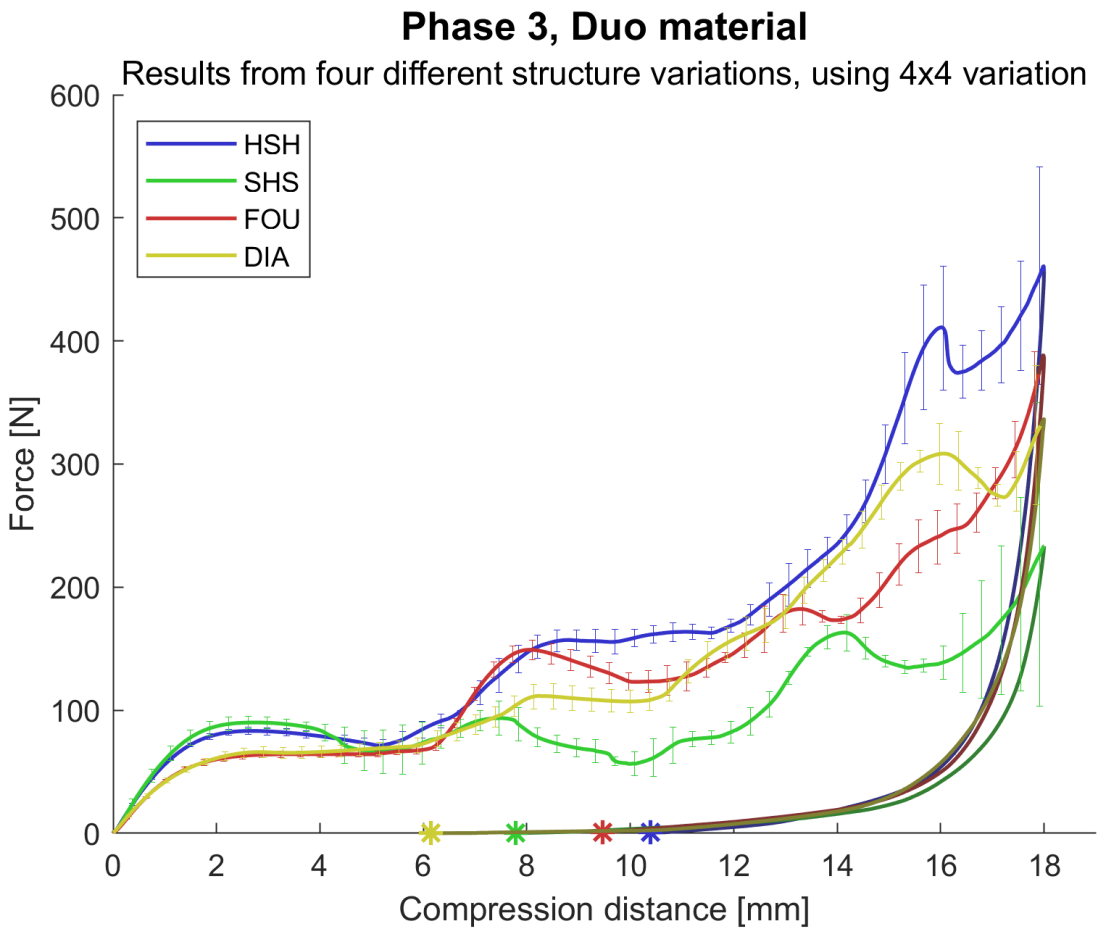

Figure 4.13: Force strain diagram for multi-material compression tests.

causes beams to buckle and fold inwards instead of bending around a cylinder. Because of this, the rotational behaviour was much more prominent within the HSH structure.

When the lower left PCL beam was the first to give way, the cylinder above this beam started to rotate before the others. This in combination with the lack of rotation within the upper left cylinder, caused one cylinder to be pushed slightly to the left, instead of being rotated. Once a critical distance was reached, further compressive forces were directed to push this cylinder further to the left. This behaviour could likely also be prevented if the structure continued further to the left.

This cylinder was pushed outwards in two out of three experiments. If the bottom left PCL beam deforms slightly later, the compressive behaviour of the structure changes. Leaving the cylinder inside the structure, instead of pushing it outwards. The case where all cylinders contract to the middle leads to better auxetic behaviour. This alternative behaviour can be seen in Figure 4.16. Larger structures with more cells to the left and right could compensate for this behaviour, removing the issue.

The deformation behavior of the structure with a diagonal transition between the two materials can be seen in Figure 4.15b. This shows that PCL areas deform before areas made from PLA. Leading to a diagonal area where initial failure mode takes place.

Figure 4.15b-5 shows the structure after the load has been removed. This shows that the left side was much more elastic, compared to the right half. This was expected, as the flexible PCL is concentrated on this side of the structure.

The central beam, made from half PCL and half PLA deformed in a V-shape. This is undesired behaviour. Beams which are placed under compression should cause a rotational behaviour

in the cylinders they are attached to. This does not happen if they can deform easily. This result shows that the PCL and PLA end-to-end connections were not strong enough. Another point to mention is the permanency of this deformation. This end-to-end transition acts like a hinge, with limited strength and elasticity.

Initial deformation within the flexible outside variant takes place in stages, see Figure 4.15d. First four vertical PCL beams deform, see Figure 4.15d2. Thereafter, Figure 4.15d4 shows that two more PCL beams have deformed in combination with a more gradual deformation of the PLA part. The same V-shaped deformation of beams with a multi-material end-to-end connection appear. These connections are a structural weak point and limit the overall auxetic behaviour of the structure.

Lastly, Figure 4.15d8 shows that the upper PCL half is more elastic than the lower PLA half.

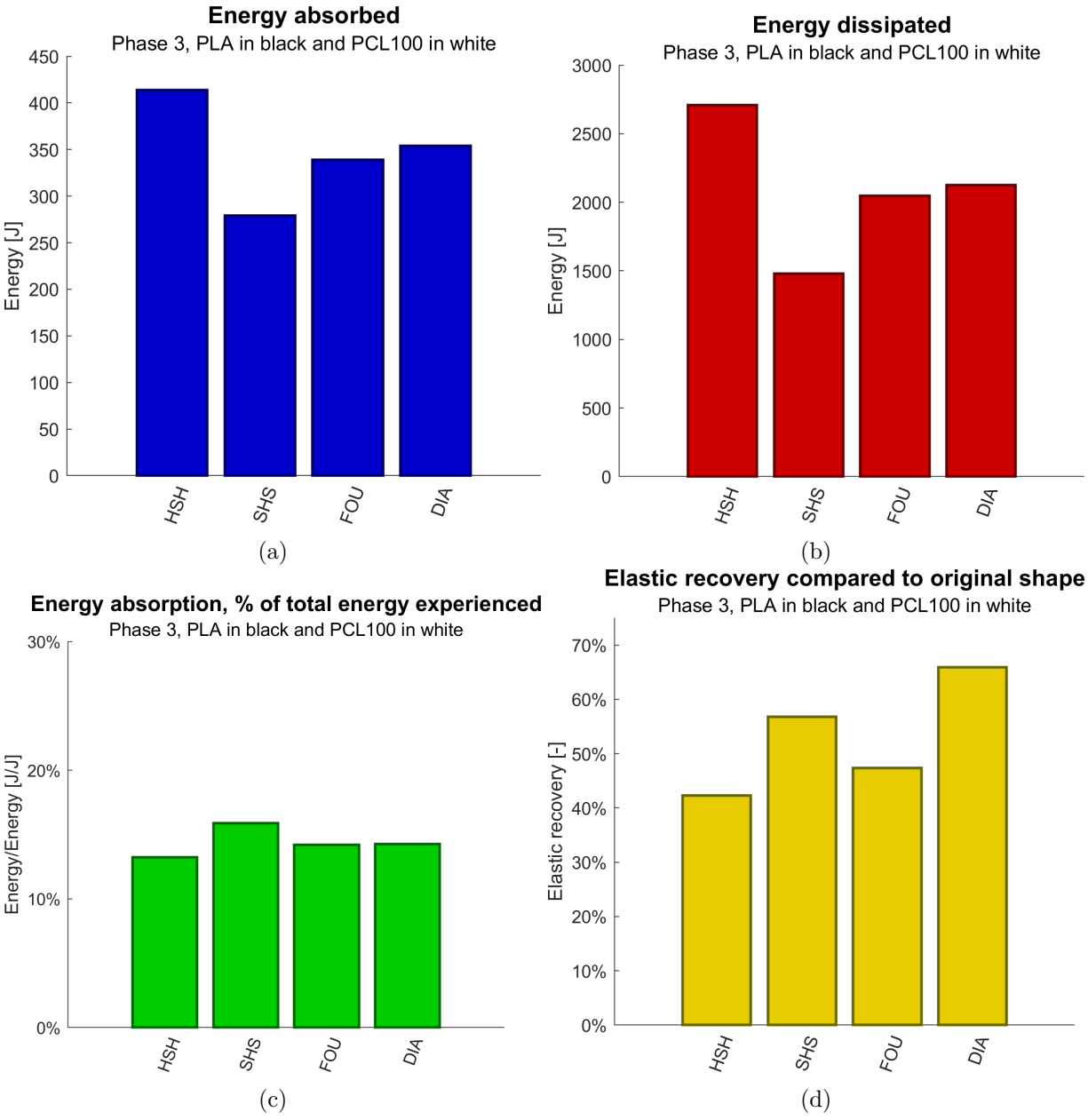

Figure 4.14: Results from phase 3, multi material variations

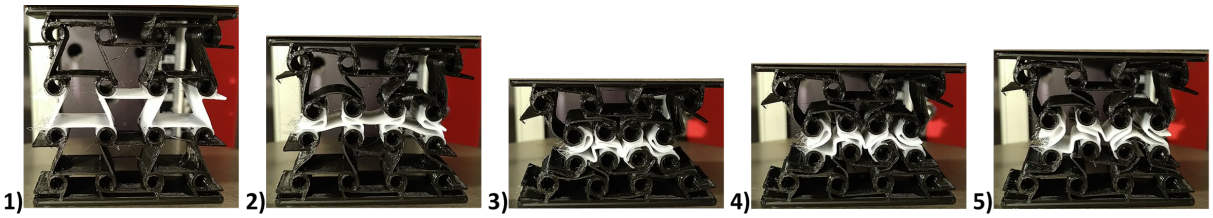

(a)

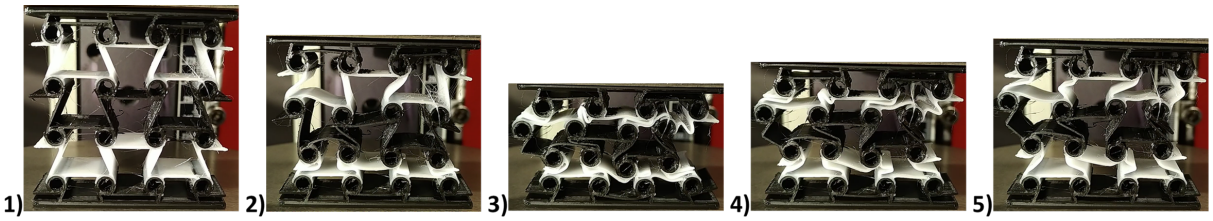

(b)

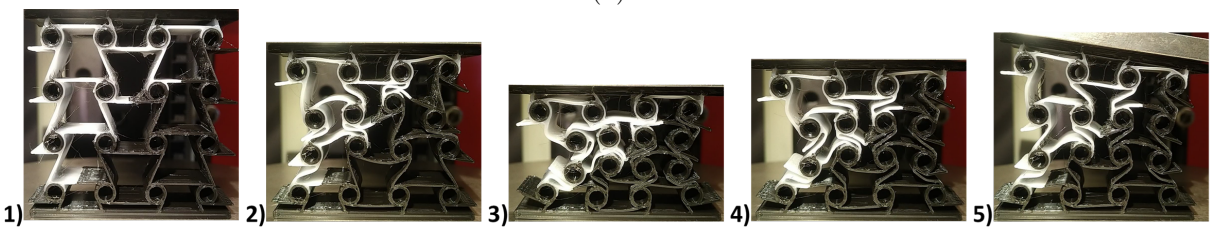

(c)

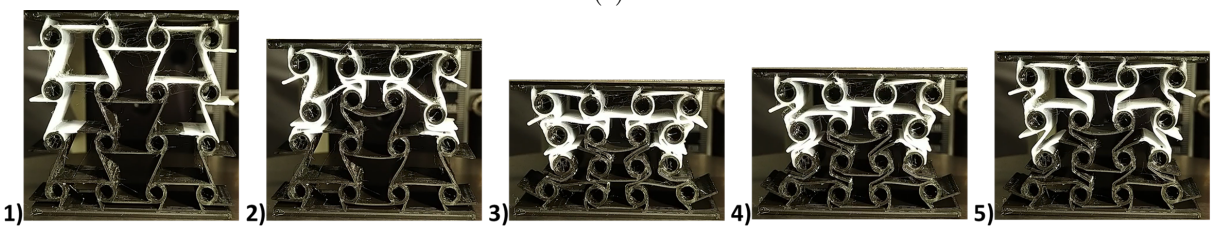

(d)

Figure 4.15: Deformation process of the multi-material designs, PLA in black and PCL in white. Pictures were taken at the start, middle, end and midway points. a) HSH. b) SHS. c) DIA. d) FOU. Larger version are placed in Appendix J.

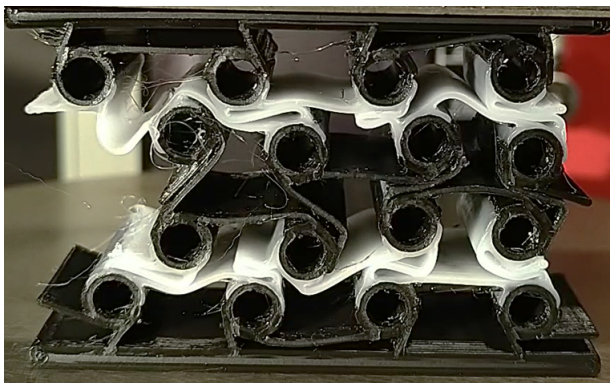

Figure 4.16: Different deformation behaviour of one out of three SHS structures.

4.3.3 Conclusions on multi-material experiments

A method was developed to 3D print the Chiral N4 structure with different hard and soft sections. This method has functioned mechanically, leading so similar auxetic compressive behaviour in mono material structures and multi material structures. With the exception of multi material beams, where two polymers are connected end-to-end, which deformed into V-shapes under axial compression.

It is possible to program different responses within the ChiralN4 structure, by the selectively using hard and soft materials. Experiments showed consistent results between samples, with no critical mechanical failures.

The programmed patterns had no significant impact on the energy absorption properties of the structures. Each structure absorbed between 13,2% and 15,9% of the total energy experienced. This is less than the 19,6% which a 5x5 sample made from pure PLA experienced, and far less than the 46% by samples from pure PCL. Changing from 25 cells to 16 cells is decreases the cellular density and is beneficial for the energy absorption performance. The difference is likely caused by the reinforcements within the cylinders of the multi material experiments. These were added to create a structure where buckling of cylinders made from soft materials would not cause structural failure during compression. However, this addition likely subtracted from the elasticity these cylinders were able to provide with thinner walls in earlier experiments.

Another comparison can be drawn to investigate the impact of inner cylinder from hard polymers on energy absorption performance. Figure 4.11b shows a structure made from PCL with hard inner cylinders. This structure had 25 cells, the same as the models which were used for experiments within the second experiment. The results from compressing the reinforced structure to the structure made from pure PCL can be compared. Showing 20% energy absorption and 46% respectively. Energy absorption occurs not only within the deformation of the beams, but also within the compression of the cylinders.

Different multi material designs did show differences in elastic performance. The HSH variant was made with the most hard material and showed the least elasticity with 43%. Whereas the diagonal variant, with a full column of flexible material, showed the highest elastic recovery with 66%. These results are in line with previous observations that the elastic recovery of a structure does not necessarily correlate with the energy absorption performance.

A difference was noticed between the compression behaviour of samples with 16 cells and samples with 25 cells. The lower density caused the cylinders neighbouring the top and bottom plates to be more active in the deformation. A longer connection between the cylinder and the wall gave more room for movement. The greater movement is beneficial for the auxetic behaviour of the sample.

4.3.4 Discussion on multi-material experiments

The flexibility of the beams influences when the structure experiences densification. More flexible material extends the initial lower stress plateau slightly, before stresses rise again due to densification.

A sufficiently flexible connection is needed between cylinders and the top and bottom plates to allow for a rotational motion in all cylinders. Some asymmetric behaviour such as with SHS could possibly be prevented by extending the structure.

The end-to-end connection of hard and soft polymers did not perform well under axial compression. This method of connecting two different materials might function under tension, but this requires further testing. A different connection would need to be designed for future design iterations. One possibility could be to extend the serrated profile from one cylinder to another. Substituting a sudden transition for a gradual transition.

During the design iteration, there was a problem where cylinders from soft polymers deformed and buckled. This buckling behaviour was prevented by reinforcing the cylinders with an inner

cylinder made from a harder material. This solution worked, no cylinders deformed during the multi material experiments. However, it was also found that this took away the ability from these cylinders to absorb energy. The reinforcements made the cylinders to ridged, reducing the energy absorption performance of the structures. This showed that this solution is not the most optimal design method.

An ideal solution would use cylinders made from soft polymers without reinforcements. Letting the connecting beams made from hard polymers bend, deform and wind around cylinders before cylinders from soft materials start to buckle. This could be done with the aid of numerical simulations, where local wall thicknesses are varied and optimised. Effectively calculating the force needed to bend beams from hard polymers, and calculating the wall thickness is needed for soft cylinders to not buckle at these same forces.

Chapter 5

Conclusion

At the start of this project, five sub questions and one main question were stated. The first two questions were set to guide the literary research. The other three correspond to the three main experiments which were conducted. At the end of the project, this research proved the viability of the Chiral N4 shape. It is possible to create programmed metamaterials which function in a similar vein to other programmed metamaterials, such as the honeycomb re-entrant.

The first sub question was: Which beneficial properties do auxetic structures exhibit? Auxetic structures are structures with a negative Poisson's ratio. This causes material to flow towards the area of impact instead of being pushed away from the impact. This behaviour is interesting for applications where energy absorption is an interesting property. These sandwich structures have enhanced energy absorption properties, allowing them to excel in dissipating energy. The negative Poisson's ratio has a relationship with compressive strength. Under similar relative densities, greater negative values of Poisson's ratio will increase the compressive strength. Auxetic structures show an interesting stress-strain behaviour when compressed. They experience an initial elastic stage, followed by an extensive plateau stage, before finally experiencing densification in the strain hardening stage. This behaviour lends itself to multi-material designs to create a gradual response under compression.

The second sub question was: How do process parameters during 3D printing affect the functionality of the structure. Changing certain printing parameters can improve a parts strength. The most important parameters are: lowering layer thickness, increasing infill percentage, increasing the extrusion temperature up to a point, and build orientation. The layer direction affects a parts strength, due to the anisotropic nature of 3D printed parts. The delicate interplay between print settings and their various impacts can be optimized on a case by case basis.

The third sub question was: Which auxetic shape has the best energy absorption properties? To answer this question, seven different shapes were tested. The two shapes which showed optimal energy absorption properties were S-shape and ChiralN4. The S-shape showed the greatest potential for energy absorption properties, but does not lend itself well to multi-material designs. Which was why the ChiralN4 shape was selected for further research. Other shapes performed better in different areas, such as highest stress levels, maximum area reduction, or a steadily increasing resistance to compression.

The fourth sub question was: Which materials have the best energy absorption properties, when using FDM 3D printing? To answer this question, four different materials were compared within an experiment. The shape which was chosen in the first experiment, ChiralN4, was used for this experiment. Two hard materials were used, PLA and C8. Two soft or flexible materials were used, PCL100 and TPC-91a . Results showed that PLA and TPC had the best energy absorption properties. However, TPC and PLA did not adhere well to each other. Which is why PCL and PLA were ultimately used to create multi-material structures.

The fifth and last sub question was: How can the chosen shape and materials be combined to

create multimaterial auxetic metamaterials? Several design iterations were made before structures were created which did not fail under compression. Four different designs were selected, printed and tested. The results showed behaviours which were clearly distinct from each other. This behaviour can be traced back to how the division between hard and soft materials was made within the structure.

Finally, the main question of this thesis was: How to maximize energy absorption of multimaterial auxetic metamaterials during compression? The right shape is important. Auxetics excel in energy absorption, and small changes in a structures shape can have large impacts to the behaviour of the larger structure. Eight shapes were examined in this study, and for multimaterial applications the ChiralN4 was found to outperform the others. Furthermore, reducing the density within the sandwich structure is beneficial for the energy absorption properties. This does come at the cost of the maximum stress values a structure can resist during compression. Materials are the second important factor. As a general rule, elastic materials will have better energy absorption properties. However, when two or more materials are combined within the same structure, they must adhere well to each other. When maximizing energy absorption, mono material designs with flexible materials will outperform shapes which combine hard and soft materials together.

Chapter 6

Recommendations and future work

Different auxetic shapes and patterns can be looked into. The eight shapes which were considered in this study are but a select number among many. Furthermore, for each shape minor changes in their geometry can be made. Each auxetic shape has the potential to be optimized in their own way. Creating larger structures with more nodes within will allow for more diverse multi-material designs. Auxetics sandwich structures are not limited to using a single shape. Several can be combined to benefit from different qualities. Two dimensional structures are the easiest to analyse, but all mentions above also hold for three dimensional shapes.

The impact of compression distance could be worth investigating. It can be hypothesised that higher strain distances will diminish energy absorption properties. As the elastic stage encompasses a larger ratio of the total energy experienced. The energy absorption properties of a structure might also change depending on how far they reach into the densification area. Both of these behaviours could differ per auxetic shape.

During this project, the ChiralN4 shape was investigated further. A sample was created and tested where the cellular pattern was roted 90 degrees. This removed the auxetic properties of the structure, as material is pushed sideways. The result can be seen in Appendix J.

When starting an academic project for which flexible materials will be used. It is recommended to have experience with 3D printing of flexible materials. Or to have connection with a person with experience. The process of finding optimal printing parameters can take significant time for flexible materials such as PCL.

Experience will significantly speed up the initial setup, troubleshooting unexpected errors, analysing failed prints, and knowing how improve a next iteration. When studying this alone, look sources as YouTube over academic papers for help.

The latest designs used PLA inner cylinders to circumvent several issues. Both in the manufacturing process and during the compression experiments. Shapes which do not rely on end-to-end connections could be created with TPC. For example, the HSH and SHS variants from this thesis. TPC outperformed other materials significantly, showing up to 90% energy absorption. Instead of using TPC, a more thorough research into printable flexible materials may deliver a substitute which adheres better to PLA.

The second method for increasing energy absorption properties would be to remove the inner cylinder. These currently reinforce the cylinders made from soft polymers to prevent buckling, but they also remove the flexibility of these cylinders. It might be possible to replace these reinforcements with local increases of the wall thickness. The soft cylinders must buckle after the connection beams made from hard polymers have been folded into place.

The topic of shape memory polymers was briefly mentioned, but could not be further explored. Their effect could be used to create shock absorbers, which could be restored and repaired after being used. This re-usability could be interesting, but needs to be further investigated. Different auxetic shapes and changing compressive distances could optimize the number of repair cycles before significant performance losses.

Chapter 7

Bibliography

[1] D. J. N. Amorim, T. Nachtigall, and M. B. Alonso. Exploring mechanical meta-material structures through personalised shoe sole design. Association for Computing Machinery, 2019.

[2] M. Barletta, A. Gisario, and M. Mehrpouya. 4d printing of shape memory polylactic acid (pla) components: Investigating the role of the operational parameters in fused deposition modelling (fdm). *Journal of Manufacturing Processes*, 61:473–480, 2021.

[3] S. R. G. Bates, I. R. Farrow, and R. S. Trask. Compressive behaviour of 3d printed thermoplastic polyurethane honeycombs with graded densities. *Materials & Design*, 162:130–142, 2019.

[4] M. Bodaghi, A. R. Damanpack, and W. H. Liao. Self-expanding/shrinking structures by 4d printing. *Smart Materials and Structures*, 25:105034, 9 2016.

[5] M. Bodaghi, A. Serjouei, A. Zolfagharian, M. Fotouhi, H. Rahman, and D. Durand. Reversible energy absorbing meta-sandwiches by fdm 4d printing. *International Journal of Mechanical Sciences*, 173:105451, 2020.

[6] J. Dong, G. Ye, W. Yongjun, F. Jin, and H. Fan. Design, manufacture and crushing behaviors of buckling-inspired auxetic meta-lattice structures. *International Journal of Smart and Nano Materials*, 12:1–20, 9 2021.

[7] Z. Dong, Y. Li, T. Zhao, W. Wu, D. Xiao, and J. Liang. Experimental and numerical studies on the compressive mechanical properties of the metallic auxetic reentrant honeycomb. *Materials & Design*, 182:108036, 2019.

[8] Dongsik, K. D.-N. C. Hyeonho, and Seo. Mechanics of auxetic materials. *Handbook of Mechanics of Materials*, pages 733–757, 2019.

[9] P. D. Dubrovski, N. Novak, M. Borovinšek, M. Vesenjak, and Z. Ren. In-plane behavior of auxetic non-woven fabric based on rotating square unit geometry under tensile load. *Polymers*, 11, 6 2019.

[10] J. Elipe and A. D. Lantada. Comparative study of auxetic geometries by means of computer-aided design and engineering. *Smart Materials and Structures - SMART MATER STRUCT*, 21, 2 2012.

[11] L. Geng, X. L. Ruan, W. Wu, R. Xia, and D. N. Fang. Mechanical properties of selective laser sintering (sls) additive manufactured chiral auxetic cylindrical stent. *Experimental Mechanics*, 59, 9 2019.

[12] I. Gibson, D. Rosen, and B. Stucker. *Additive Manufacturing Technologies*. Springer New York, second edition edition, 2015.

[13] T. Gordelier, P. Thies, L. Turner, and L. Johanning. Optimising the fdm additive manufacturing process to achieve maximum tensile strength: a state-of-the-art review. *Rapid Prototyping Journal*, ahead-of-print, 07 2019.

[14] J. Grima and K. Evans. Auxetic behavior from rotating squares. *Journal of Materials Science Letters*, 19:1563–1565, 09 2000.

[15] Y. Guo, J. Zhang, L. Chen, B. Du, H. Liu, L. Chen, W. Li, and Y. Liu. Deformation behaviors and energy absorption of auxetic lattice cylindrical structures under axial crushing load. *Aerospace Science and Technology*, 98:105662, 2020.

[16] W. M. Huang, Y. Zhao, C. C. Wang, Z. Ding, H. Purnawali, C. Tang, and J. L. Zhang. Thermo/chemo-responsive shape memory effect in polymers: a sketch of working mechanisms, fundamentals and optimization. *Journal of Polymer Research*, 19:9952, 2012.

[17] B. Z. Jang, D. R. Uhlmann, and J. B. V. Sande. Ductile–brittle transition in polymers. *Journal of Applied Polymer Science*, 29:3409–3420, 1984.

[18] R. Johnston and Z. Kazancı. Analysis of additively manufactured (3d printed) dual-material auxetic structures under compression. *Additive Manufacturing*, 38:101783, 2021.

[19] M. W. P. C. X. K. The manufacture and characterisation of a novel, low modulus, negative poisson's ratio composite. *Composites Science and Technology*, 69:651–655, 2009.

[20] P. U. Kelkar, H. S. Kim, K.-H. Cho, J. Y. Kwak, C.-Y. Kang, and H.-C. Song. Cellular auxetic structures for mechanical metamaterials: A review. *Sensors*, 20, 2020.

[21] N. Khatri and P. Egan. Tailored energy absorption for 3d printed multi-material cellular structures using abs and tpu. In *Mechanics of Solids, Structures, and Fluids; Micro- and Nano- Systems Engineering and Packaging*, ASME International Mechanical Engineering Congress and Exposition, Proceedings (IMECE). American Society of Mechanical Engineers (ASME), 2021. Funding Information: Dr. Burak Aksak provided aid via research discussions. Publisher Copyright: Copyright © 2021 by ASME; null ; Conference date: 01-11-2021 Through 05-11-2021.

[22] D. M. Kochmann and K. Bertoldi. Exploiting microstructural instabilities in solids and structures: From metamaterials to structural transitions. *Applied Mechanics Reviews*, 69, 10 2017.

[23] R. S. Kshetrimayum. A brief intro to metamaterials. *IEEE Potentials*, 23:44–46, 2005.

[24] N. Kulkarni, S. J. Franklin, G. Fadel, G. Li, N. Coutris, and M. P. Castanier. Multi-objective design of meta-materials exhibiting a targeted non-linear deformation response. *International Journal on Interactive Design and Manufacturing (IJIDeM)*, 14:1357–1377, 2020.

[25] R. Lakes. Foam structures with a negative poisson's ratio. *Science*, 235:1038–1040, 1987.

[26] Z. Li and J. Lambros. Strain rate effects on the thermomechanical behavior of polymers. *International Journal of Solids and Structures*, 38:3549–3562, 2001.

[27] H. Lim and S. Hoag. Plasticizer effects on physical–mechanical properties of solvent cast soluplus® films. *AAPS PharmSciTech*, 14, 05 2013.

[28] T.-C. Lim. Auxetic materials and structures. In T.-C. Lim, editor, *Auxetic Materials and Structures*, pages XV, 587. Springer Singapore, 2015.

[29] Y.-B. Luo, X.-L. Wang, and Y.-Z. Wang. Effect of tio2 nanoparticles on the long-term hydrolytic degradation behavior of pla. *Polymer Degradation and Stability*, 97:721–728, 12 2012.

[30] W. Lv, D. Li, and L. Dong. Study on blast resistance of a composite sandwich panel with isotropic foam core with negative poisson's ratio. *International Journal of Mechanical Sciences*, 191:106105, 2021.

[31] A. V. Mazaev, O. Ajeneza, and M. V. Shitikova. Auxetics materials: classification, mechanical properties and applications. *IOP Conference Series: Materials Science and Engineering*, 747:12008, 1 2020.

[32] K. Meena and S. Singamneni. An elongated s-shaped auxetic mechanical meta-material structure. *Materials Today: Proceedings*, 33, 2 2020.

[33] K. Meena and S. Singamneni. Investigation of a novel chiral s-shaped auxetic structure under large tensile deformation. *physica status solidi (b)*, 257:2000239, 2020.

[34] K. Meena and S. Singamneni. Novel hybrid auxetic structures for improved in-plane mechanical properties via additive manufacturing. *Mechanics of Materials*, 158:103890, 2 2021.

[35] M. Mehrpouya, A. Azizi, S. Janbaz, and A. Gisario. Investigation on the Functionality of Thermo-Responsive Origami Structures. *Advanced Engineering Materials*, 22, 2020.

[36] M. Mehrpouya, A. Gisario, A. Azizi, and M. Barletta. Investigation on shape recovery of 3d printed honeycomb sandwich structure. *Polymers for advanced technologies*, 31(12):3361–3365, Dec. 2020.

[37] J. Mueller, J. Lewis, and K. Bertoldi. Architected multimaterial lattices with thermally programmable mechanical response. *Advanced Functional Materials*, 32, 2 2022.

[38] N. Namvar, A. Zolfagharian, F. Vakili-Tahami, and M. Bodaghi. Reversible energy absorption of elasto-plastic auxetic, hexagonal, and auxhex structures fabricated by fdm 4d printing. *Smart Materials and Structures*, 31:55021, 4 2022.

[39] Z. M. Nejad, A. Zamanian, M. Saeidifar, H. R. Vanaei, and M. S. Amoli. 3d bioprinting of polycaprolactone-based scaffolds for pulp-dentin regeneration: Investigation of physicochemical and biological behavior. *Polymers*, 13, 2021.

[40] S. P. Patil, A. Kulkarni, and B. Markert. Mechanical properties of dragline silk fiber using a bottom-up approach. *Journal of Composites Science*, 6, 2022.

[41] W. Pattanasuttichonlakul, N. Sombatsompop, and B. Prapagdee. Accelerating biodegradation of pla using microbial consortium from dairy wastewater sludge combined with pla-degrading bacterium. *International Biodeterioration and Biodegradation*, 132:74–83, 2018.

[42] D. Prall and R. S. Lakes. Properties of a chiral honeycomb with a poisson's ratio of — 1. *International Journal of Mechanical Sciences*, 39:305–314, 1997.

[43] Ruopeng, S. D. R. C. T. Jun, and Liu. Introduction to metamaterials. *Metamaterials: Theory, Design, and Applications*, pages 1–19, 2010.

[44] D. L. Safranski and K. Gall. Effect of chemical structure and crosslinking density on the thermo-mechanical properties and toughness of (meth)acrylate shape memory polymer networks. *Polymer*, 49:4446–4455, 2008.

[45] S. Saufi, M. Z. M. Yusoff, M. Lalegani, S. Sapuan, I. R.A., A. As'arry, M. Ariffin, and M. Bodaghi. Compression behaviour of bio-inspired honeycomb reinforced starfish shape structures using 3d printing technology. *Polymers*, 13:13244388, 9 2021.

[46] K. K. Saxena, R. Das, and E. P. Calius. Three decades of auxetics research – materials with negative poisson's ratio: A review. *Advanced Engineering Materials*, 18:1847–1870, 2016.

[47] M. Schenk and S. Guest. Geometry of miura-folded metamaterials. *Proceedings of the National Academy of Sciences of the United States of America*, 110:3276–81, 02 2013.

[48] A. Serjouei, A. Yousefi, A. Jenaki, M. Bodaghi, and M. Mehrpouya. 4d printed shape memory sandwich structures: experimental analysis and numerical modeling. *Smart Materials and Structures*, 31:55014, 4 2022.

[49] Y. Shao, J. Meng, G. Ma, S. Ren, L. Fang, X. Cao, L. Liu, H. Li, W. Wu, and D. Xiao. Insight into the negative poisson's ratio effect of the gradient auxetic reentrant honeycombs. *Composite Structures*, 274:114366, 2021.

[50] R. Singh, R. Kumar, I. Farina, F. Colangelo, L. Feo, and F. Fraternali. Multi-material additive manufacturing of sustainable innovative materials and structures. *Polymers*, 11, 2019.

[51] C. W. Smith, J. N. Grima, and K. E. Evans. A novel mechanism for generating auxetic behaviour in reticulated foams: missing rib foam model. *Acta Materialia*, 48:4349–4356, 2000.

[52] G. M. Swallowe. Strain rate effects. In G. M. Swallowe, editor, *Mechanical Properties and Testing of Polymers*, pages 214–218. Springer Netherlands, 1999.

[53] D. Syrlybayev, B. Zharylkassyn, A. Seisekulova, M. Akhmetov, A. Perveen, and D. Talamona. Optimisation of strength properties of fdm printed parts—a critical review. *Polymers*, 13, 2021.

[54] M. Wallbanks, M. Khan, M. Bodaghi, A. Triantaphyllou, and A. Serjouei. On the design workflow of auxetic metamaterials for structural applications. *Smart Materials and Structures*, 31:23002, 2 2021.

[55] Z. Wan, P. Zhang, Y. Liu, L. Lv, and Y. Zhou. Four-dimensional bioprinting: Current developments and applications in bone tissue engineering. *Acta Biomaterialia*, 101:26–42, 2020.

[56] K. Wang, Y.-H. Chang, Y. Chen, C. Zhang, and B. Wang. Designable dual-material auxetic metamaterials using three-dimensional printing. *Materials & Design*, 67:159–164, 2015.

[57] K. Wang, Y. Zhao, Y.-H. Chang, Z. Qian, C. Zhang, B. Wang, M. A. Vannan, and M.-J. Wang. Controlling the mechanical behavior of dual-material 3d printed meta-materials for patient-specific tissue-mimicking phantoms. *Materials & Design*, 90:704–712, 2016.

[58] Q. Wang, Z. Yang, Z. Lu, and X. Li. Mechanical responses of 3d cross-chiral auxetic materials under uniaxial compression. *Materials & Design*, 186:108226, 2020.

[59] Y. Xue, X. Wang, W. Wang, X. Zhong, and F. Han. Compressive property of al-based auxetic lattice structures fabricated by 3-d printing combined with investment casting. *Materials Science and Engineering: A*, 722:255–262, 2018.

[60] C. Yuan, X. Mu, C. Dunn, J. Haidar, T. Wang, and H. Qi. Thermomechanically triggered two-stage pattern switching of 2d lattices for adaptive structures. *Advanced Functional Materials*, 28:1705727, 2 2018.

[61] N. Zaaba and M. Jaafar. A review on degradation mechanisms of polylactic acid: Hydrolytic, photodegradative, microbial, and enzymatic degradation. *Polymer Engineering and Science*, 60, 12 2020.

[62] A. A. Zadpoor. Mechanical meta-materials. *Mater. Horiz.*, 3:371–381, 2016.

[63] M. H. Zamani, M. Heidari-Rarani, and K. Torabi. A novel graded auxetic honeycomb core model for sandwich structures with increasing natural frequencies. *Journal of Sandwich Structures & Materials*, 24:1313–1339, 2022.

[64] M. H. Zamani, M. Heidari-Rarani, and K. Torabi. Optimal design of a novel graded auxetic honeycomb core for sandwich beams under bending using digital image correlation (dic). *Composite Structures*, 286:115310, 2022.

[65] J. Zhang, G. Lu, and Z. You. Large deformation and energy absorption of additively manufactured auxetic materials and structures: A review. *Composites Part B: Engineering*, 201:108340, 2020.

Appendix A

Calculation for Poisson's ratio of chiral N6 structures.

The appendices including calculations, detailed experiment descriptions, result tables, graphs and drawing.

A.1 Poisson's ratio for chiral structures with six beams

The poisson's ratio for chiral structures with six beams can be calculated to be equal to -1 for small deformations [42]. For larger deformations, the ratio will deviate from -1 and approach a value closer to 0 as the strain on the structure increases.

Starting with the state as seen in Figure A.2, which describes the undeformed state between two nodes of the structure connected with a beam. The distance between two nodes is equal to R, and the radius of a node is equal to r. By definition of the six-fold symmetry, θ is equal to 30°.

Figure A.3 shows the same two nodes, but under a deformed state. The rotational behavior of the nodes reduces the length R by two times the length e.

From Figure A.3, e can be defined as:

$$e = r \cdot sin(\Theta) \tag{A.1}$$

assuming small deformations results in

$$\begin{aligned} \Theta &\approx 0 \\ e = r \cdot sin(\Theta) &\approx r \cdot \Theta \end{aligned} \tag{A.2}$$

Now looking at Figure A.4

$$\begin{aligned} e_1 = e \cdot cos(\Theta) = e_1 &= r \cdot \Theta \cdot \cos(\theta) \\ e_2 = e \cdot sin(\theta) = e_2 &= r \cdot \Theta \cdot sin(\theta) \end{aligned} \tag{A.3}$$

By definition we know for the elongation:

$$\epsilon_1 = \frac{\text{elongation}}{\text{original length}} = \frac{e_1}{\text{Length of x-axis between the centers of the two nodes}} \tag{A.4}$$

therefore

$$\begin{aligned} \epsilon_1 &= \frac{e_1}{R \cdot cos(\Theta)} \\ \epsilon_2 &= \frac{e_2}{R \cdot sin(\Theta)} \end{aligned} \tag{A.5}$$

combined with Equation A.3 gives

$$\begin{aligned} \epsilon_1 &= \frac{r \cdot \Theta}{R} \cdot \frac{cos(\theta)}{cos(\theta)} \\ \epsilon_2 &= \frac{r \cdot \Theta}{R} \cdot \frac{sin(\theta)}{sin(\theta)} \end{aligned} \tag{A.6}$$

Which leads to combined with Equation A.3 gives

$$\begin{aligned} \nu_{12} &= -\frac{\epsilon_2}{\epsilon_1} \\ \nu_{21} &= -\frac{\epsilon_1}{\epsilon_2} \\ \epsilon_1 &= \epsilon_2 \\ \nu_{12} &= \nu_{21} = -1 \end{aligned} \tag{A.7}$$

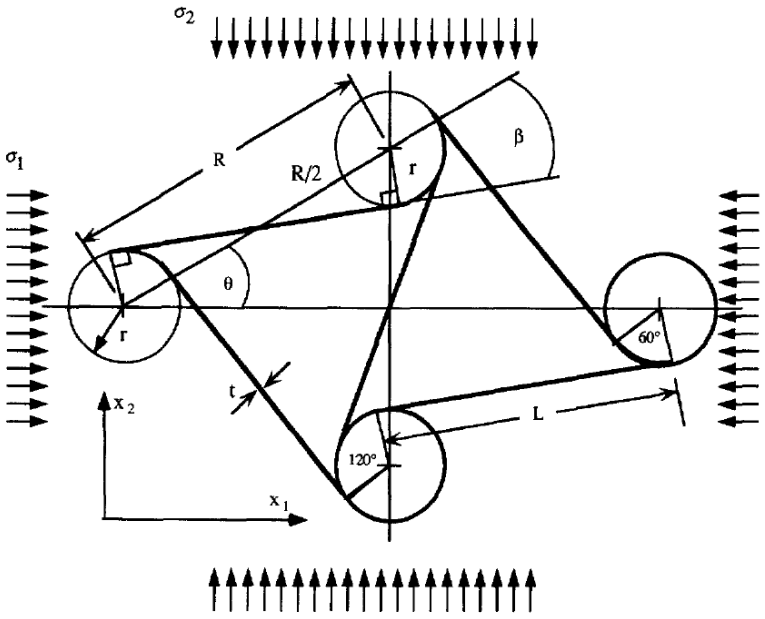

Figure A.1: Overview of the structure, drawing from [42].

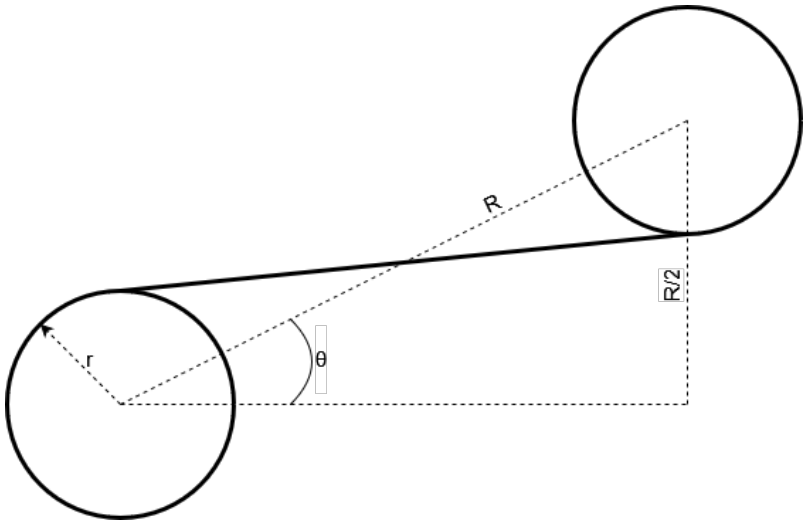

Figure A.2: Two undeformed nodes of a chiral structure

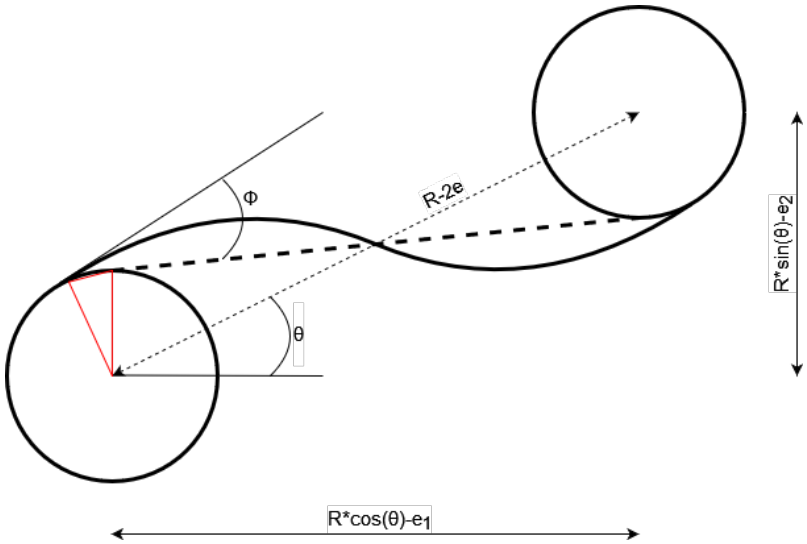

Figure A.3: Deformed state of the chiral structure

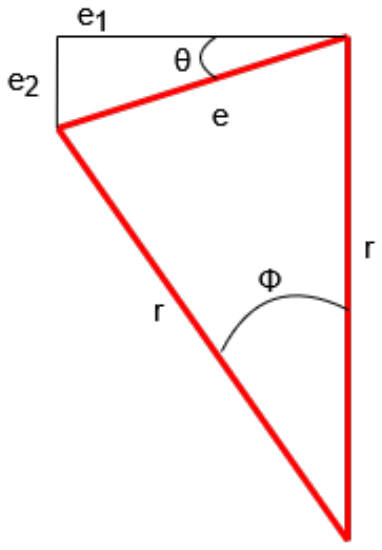

Figure A.4: Detailed section of the red triangle from the deformed state

Appendix B

Plagiarism report

PAPER NAME

CONCEPT_V2_MSc_Thesis_Jonne_Postmes_21_okt.pdf

AUTHOR

Jonne Postmes

WORD COUNT

24243 Words

CHARACTER COUNT

129553 Characters

PAGE COUNT

104 Pages

FILE SIZE

71.9MB

SUBMISSION DATE

Oct 24, 2022 3:38 PM GMT+2

REPORT DATE

Oct 24, 2022 3:41 PM GMT+2

7% Overall Similarity

The combined total of all matches, including overlapping sources, for each database.

- 5% Internet database
- 4% Publications database
- Crossref database
- Crossref Posted Content database
- 2% Submitted Works database

Excluded from Similarity Report

- Bibliographic material

Appendix C

Technical drawings of experiment 1

This appendix contains eight technical drawings. Detailing the dimensions of the structures used for experiment 1.

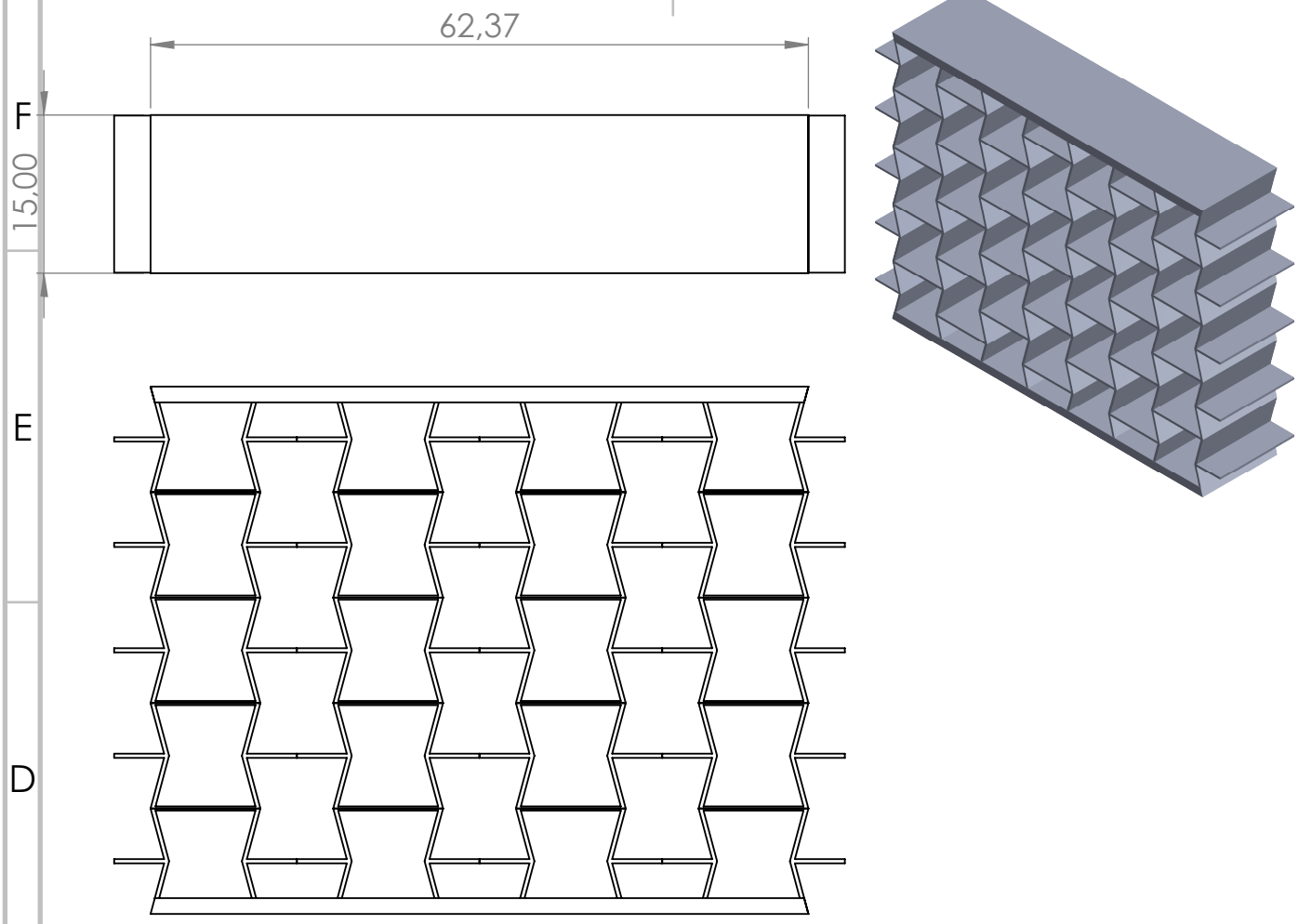

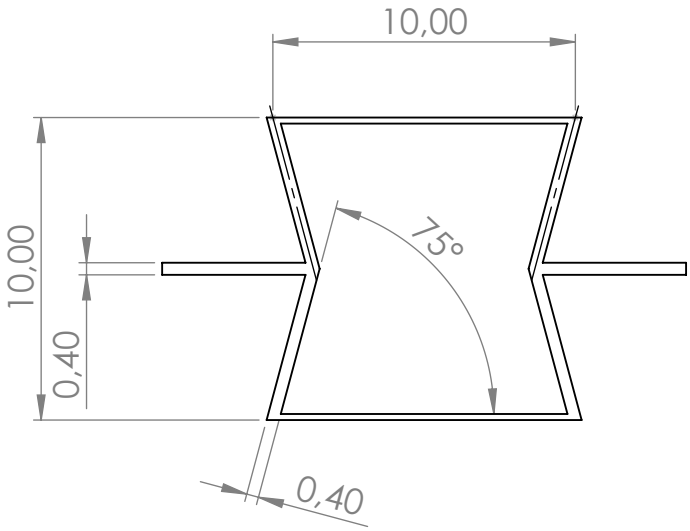

UNLESS OTHERWISE SPECIFIED: DIMENSIONS ARE IN MILLIMETERS SURFACE FINISH: TOLERANCES: LINEAR: ANGULAR:	FINISH:	DEBURR AND BREAK SHARP EDGES	DO NOT SCALE DRAWING / REVISION

	NAME	SIGNATURE	DATE
DRAWN			
CHK'D			
APPV'D			
MFG			
Q.A			

TITLE:

MATERIAL:

DWG NO. Assembly_Re-entrant

A4

WEIGHT:

SCALE:1:1

SHEET 1 OF 1

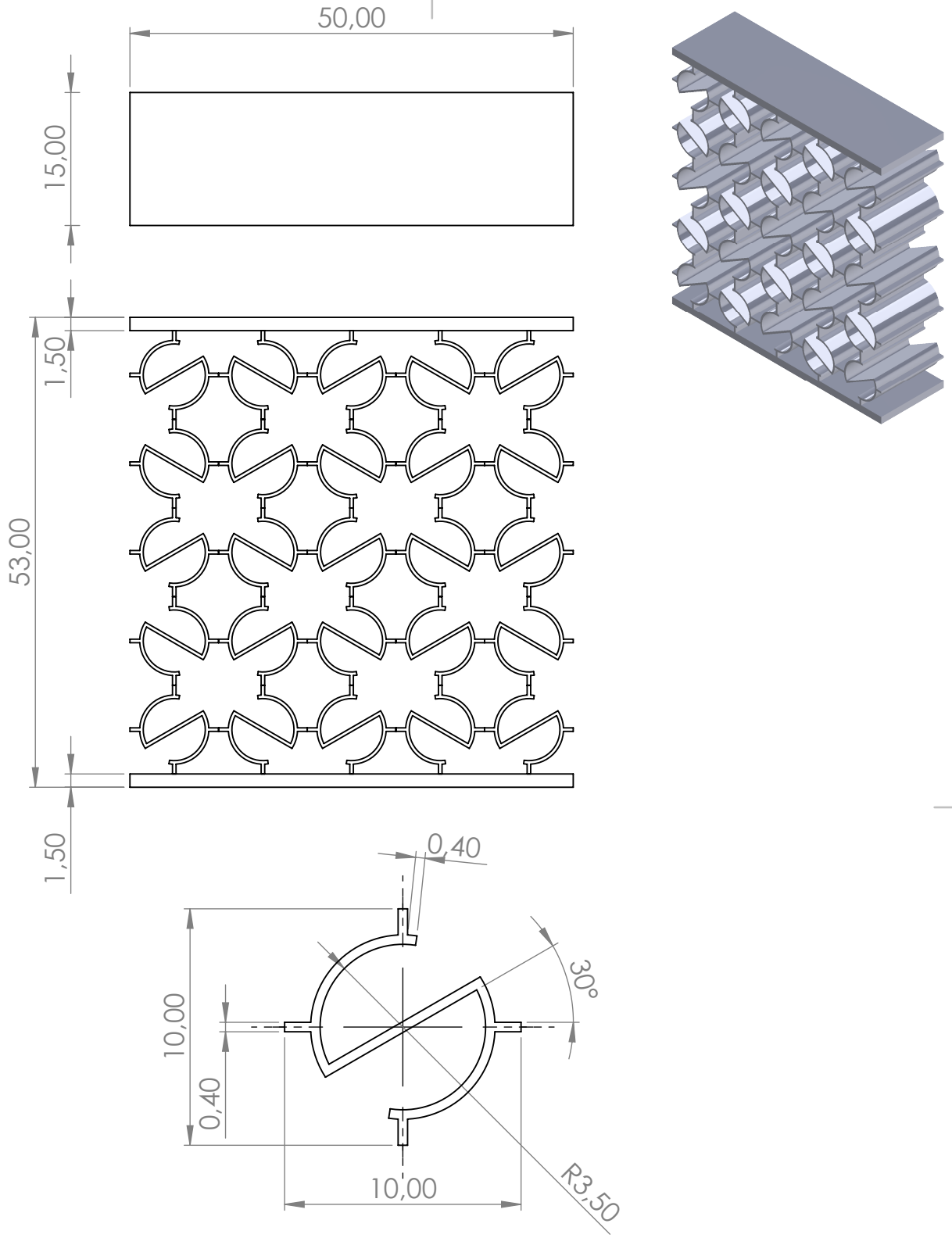

UNLESS OTHERWISE SPECIFIED: DIMENSIONS ARE IN MILLIMETERS SURFACE FINISH: TOLERANCES: LINEAR: ANGULAR:	FINISH:	DEBURR AND BREAK SHARP EDGES	DO NOT SCALE DRAWING / REVISION

	NAME	SIGNATURE	DATE
DRAWN			
CHK'D			
APPV'D			
MFG			
Q.A			

TITLE:

MATERIAL:

DWG NO. Assembly_S-shape A4

WEIGHT:

SCALE:1:1

SHEET 1 OF 1

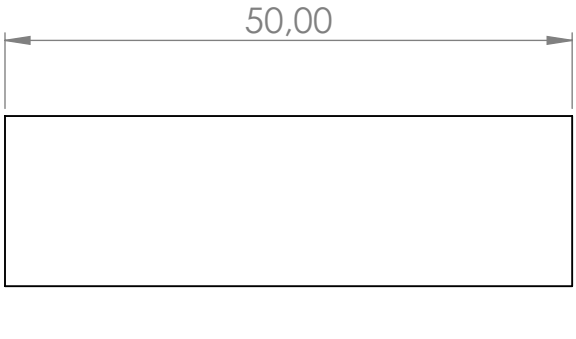

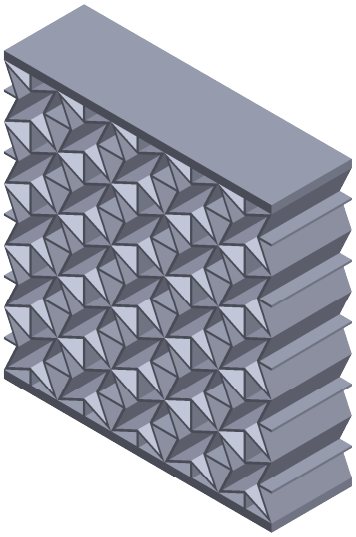

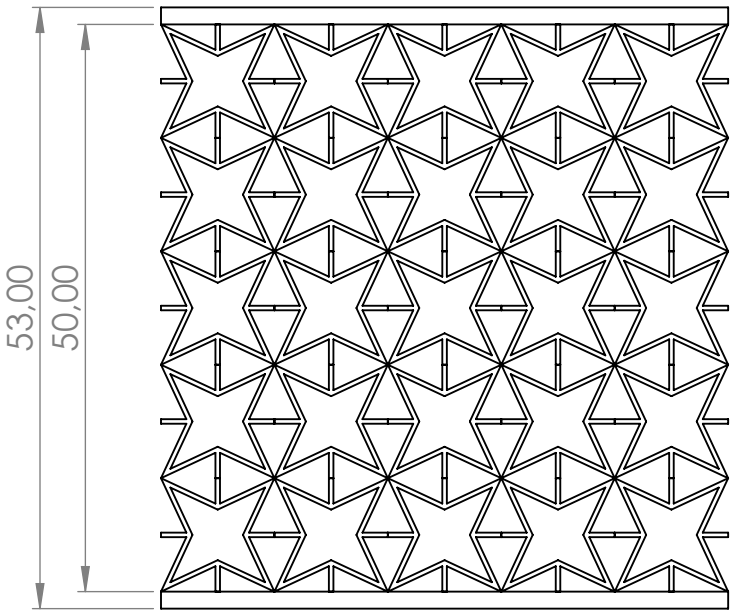

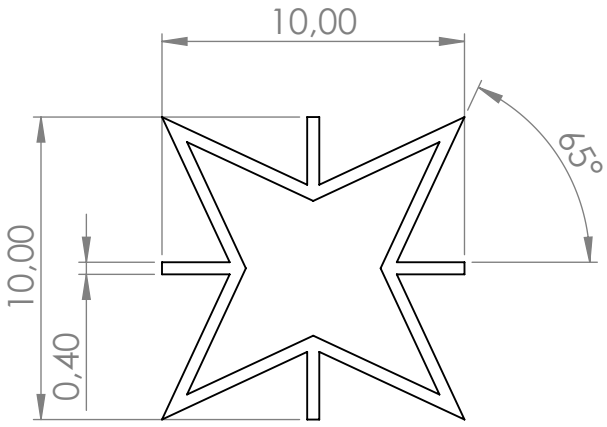

UNLESS OTHERWISE SPECIFIED: DIMENSIONS ARE IN MILLIMETERS SURFACE FINISH: TOLERANCES: LINEAR: ANGULAR:	FINISH:	DEBURR AND BREAK SHARP EDGES

	DO NOT SCALE DRAWING	REVISION

	NAME	SIGNATURE	DATE
DRAWN			
CHK'D			
APPV'D			
MFG			
Q.A			

TITLE:

MATERIAL:

DWG NO. Assembly_Star-re-entrant

A4

WEIGHT:

SCALE:1:1

SHEET 1 OF 1

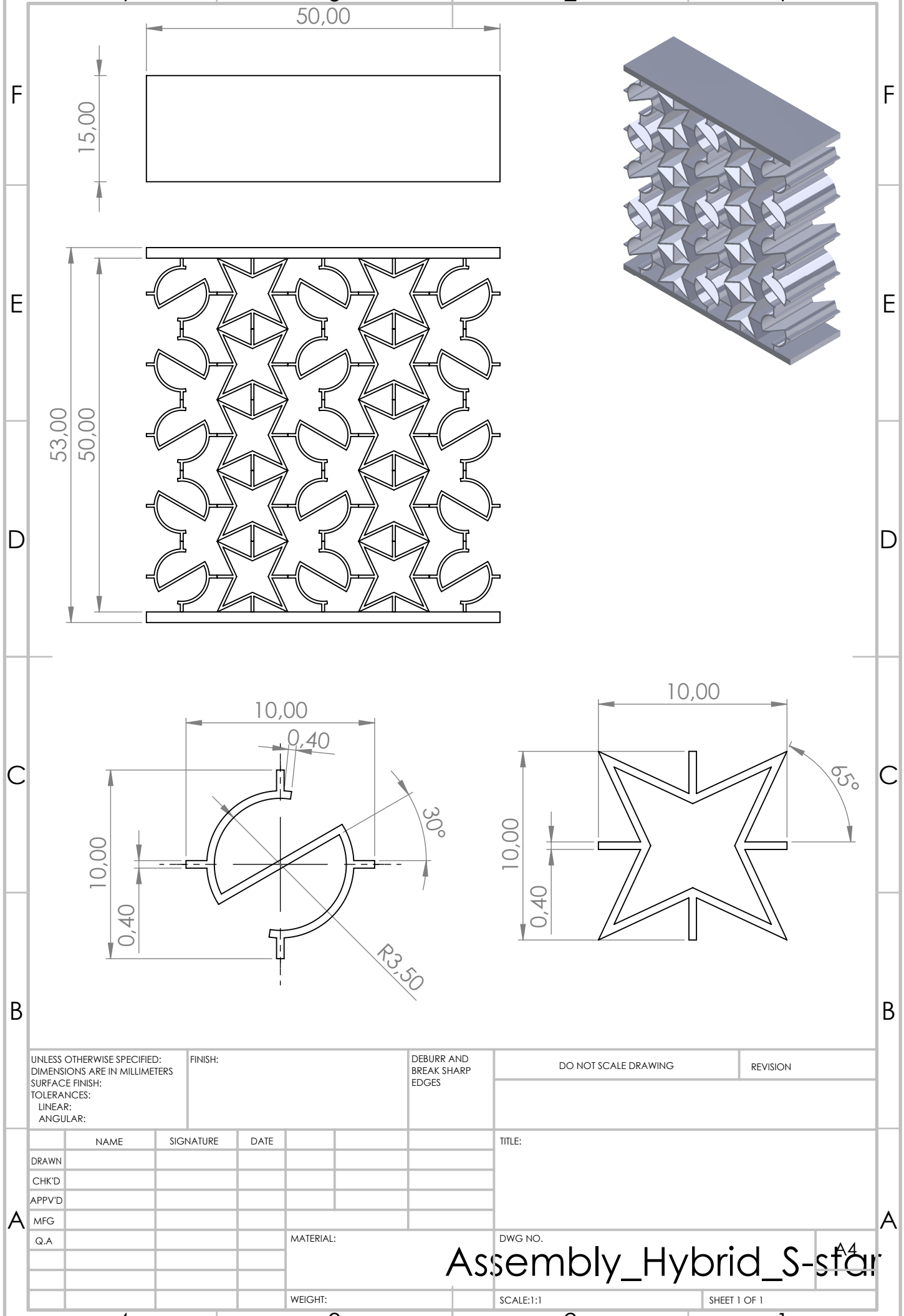

UNLESS OTHERWISE SPECIFIED: DIMENSIONS ARE IN MILLIMETERS SURFACE FINISH: TOLERANCES: LINEAR: ANGULAR:	FINISH:	DEBURR AND BREAK SHARP EDGES	DO NOT SCALE DRAWING / REVISION

	NAME	SIGNATURE	DATE
DRAWN			
CHK'D			
APPV'D			
MFG			
Q.A			

TITLE:

MATERIAL:

DWG NO. Assembly_Hybrid_S-star

A4

WEIGHT:

SCALE:1:1

SHEET 1 OF 1

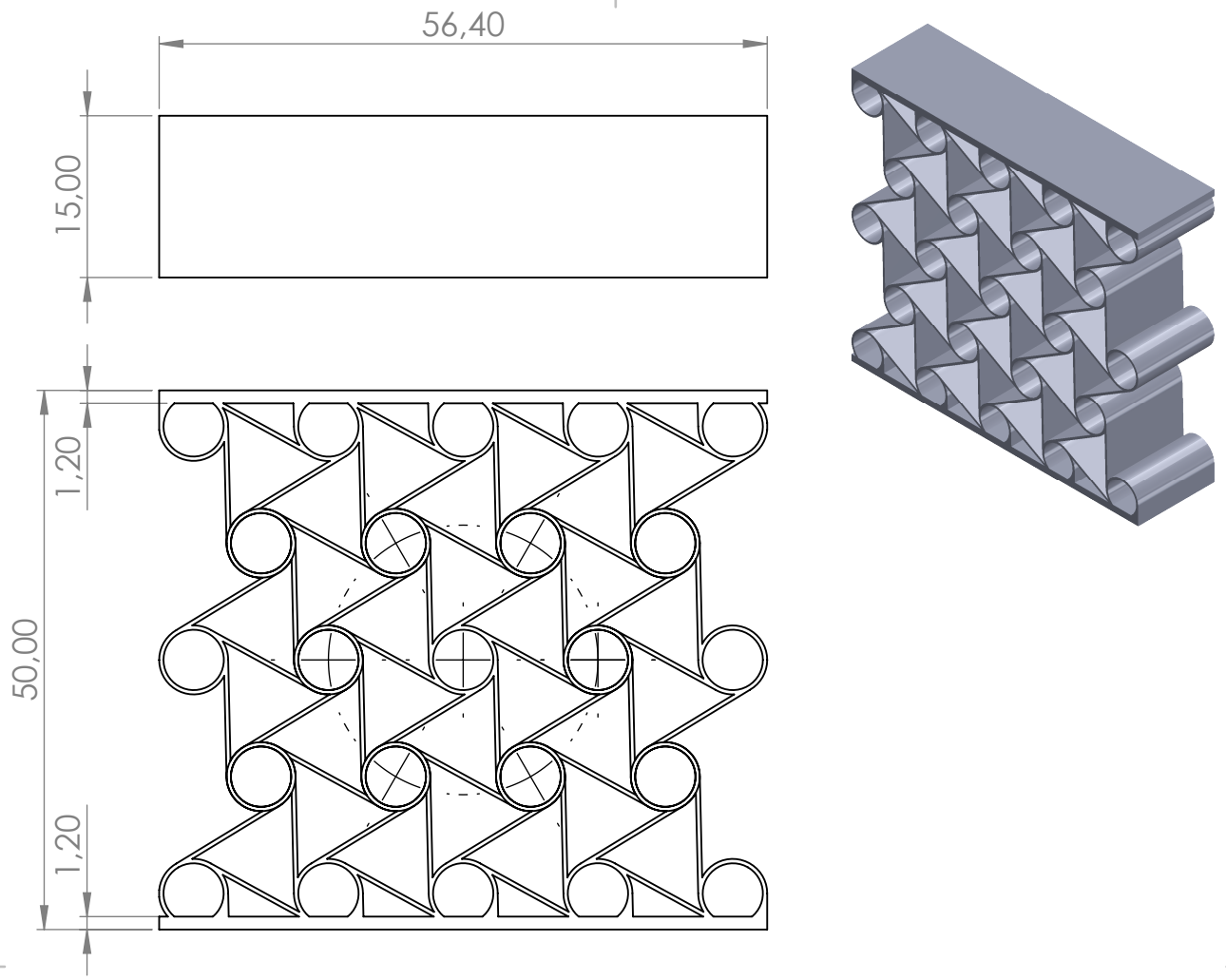

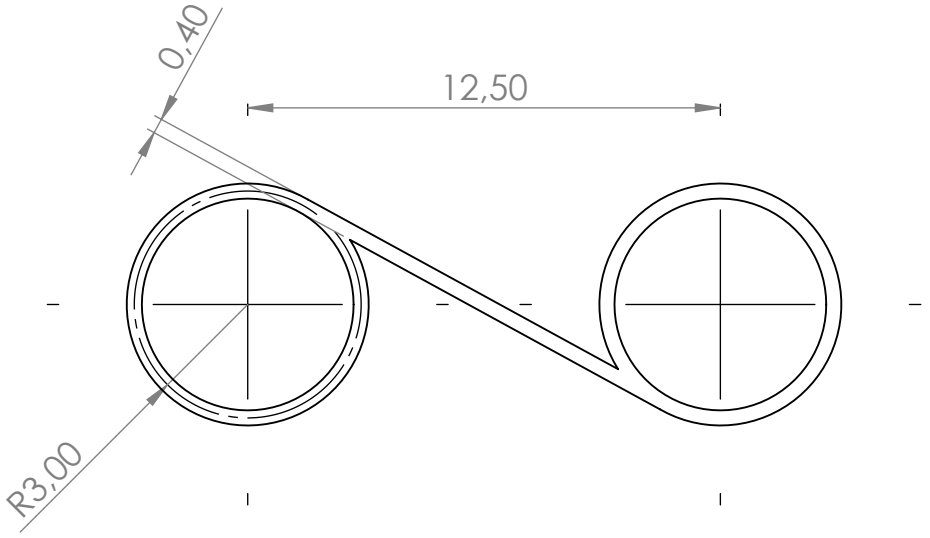

UNLESS OTHERWISE SPECIFIED: DIMENSIONS ARE IN MILLIMETERS SURFACE FINISH: TOLERANCES: LINEAR: ANGULAR:	FINISH:	DEBURR AND BREAK SHARP EDGES	DO NOT SCALE DRAWING / REVISION

	NAME	SIGNATURE	DATE
DRAWN			
CHK'D			
APPV'D			
MFG			
Q.A			

TITLE:

MATERIAL:

DWG NO. Chiral_N6

A4

WEIGHT:

SCALE:1:1

SHEET 1 OF 1

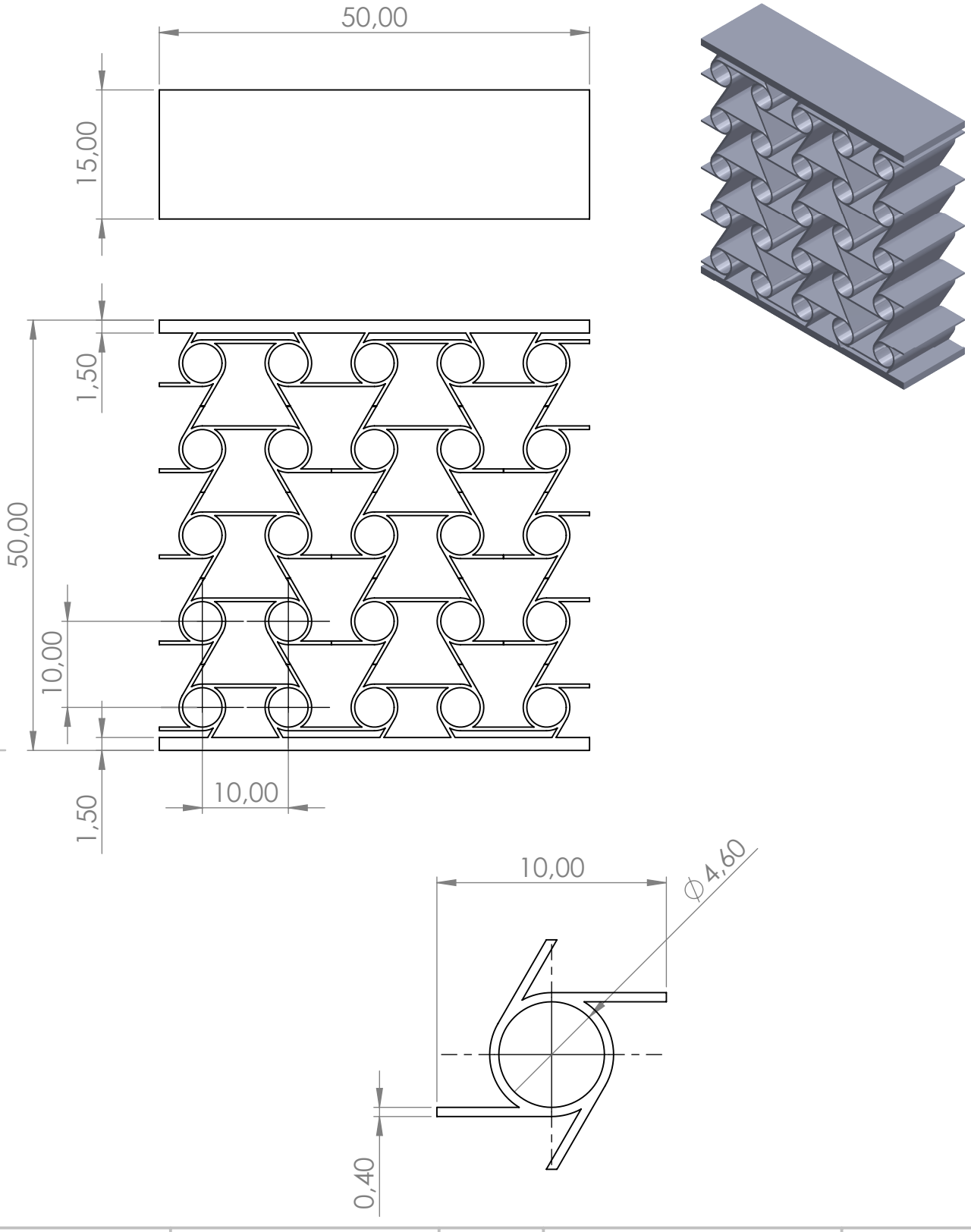

UNLESS OTHERWISE SPECIFIED: DIMENSIONS ARE IN MILLIMETERS SURFACE FINISH: TOLERANCES: LINEAR: ANGULAR:	FINISH:	DEBURR AND BREAK SHARP EDGES	DO NOT SCALE DRAWING / REVISION

	NAME	SIGNATURE	DATE
DRAWN			
CHK'D			
APPV'D			
MFG			
Q.A			

TITLE:

MATERIAL:

DWG NO.

A4

Chiral_n4_circular_Symmetric

WEIGHT:

SCALE:1:1

SHEET 1 OF 1

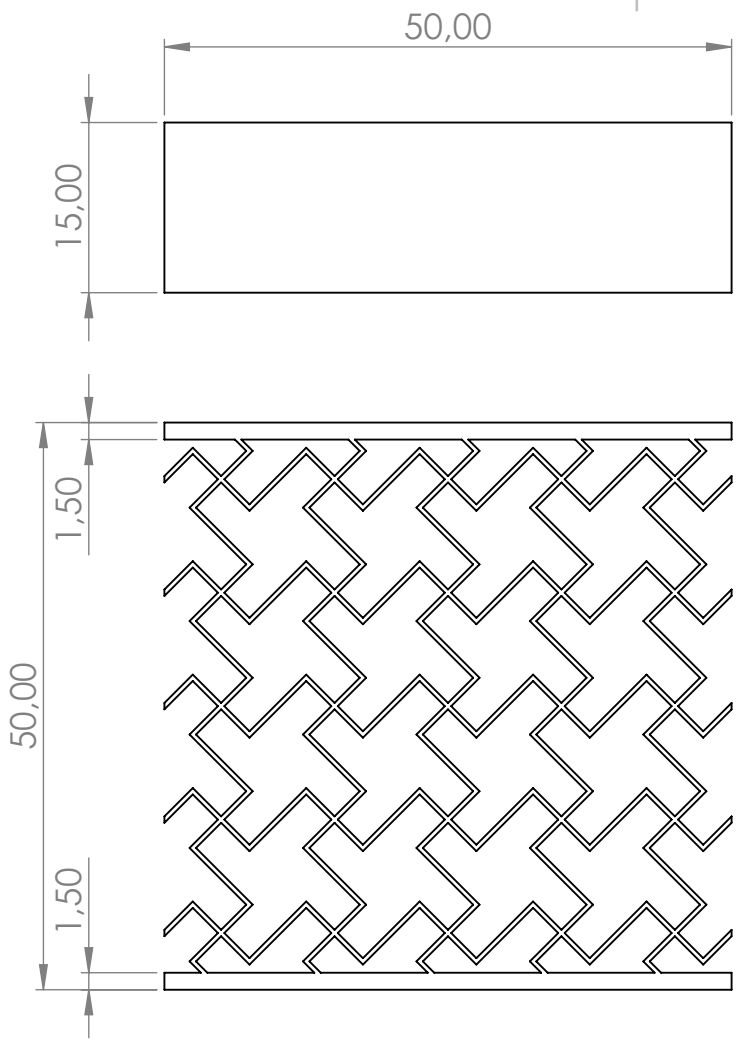

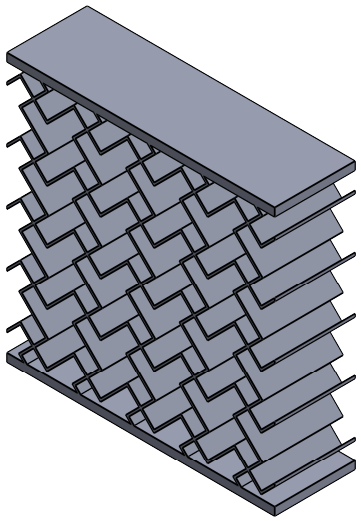

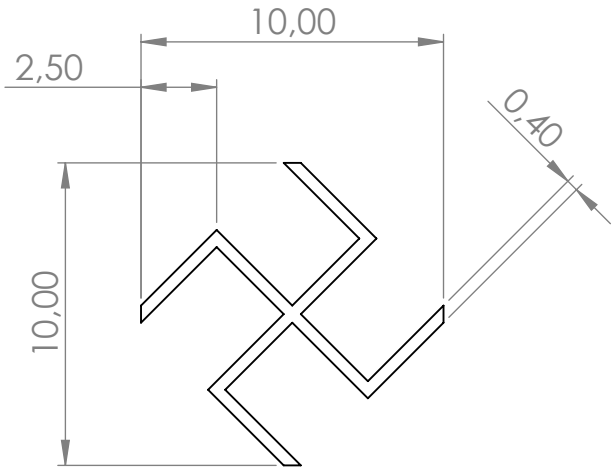

UNLESS OTHERWISE SPECIFIED: DIMENSIONS ARE IN MILLIMETERS SURFACE FINISH: TOLERANCES: LINEAR: ANGULAR:	FINISH:		DEBURR AND BREAK SHARP EDGES	DO NOT SCALE DRAWING	REVISION	

	NAME	SIGNATURE	DATE			
DRAWN						
CHK'D						
APPV'D						
MFG						
Q.A				MATERIAL:	DWG NO.	A4
					Lozenge_grid_square	
				WEIGHT:	SCALE:1:1	SHEET 1 OF 1

TITLE:

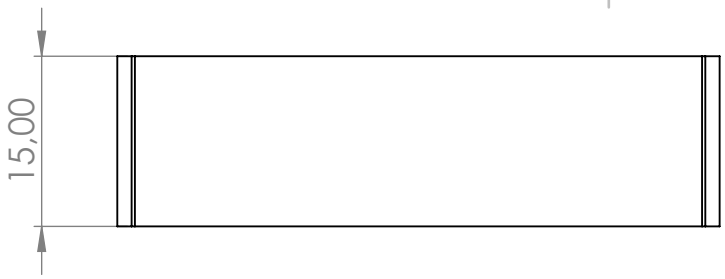

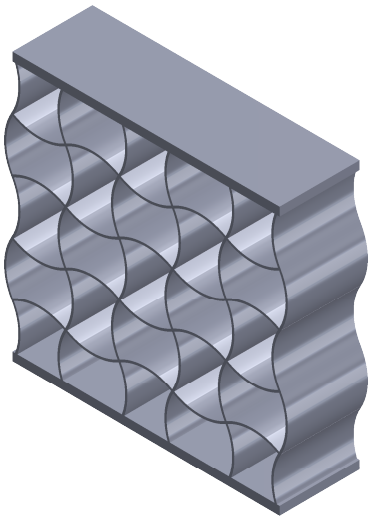

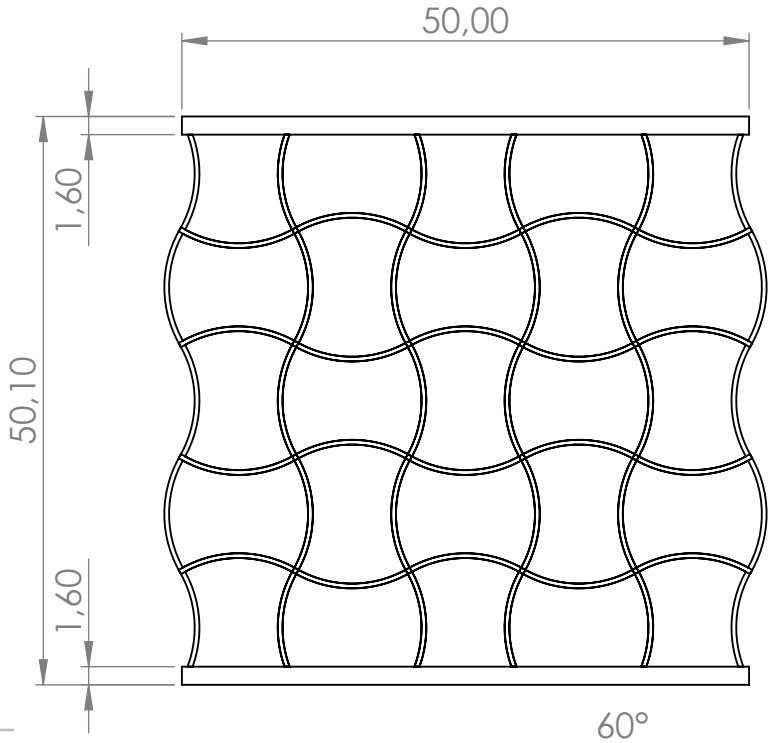

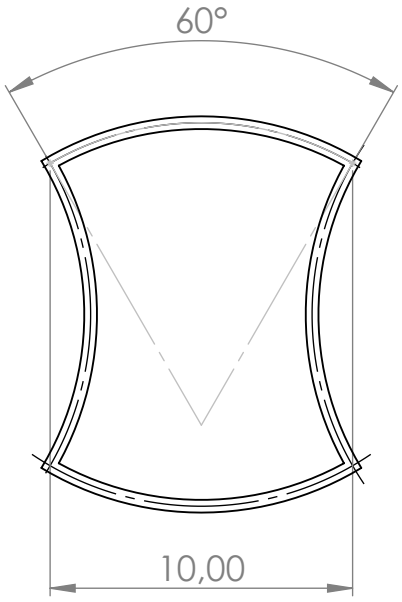

UNLESS OTHERWISE SPECIFIED: DIMENSIONS ARE IN MILLIMETERS SURFACE FINISH: TOLERANCES: LINEAR: ANGULAR:	FINISH:		DEBURR AND BREAK SHARP EDGES		DO NOT SCALE DRAWING		REVISION
	NAME	SIGNATURE	DATE				TITLE:
DRAWN							
CHK'D							
APPV'D							
MFG							
Q.A				MATERIAL:		DWG NO.	A4
						Assembly_sinusoda1	
				WEIGHT:		SCALE:1:1	SHEET 1 OF 1

Appendix D

Test results of intermediate iterations preceding final duo-material design

This appendix contains the test results which were made during the iteration process before the final duo-material design was selected.

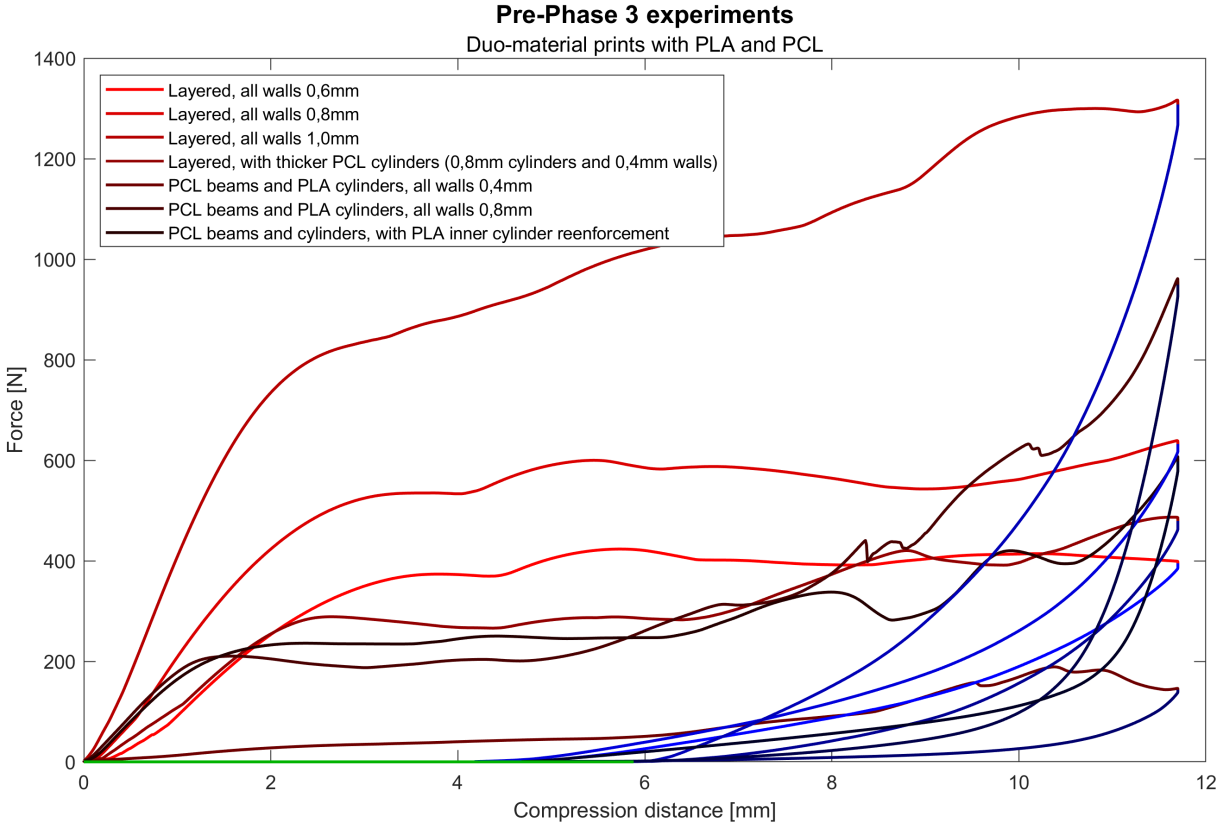

Figure D.1: Stress strain diagram of the first seven iterations

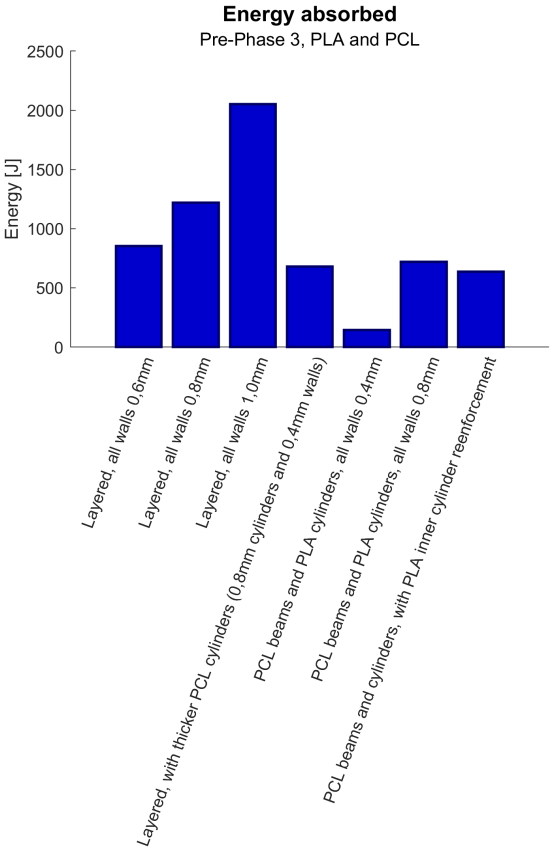

(a)

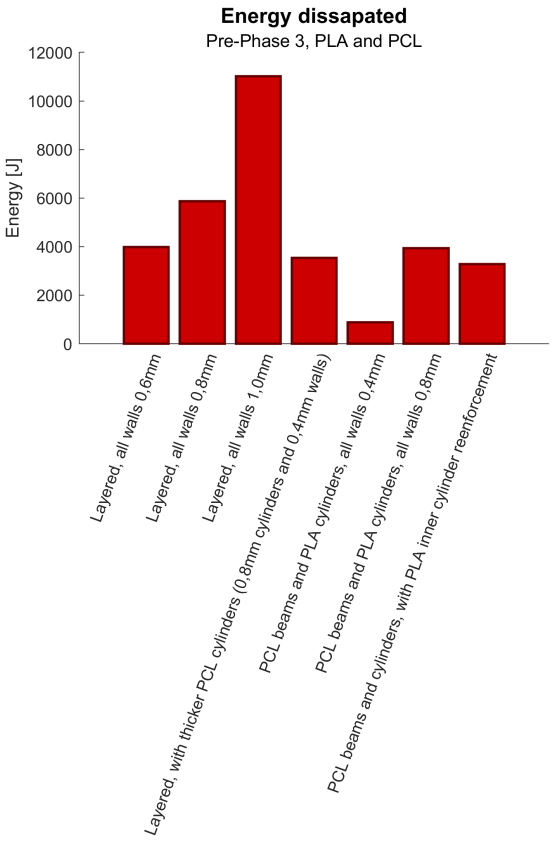

(b)

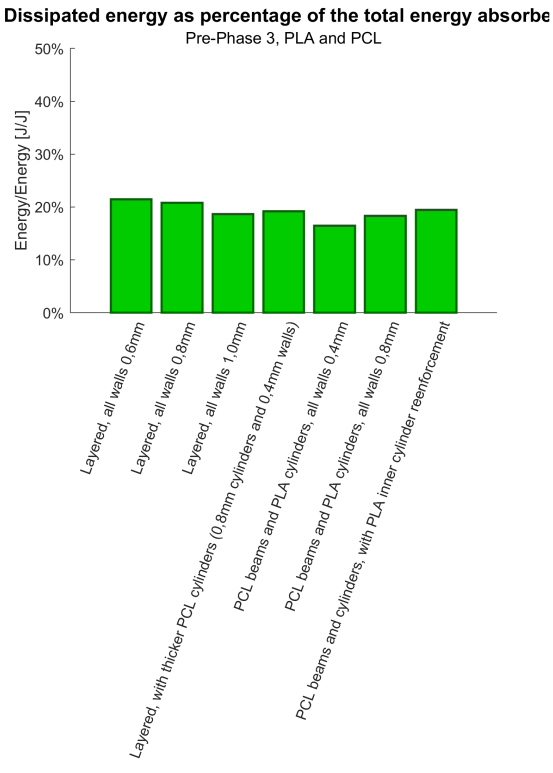

(c)

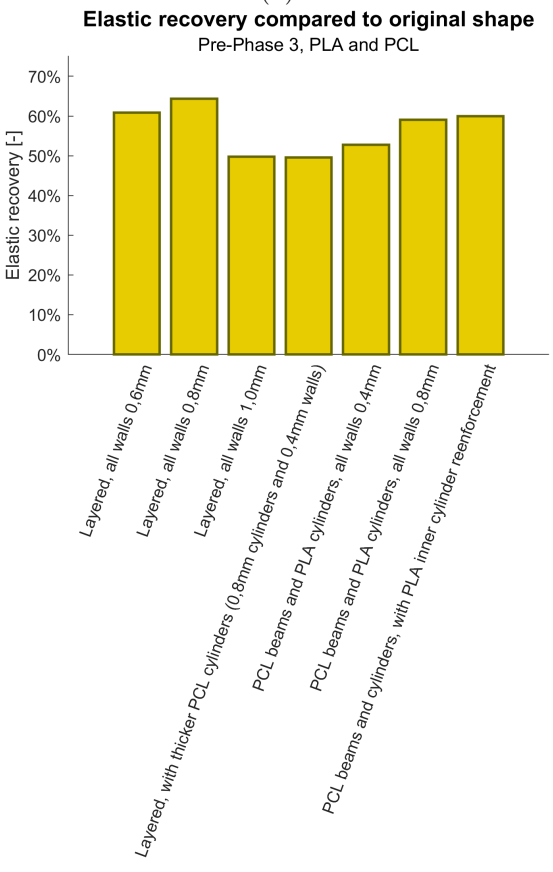

(d)

Figure D.2: Bar chart analysis of the first seven iterations.

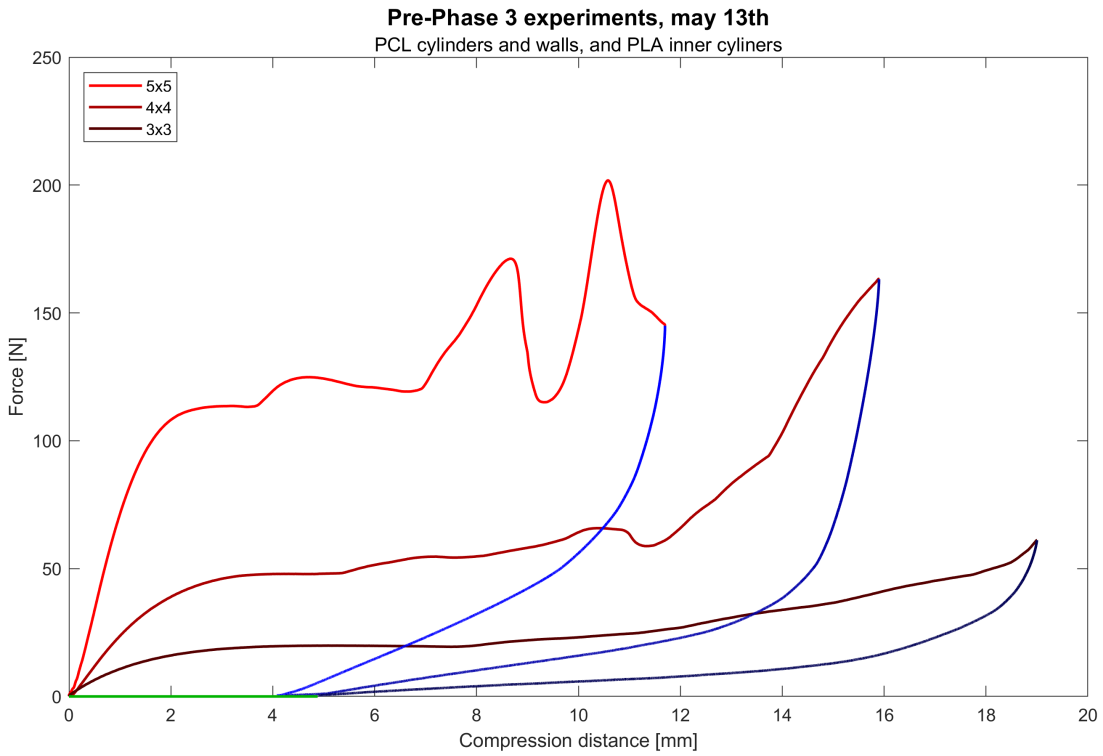

Figure D.3: Stress strain diagram of the sandwich structures with decreasing inner density.

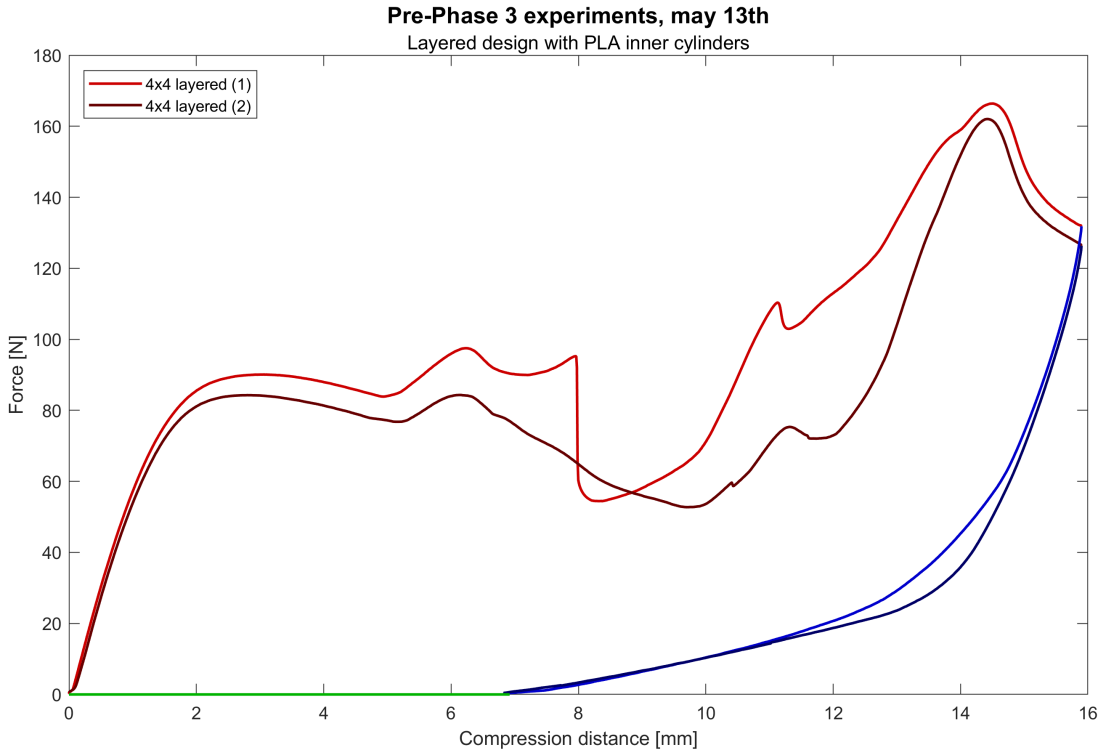

Figure D.4: Stress strain diagram, created when testing the final iteration for the duo-material design.

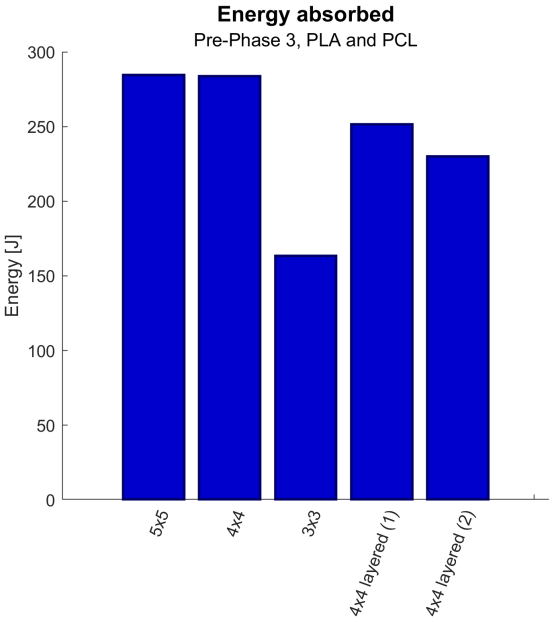

(a)

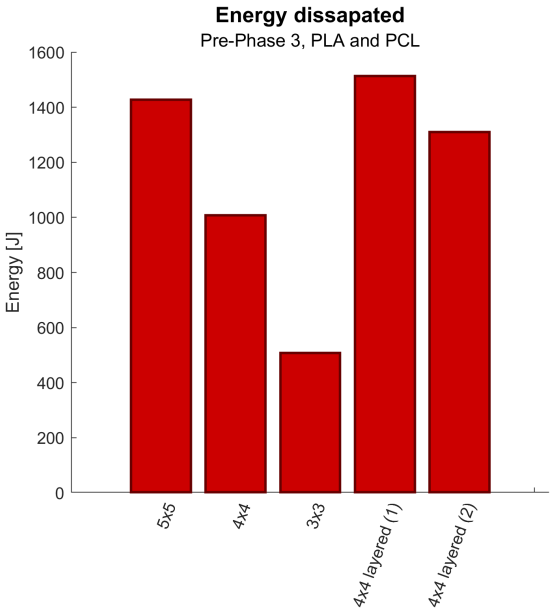

(b)

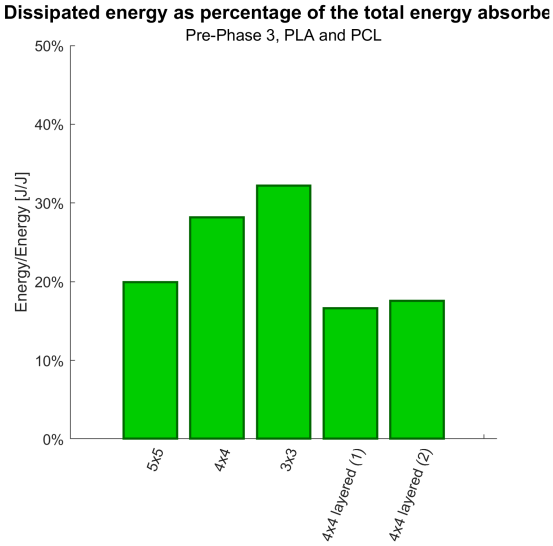

(c)

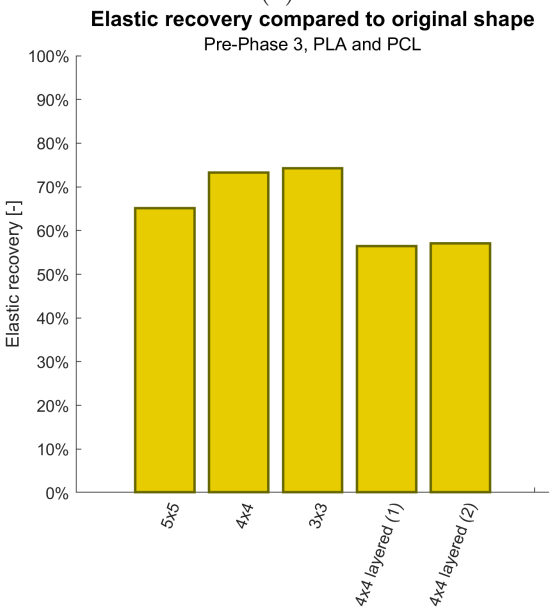

(d)

Figure D.5: Bar chart analysis of the last 5 iterations.

Appendix E

Results of Chiral N6 strain rate experiment

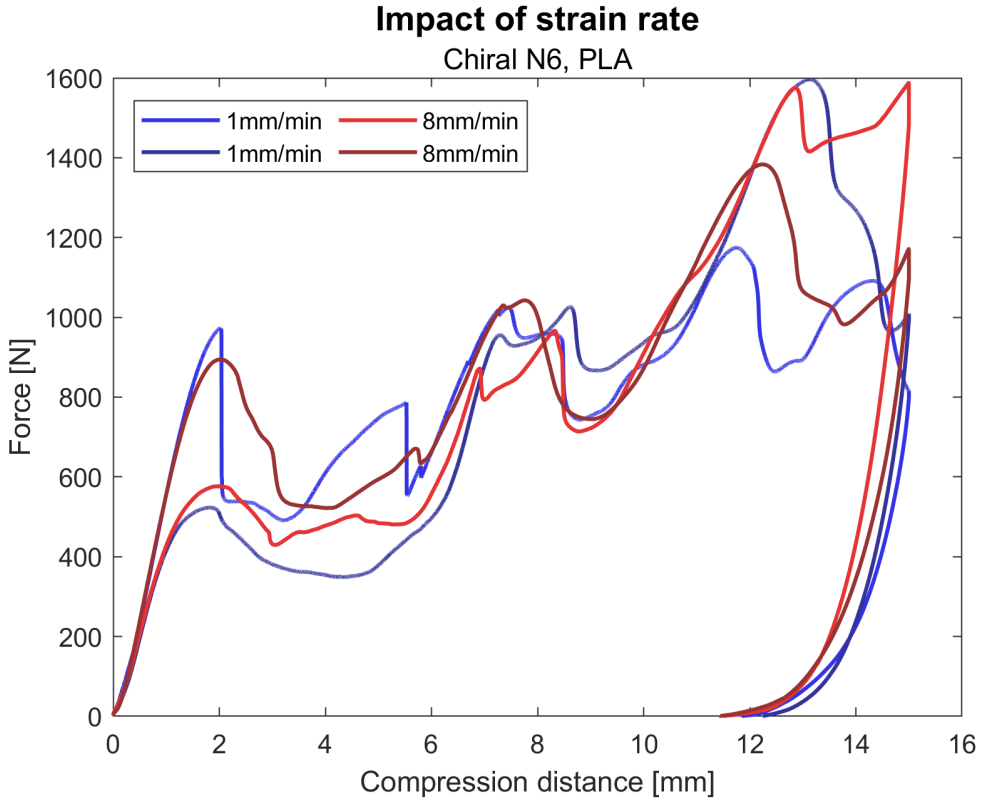

Figure E.1: Impact of strain rates on a Chiral N6 structure.

When testing the impact of strain rate, a chiral N6 structures was tested alongside the honeycomb re-entrant structure mentioned in the main report. The results from the chiral structure are ambiguous and not suited for strong conclusions. However, one of the conclusions drawn can be seen here as well. The initial peek force at a strain of 2mm is roughly equal. Even if the randomness of buckling behaviour caused this force to appear at two different values.

The other two observations cannot be confirmed with this experiment. These are the greater compression resistance at higher strain rates, and the more elastic behaviour on the backstroke for higher strain rates.

Appendix F

Printing Guide

Reference guide for 3D printing sandwich structures with PCL, TPC and C8.

Date September 2022

Written by Jonne Postmes, MSc

Introduction

This document was made alongside the MSc graduation project of Jonne Postmes. Three .curaprofile are included with specific parameters which were used. 3D printing is a manufacturing method where the optimal settings can vary a lot on a per model basis. The settings I used can be a good starting off point, but are unlikely to be optimal for your project. Testing and trying different settings will likely have to happen when you wish to print with materials other than PLA. An example of the geometry I optimised my setting for can be seen below:

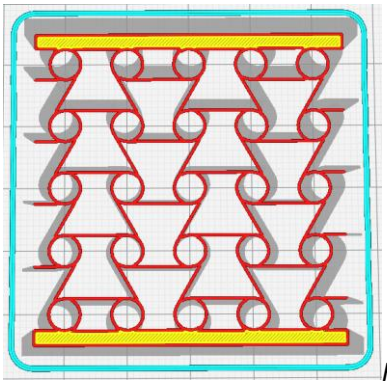

Figure: model with thin walls & a complex chape.

Materials

PCL100, https://www.3d4makers.com/products/facilan-pcl-100-filament.

C8, https://www.3d4makers.com/products/facilan-c8-filament.

TPC-91a, https://www.3d4makers.com/products/tpc-91a.

Tricks

When using Cura 4.11.0 incombination with an Ulitmaker 2. You can make the option for material temperature visible by changing the G-code flavor to marlin. Yes, the basic setting to select the nozzle temperature is not always available by default.

Switching filament

Input PLA as the material on ultimaker machines.

Appendix G

Compression of TPC-91a, 25mm

The same TPC samples used in phase 2 were also compressed to 25mm. This was done to showcase the elasticity of the sample.

Additionally, it can be seen that densification occurs at approximately 16mm. Which is later than was measured with an PLA sample. This suggests that the point of densification is material dependent.

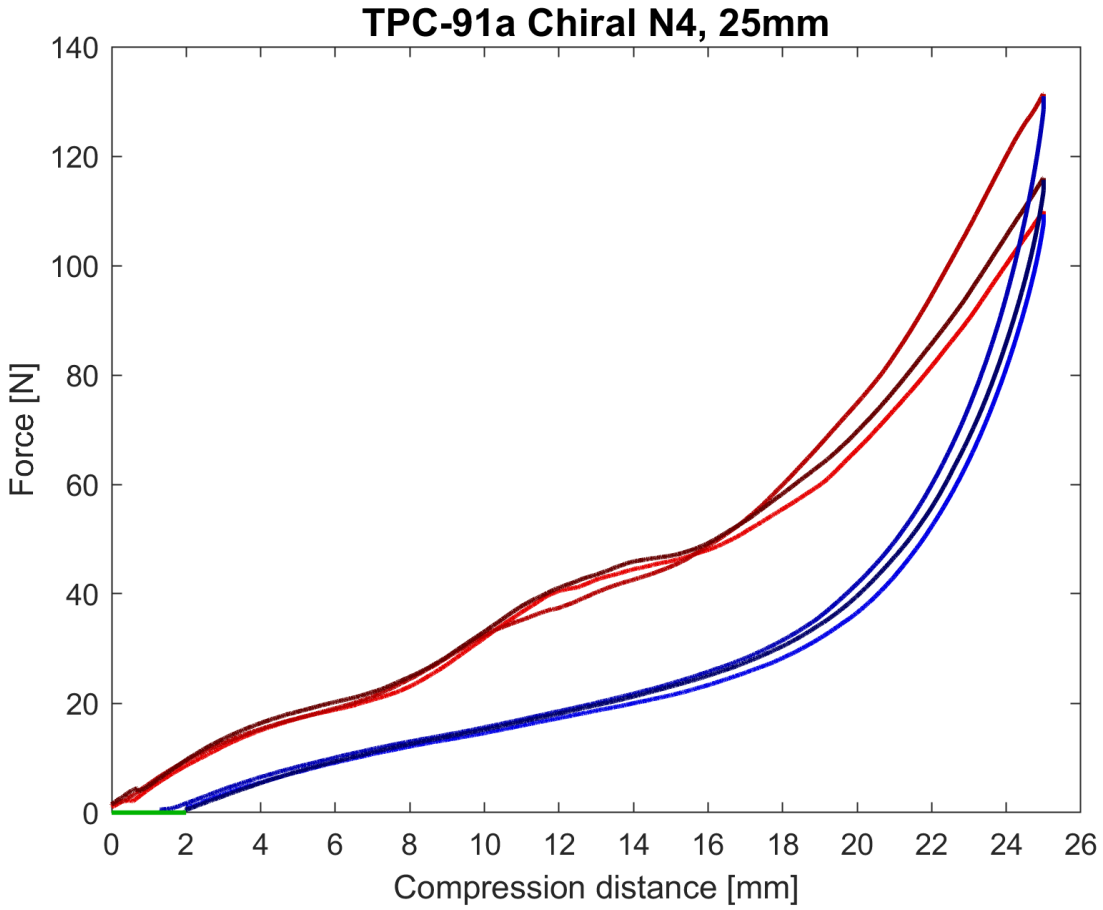

Figure G.1: Stress strain diagram for a TPC ChiralN4 sample, compressed to 25mm.

Appendix H

Design itterations for multi-material designs

This Appendix contains pictures of all models which were made during the multi material design iteration phase. The pictures are placed in chronological order, with notes placed in the captions.

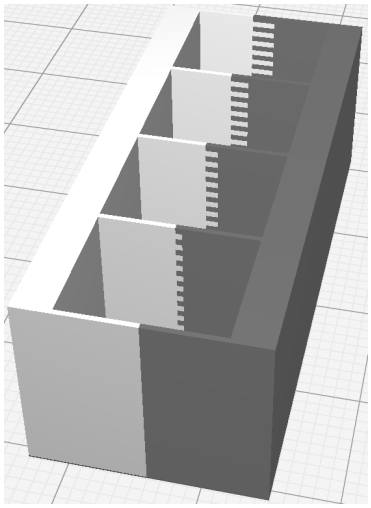

(a) Model for testing adhesion between two materials

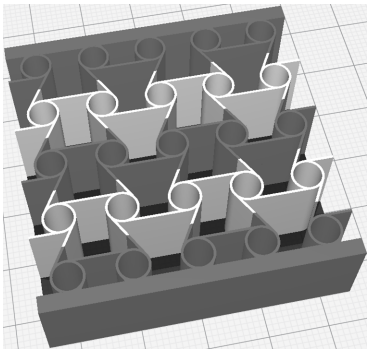

(b) Constant wall thickness, no serrated profile, TPC and PLA

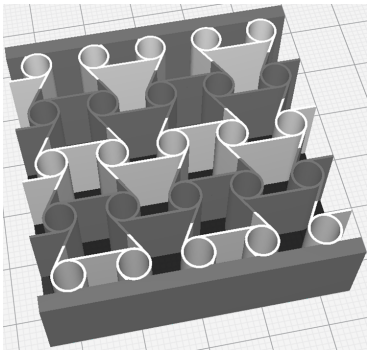

(c) Constant wall thickness, with serrated profile, TPC and PLA

Figure H.1: 3D prints with PLA and TPC.

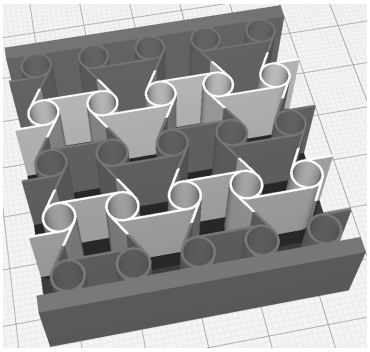

(a)

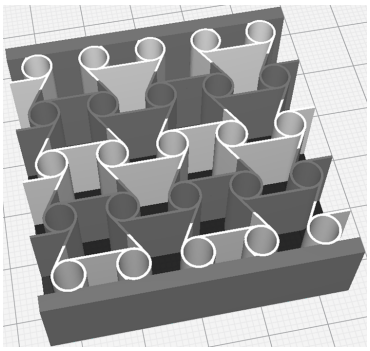

(b)

Figure H.2: Models used while tuning printing parameters for PLA and PCL

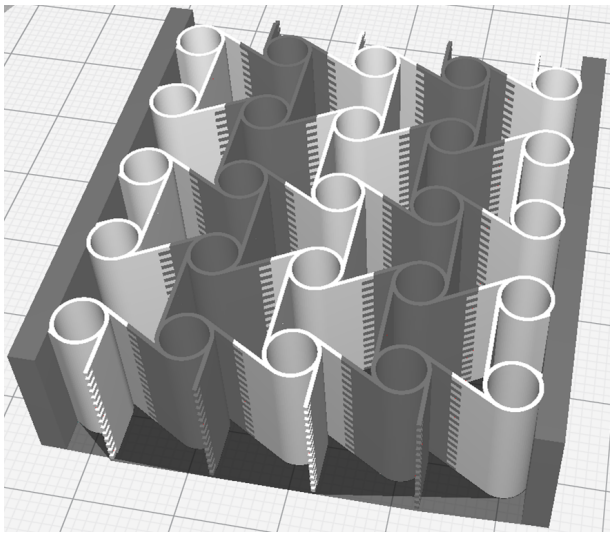

Figure H.3: Serrated profile for better adhesion between materials

Later, near the end of the thesis, it was found that other researchers have also used this method of interlocking serrated teeth to create a better adhesion between different materials [18].

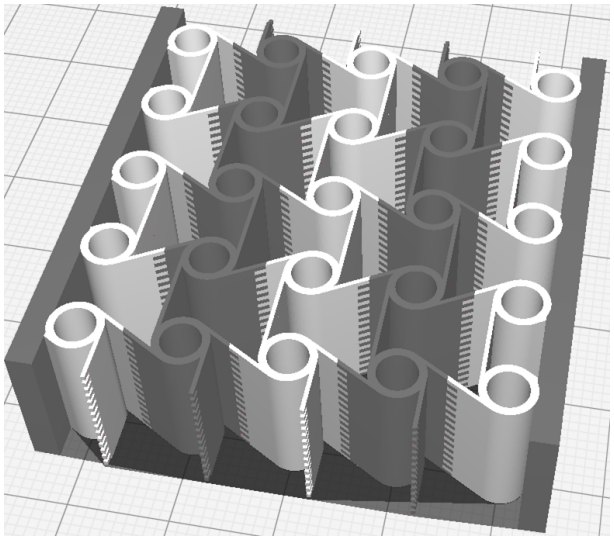

Figure H.4: 0.8mm wall thickness for cylinders to prevent re-threading of nozzle. Preventing the nozzle from yanking away material which was just placed, which created holes in the printed parts.

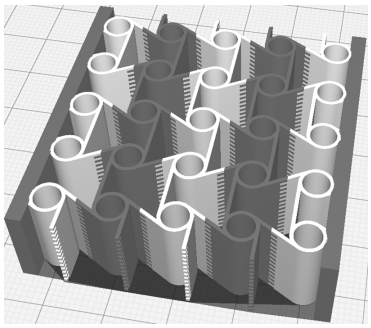

(a) Constant 0.6mm wall thickness

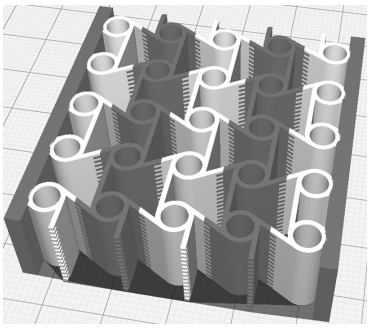

(b) Constant 0.8mm wall thickness

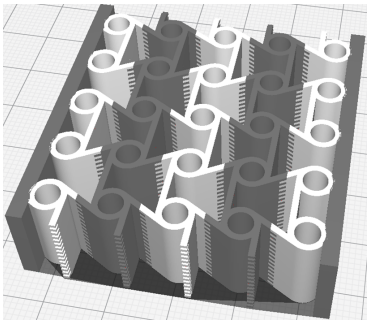

(c) Constant 1.0mm wall thickness

Figure H.5: Models used while tuning printing parameters for PLA and PCL. These were made to test if different constant wall-thicknesses would solve the buckling problem of PCL. Where PCL cylinders would deform and be squished. This did not work.

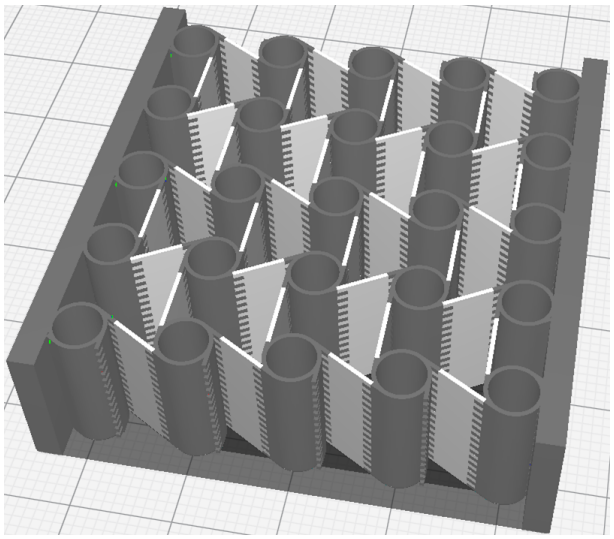

Figure H.11: PCL beams combined with PLA cylinders. This does not funciton well. The areas where two polymer are connected act as hinges with very little resistance to bending.

Figure H.6: Constant wall thickness of 0.6mm.

Figure H.7: Constant wall thickness of 0.8mm.

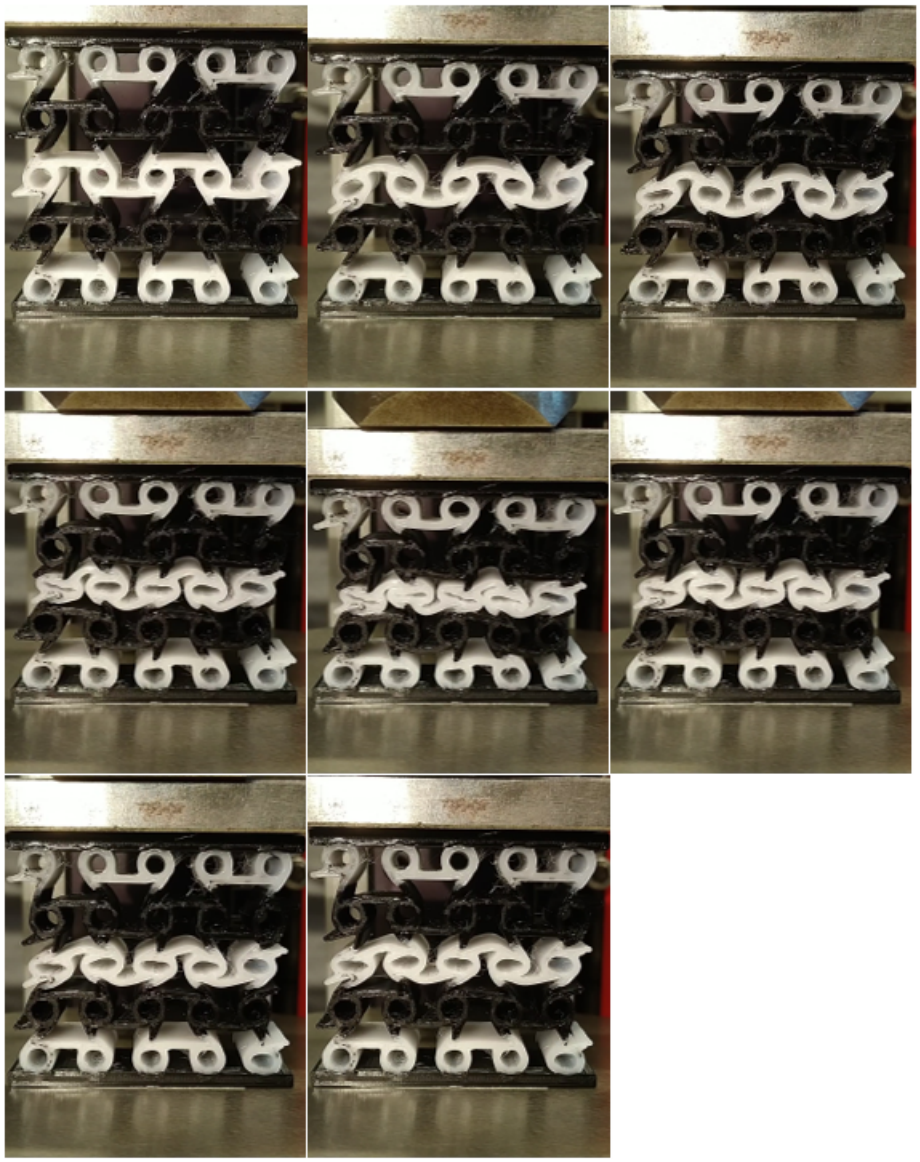

Figure H.8: Constant wall thickness of 1.0mm.

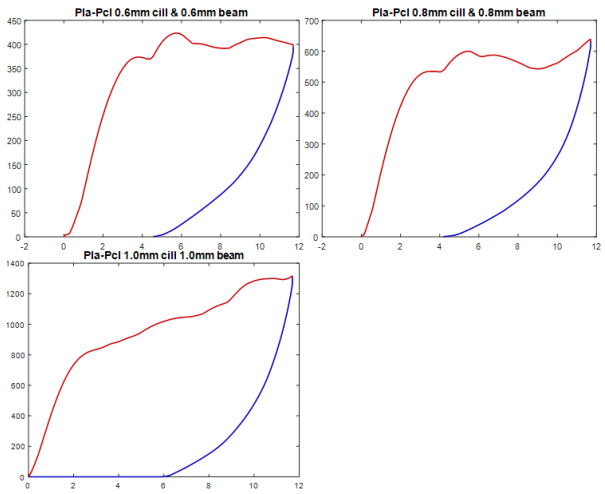

Figure H.9: The samples with varying wall thicknesses were tested. but as they experienced structural failure, they were not examined fully.

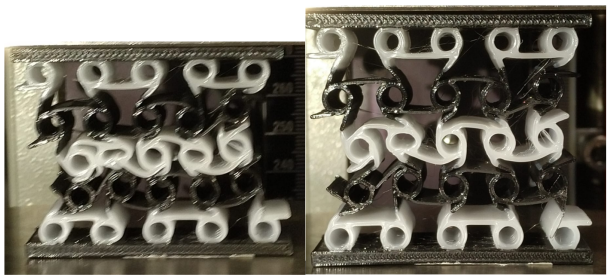

Figure H.10: 0.4mm beams combined with 0.8mm cylinder walls, still failed. This method started to work, but this method would require more fine tuning. simply doubling the wallthickness is not good enough.

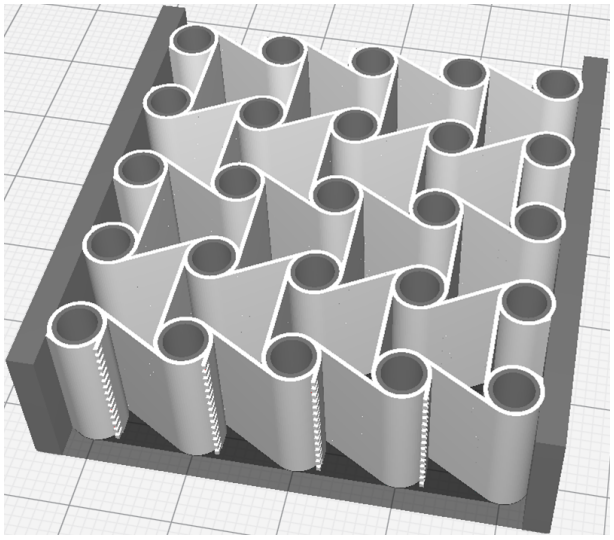

Figure H.12: PCL beams combined with PLA cylinders. This iteration showed that inner cylinders from PLA could be used. The connection between the two polymers was very solid.

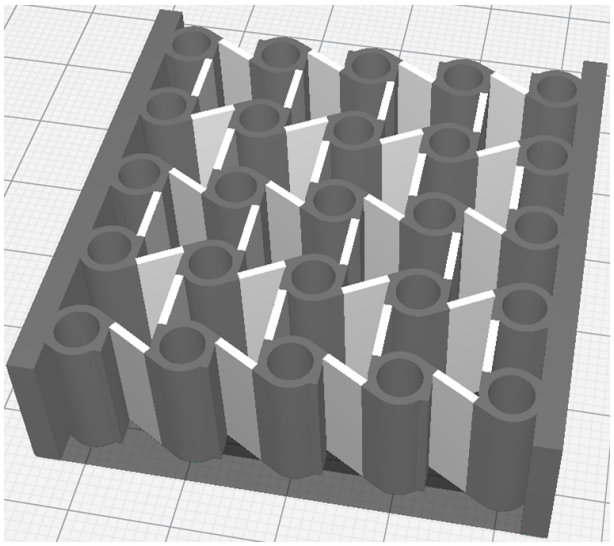

Figure H.13: PCL beams combined with PLA cylinders, serrated profile removed and increased wall thickness. This had a similar result as with Figure H.11.

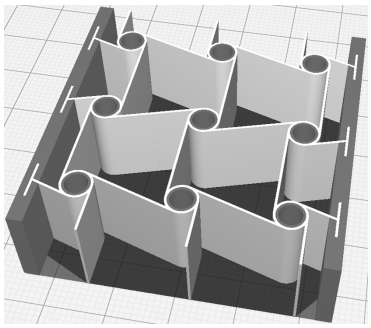

(a) 3x3, 50mm high

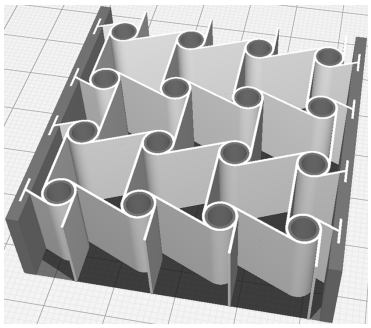

(b) 4x4, 50mm high

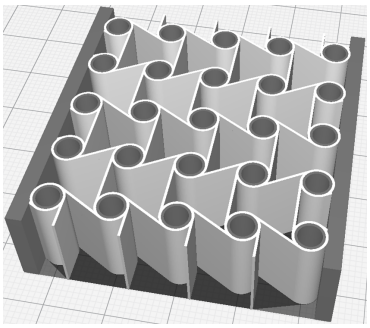

(c) 5x5, 50mm high

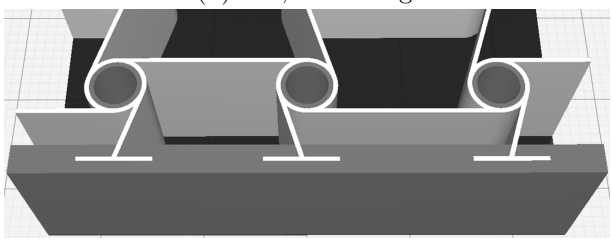

(d) Anchors used to improve adhesion between PCL beams and PLA plates.

Figure H.14: Models used while tuning printing parameters for PLA and PCL. These models were tested, their results are in Appendix I.

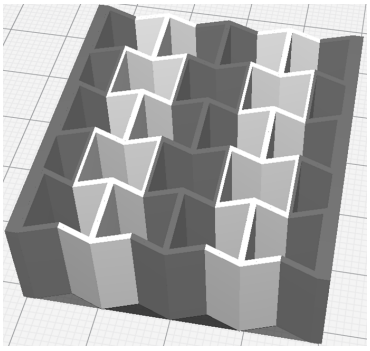

(a) Honeycomb re-entrant, PLA (black) and PCL (white)

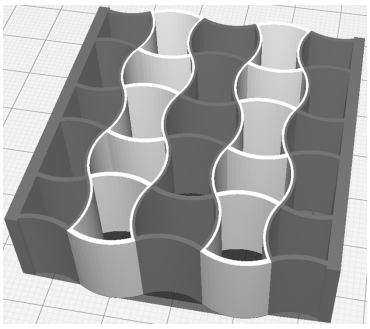

(b) Sinusoidal, PLA (black) and PCL (white)

Figure H.15: Models used while tuning printing parameters for PLA and PCL

These models in Figure H.15 were designed and created on request of the supervisor. The four models below were ideas, which were supposed to solve the problem which reinforced inner cylinders brought with them. They were rejected and not printed out. The suggestion was that the sample could be compressed even further, and to intentionally deform the cylinders. At this stage, it would be possible to alternate the material used within the reinforcements and use this to create a programmed response.

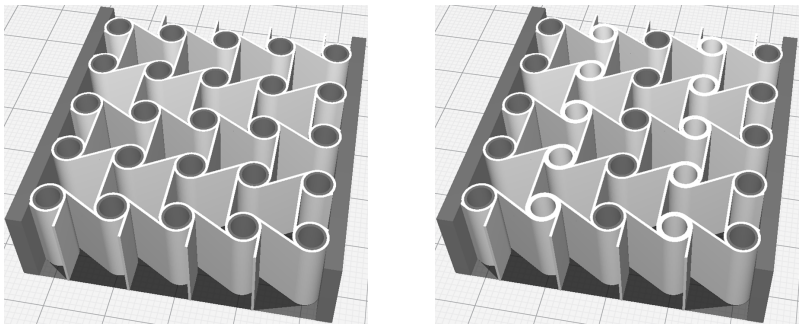

(a) (b)

Figure H.16: Discontinued idea

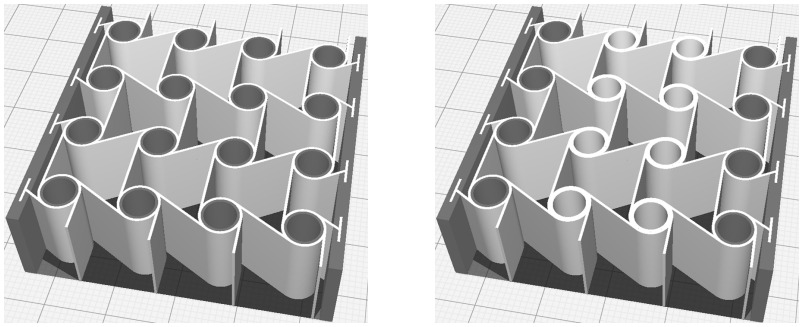

(a) (b)

Figure H.17: Discontinued idea

The Figure H.18 shows the final design method which was used in the project. It took 30 iterations to arrive at a working model.

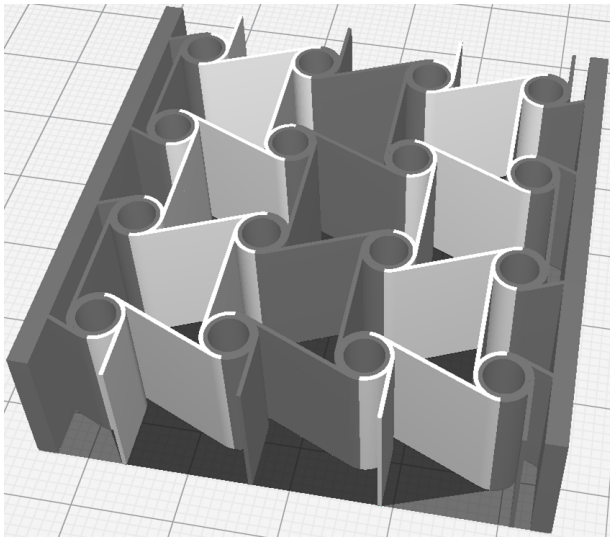

Figure H.18: Final product after design iterations

Appendix I

Experiment results of strutures with a lower inner density

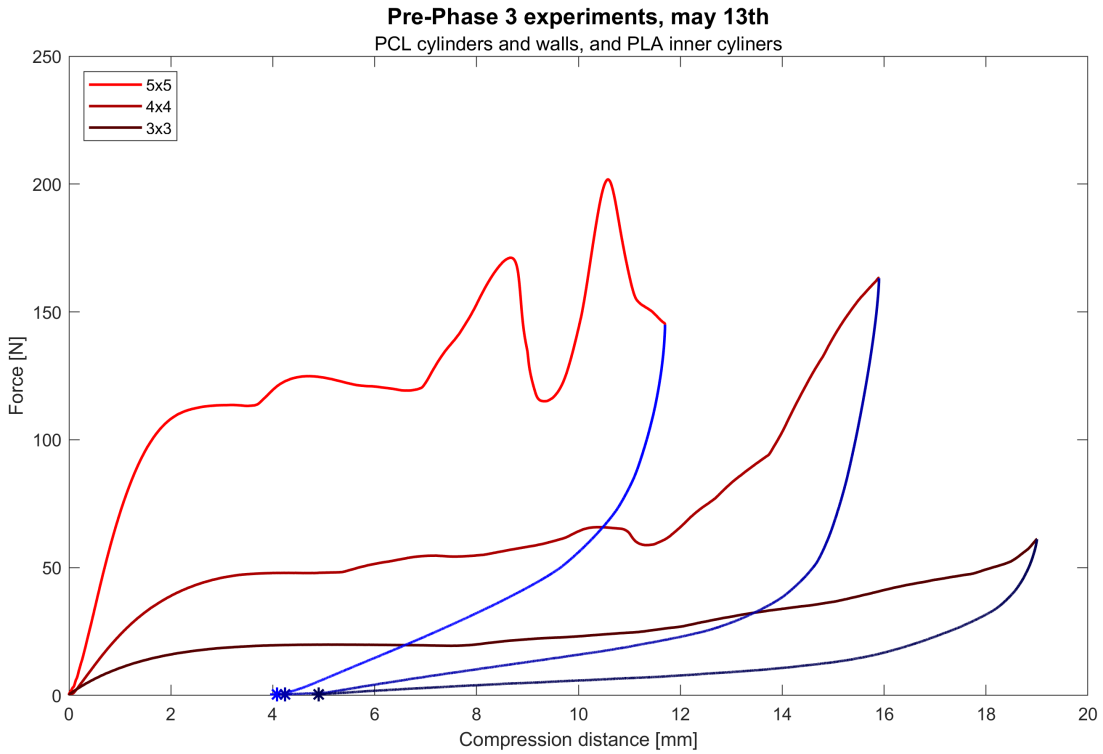

Figure I.1: Stress strain diagram, showing the results from the experiment on structure density.

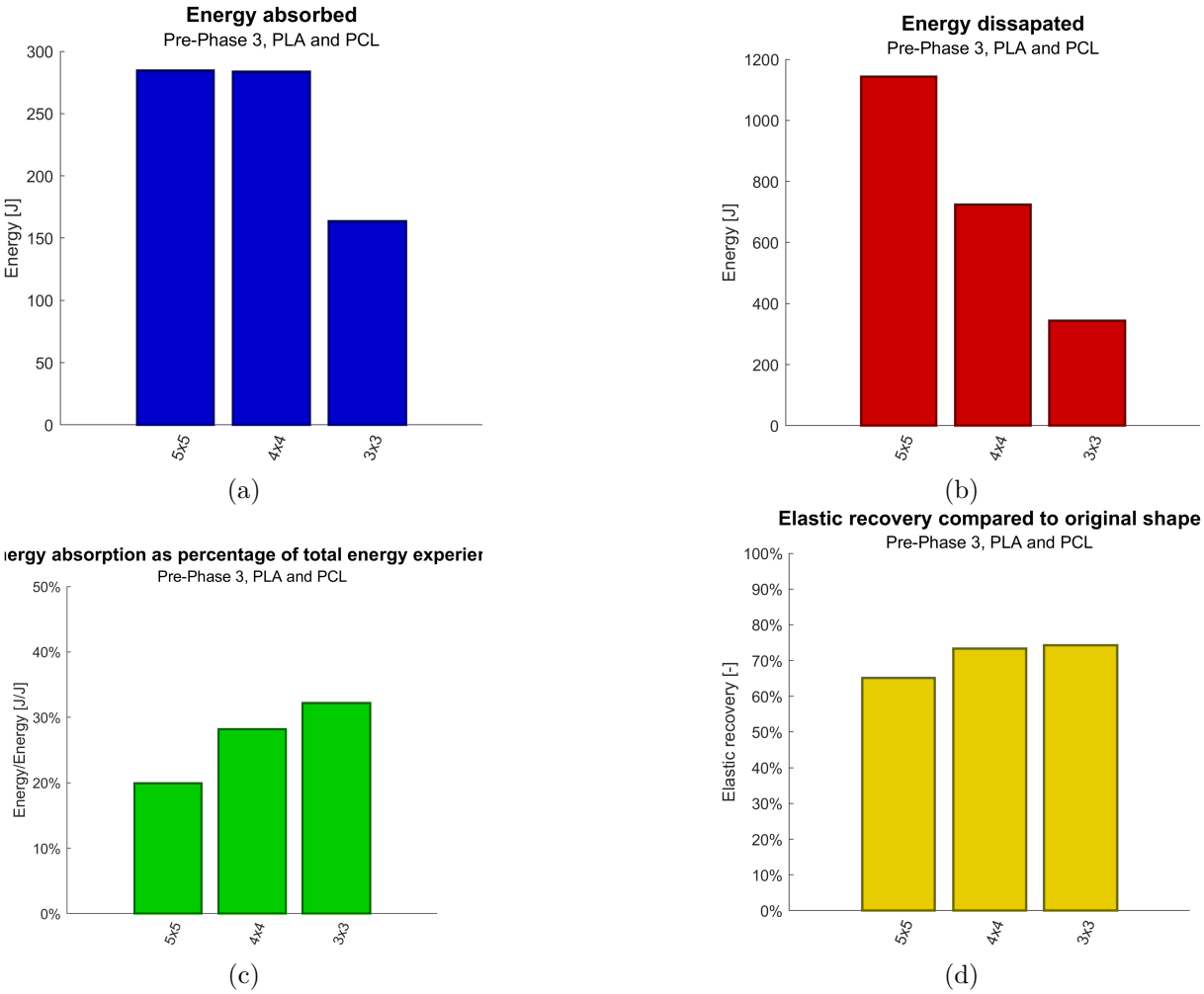

Figure I.2: Results from the experiment on structure density.

Appendix J

Enlarged results from multi-material experiments

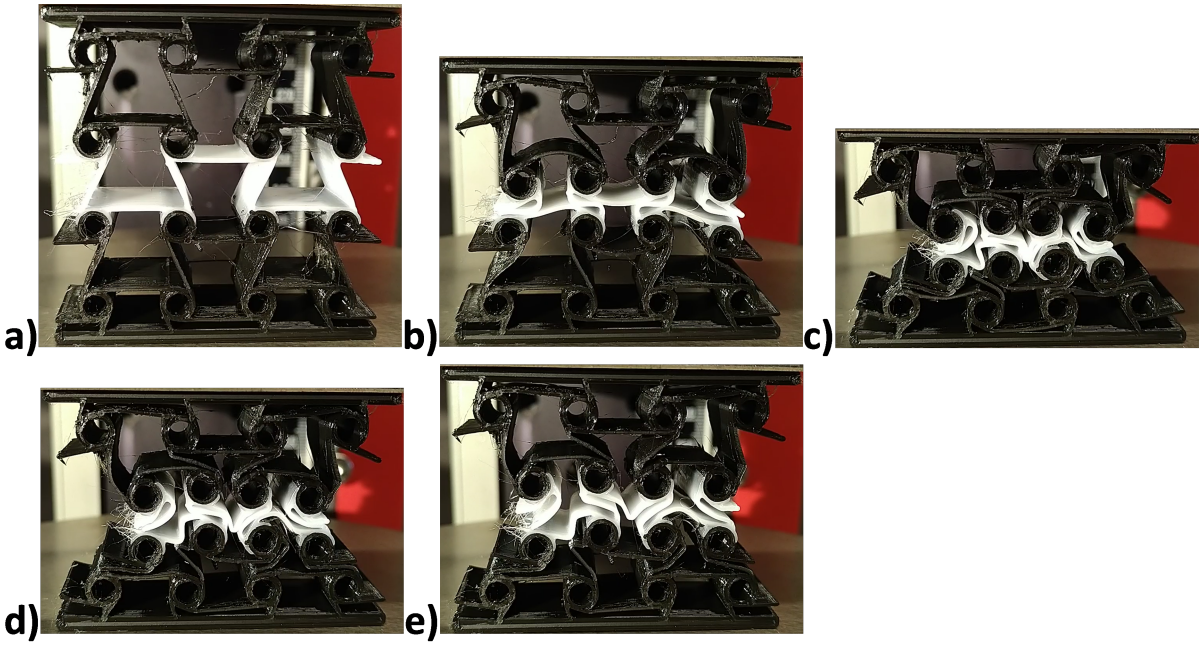

Figure J.1: BWB, PLA in black and PCL in white

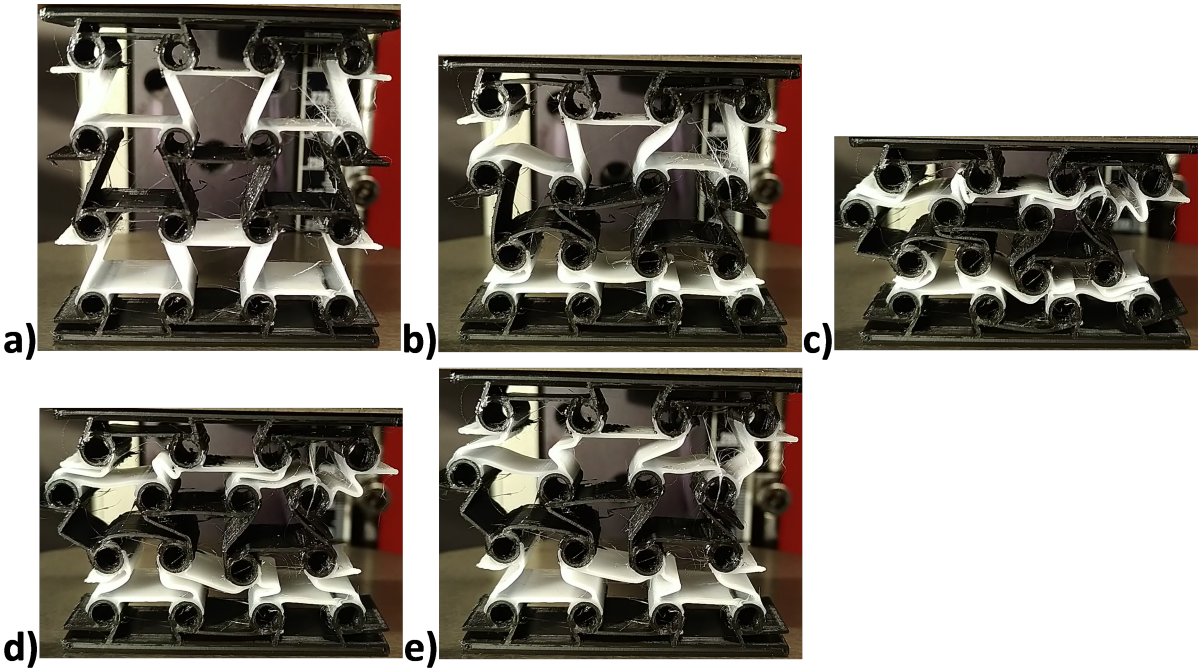

Figure J.2: WBW, PLA in black and PCL in white

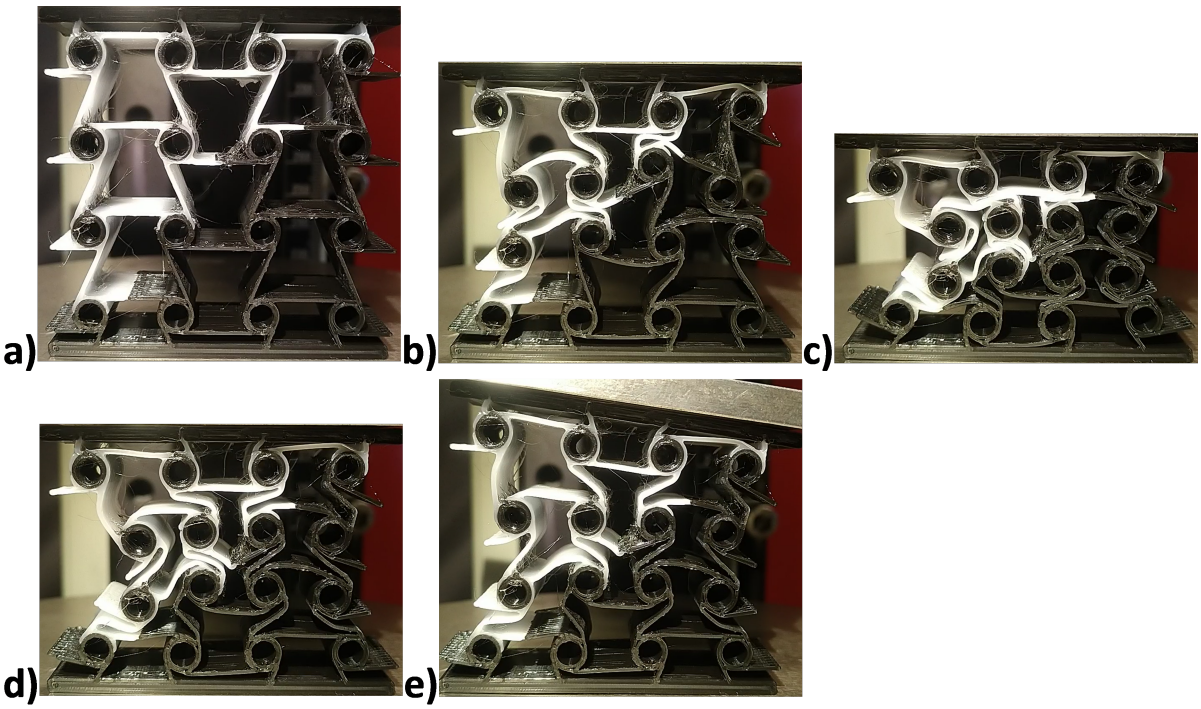

Figure J.3: Diagonal, PLA in black and PCL in white

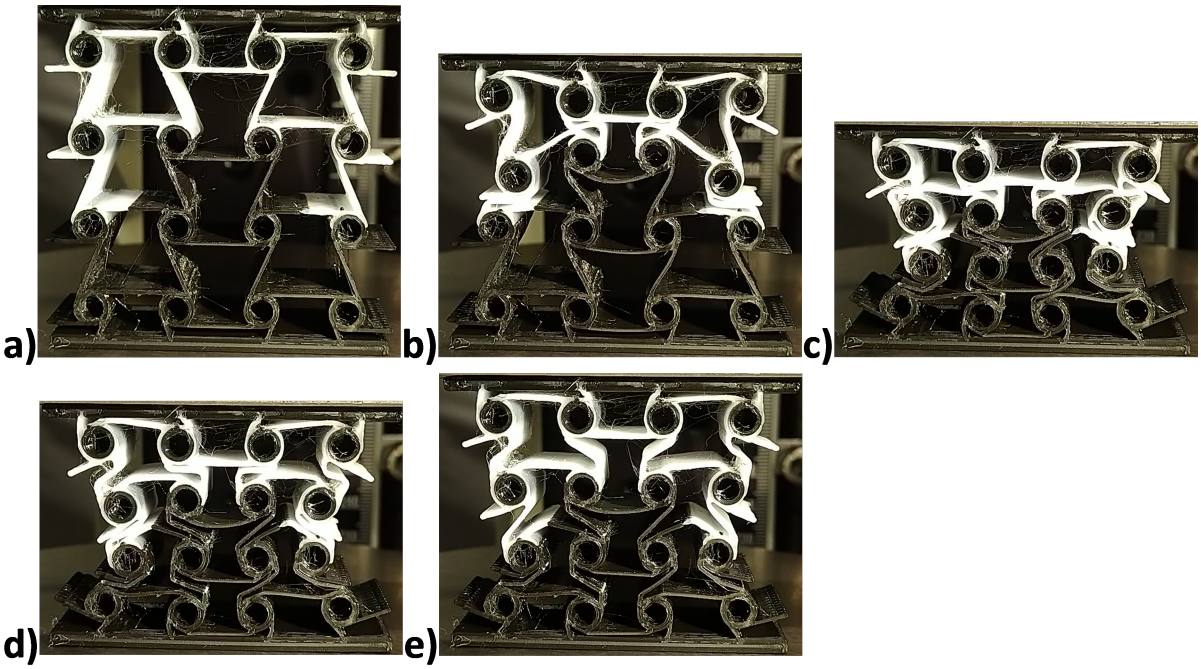

Figure J.4: , PLA in black and PCL in white

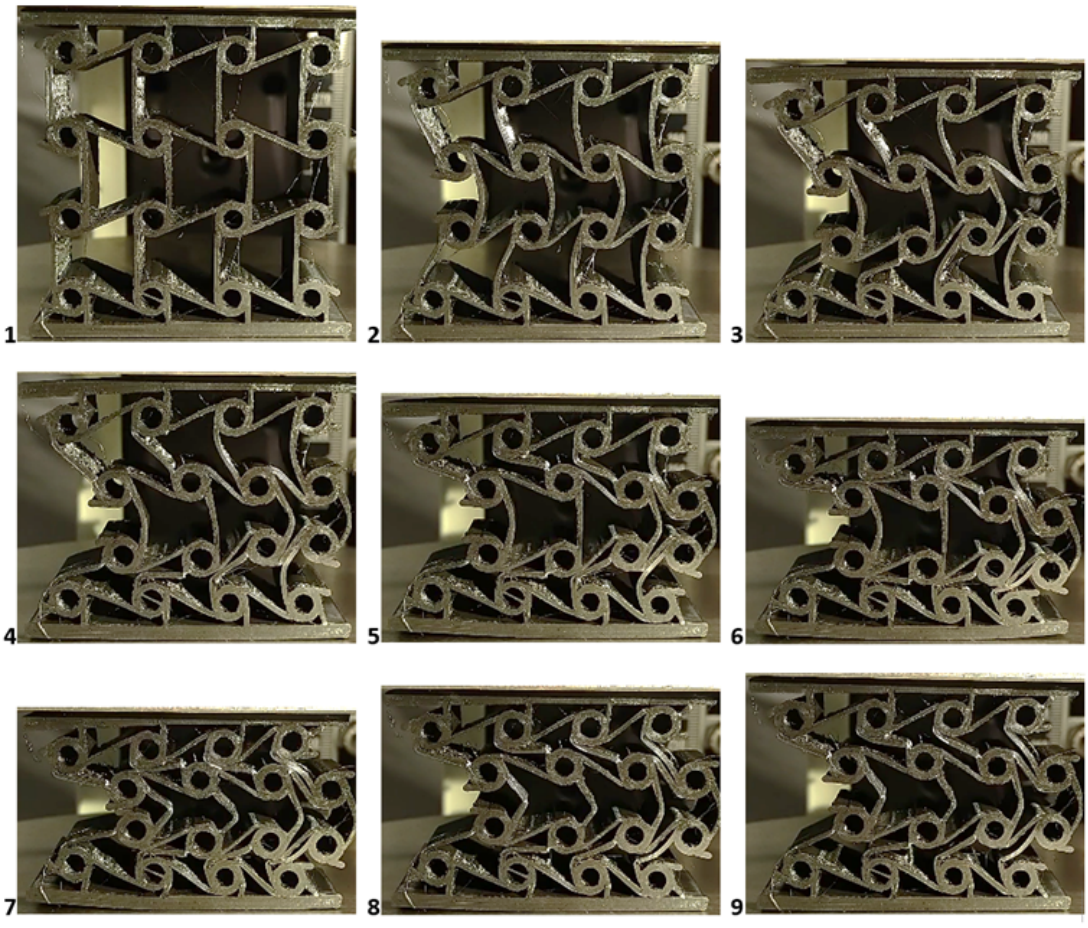

Figure J.5: The same chiralN4 pattern, but compressed sideways.

Appendix K

Literary research on Shape memory polymers and PLA biodegradability

Some subjects were researched during the project, but were not fully Incorporated within the thesis. They did not follow the main objective of the experiments. However, their work was deemed valuable at the time. Therefore, these chapters are placed here in the appendix. And to show work performed by the student.

K.1 Shape memory polymers

Off the four methods for energy absorption, only elastic is normally usable for repeated usage in a structure. Plastic deformation and structural collapse are generally seen as areas to avoid when designing structures. After all, structural failure is defined by a material experiencing a stress which causes fractures or excessive deformation. However, when these areas can be effectively used and re-used, a wider range becomes available for energy absorption. For this purpose, Shape memory polymers can be utilised. There are three basic working mechanisms behind the shape memory effect in polymers. These mechanisms are dual-state, dual-component and partial-transitioning.

Shape memory mechanisms

Although the shape memory effect is wont be studied extensively in this thesis, it does continue in the line of the previous works of the supervisor. Shape memory polymers might have an interesting application as shock absorbing material. They can be deformed during usage, and restored by applying heat. Letting the shock absorber be re-used. Furthermore, the combination of SMP, auxetics, multi-material designs, and energy absorption, has relatively little research in literature. Which makes this combination interesting.

There are three basic working mechanism for shape memory polymers. These are (I) dual-state (DSM), (II) dual-composite (DCM), and (III) partialtransition (PTM) mechanisms [2] [16] [35]. All three mechanisms follow the same steps within the memory cycle. Following Figure K.1, They start with their original shape at room temperature at a). Followed by deformation at b), depending on the material this step is performed at elevated temperatures. This step is always done with temperatures below the programming temperature. Then the temperature is lowered and forces are removed at c). At this stage, the material has been deformed, and will not change its shape without external stimuli. This part is also known as the programming step. Lastly, at stage d), the material is heated and recovers its original shape.

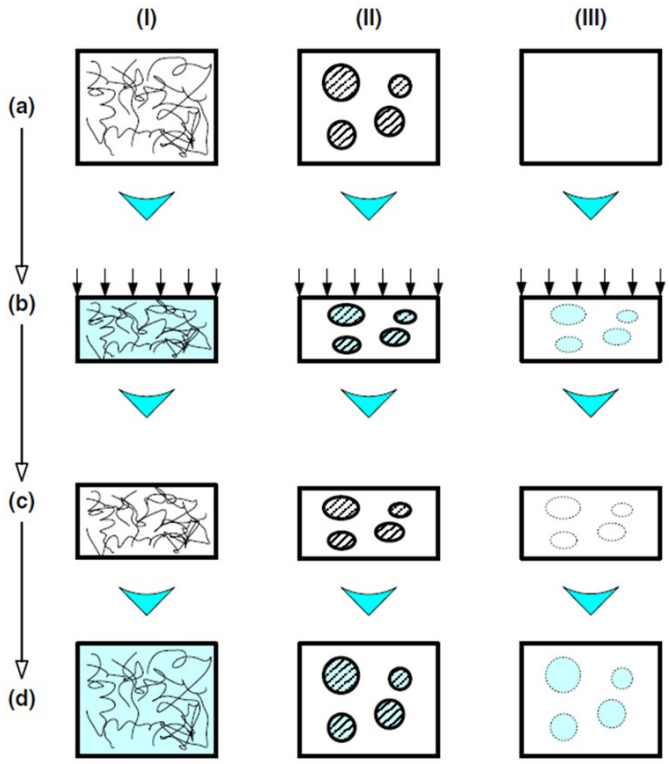

Figure K.1: Illustration of (I) dual-state (DSM), (II) dual-composite (DCM), and (III) partial-transition (PTM) mechanisms [16]. Blue colored steps are under increased temperature.

Dual-state mechanisms make use of two phases within a single polymer, the rubbery state and the glassy state. In combination with the components of a polymer, a hard segment and a soft segment. The hard segment is composed of chain entanglements or covalent bonds. This part of the component provides rigidity, and does not deform. The soft segment is made up out of the free ends of polymer chains. After programming, the soft segments have sustained deformation. Then, when the polymer is heated, Thermal vibrations allow the free chains to move and roll over one another. Allowing the crosslinks to pull the material back to its original shape. PLA is a type of polymer which falls in the DSM category, with crosslinks instead of covalent bonds. For a polymer to exhibit shape memory behaviour, a distinct transition in the E, T curve is needed. This means that a clear T_g or T_m is required.

There are two important parameters which are used to describe the effectiveness of shape memory behaviour, fixation ratio (R_f) and recovery ratio (R_r). The fixation ratio can be measured by taking a sample, elongating by 100% (ϵ_u), releasing the forces and measuring the strain after release (ϵ_m). The fixation ratio is affected by the number of times it has been elongated. The recovery ratio is measured by elongating a sample, allowing a full shape memory recovery cycle to take place, and measuring the strain after recovery (ϵ_p). See Equation K.1 and Equation K.2.

Both R_f and R_r are influenced by the crosslink density of the polymer, and the programming temperature. Changing the crosslink density changes the ratio of hard to soft components within the material. Increasing the crosslink density was found to decrease R_f at programming temperatures below T_g, but increase R_f when programming at temperatures at T_g [44]. The same study shows that it is possible to optimize the shape memory behaviour of materials by selecting appropriate crosslink densities. It was also found that crosslink density had more impact on the shame memory behaviour than the programming temperature.

$$R_f = \frac{\epsilon_u}{\epsilon_m} \tag{K.1}$$

$$R_r = \frac{\epsilon_m - \epsilon_p}{\epsilon_m} \tag{K.2}$$

Dual-composite mechanisms use two, or more, different materials to create the shape memory effect. One segment is highly elastic, and the other has a stiffness which can be controlled by external stimuli. For example, the second segment can be soft at high temperatures and hard at lower temperatures. Utilizing a reversible phase transition. In Figure K.1, the matrix is the elastic part or the soft component, and the inner included circles represent the temperature transitioning part or the hard part. At low temperatures in phase a) the material cannot easily be deformed, as the hard parts prevent deformation. After heating in phase b), the inclusions are soft and can flow to accommodate the new shape. Then after cooling in phase c), the inclusions harden and keep the flexible matrix from moving. Only when the hard material is heated again in phase d), can the flexible matrix return to the original shape.

Finally, the partial transition mechanism makes use of phase transitions. A practical example of this method would be a sponge filled with paraffin wax. At room temperature, paraffin within the pores of a sponge is solid, preventing it from deforming. Heating the paraffin will cause a phase transition and melt the wax. This allows the liquid to move in and around the sponge. Letting the structure deform. Then, if the temperature is brought back down, the paraffin will solidify. This programs the structure and keeps the sponge from changing form. Re-heating will melt the paraffin, letting the elastic sponge return to the original shape.

SME within this study

Although the shape memory effect is wont be studied extensively in this thesis, it does continue in the line of the previous works of the supervisor. Shape memory polymers might have an interesting application as shock absorbing material. They can be deformed during usage, and restored by applying heat. Letting the shock absorber be re-used. Furthermore, the combination of SMP, auxetics, multi-material designs, and energy absorption, has relatively little research in literature. Which makes this combination interesting.

K.1.1 Effect of printing parameters on shape memory effect

This thesis will not design structures with the goal of optimizing the shape memory effect. Structures will be tested to check the presence of the shape memory effect. Specialized equipment capable of controlling environmental temperatures needed to perform good quality are not currently available at the university. Instead, the impact of the most prominent parameters will be discussed. The input parameters are total thickness, layer height, activation temperature, nozzle temperature, and printing speed. Their impact on recovery time, activation time, and recovery ratio will be investigated. A general test for measuring the behaviour of shape memory polymers, is to first program the material. Then start the recovery process by placing the deformed part inside a water tank with a precisely controlled temperature. During the recovery process, measurements can be taken.

Recovery time is the time window where the material moves, and actively changes shape. The material does not necessarily starts a recovery process immediately after entering a heated environment. The time between the initial heating and the start of the shape memory effect induced movement is called the activation time. Recovery ratio is effectively how well the sample which was tested returns to its original shape. This can be measured by referencing the original length with any remaining elongation after recovery. Or if a sample started as a straight beam,

and was bend to a set angle during programming. The difference between starting angle and the shape after recovery can be used to determine the recovery ratio.

The total thickness of a part is the number of layers, multiplied with the layer height. This dimension is determined by a models geometry. Increasing the total thickness will lower both activation time and recovery ratio.

Layer height is the height of a single layer. This settings is determined by the slicing profile. FDM style printers usually print with a layer height between 0.1mm and 0.3mm. Larger layer heights are possible at the cost of surface quality or with the help of a larger nozzle size. The layer height does not normally extend beyond the nozzle size. Greater layer heights are beneficial for shape memory properties. Increasing the layer height will lower recovery time, lower activation time and increase the recovery ratio. This is likely because a greater layer height lead to better homogenity in parts.

Activation temperature is the temperature of the environment, often times water, during the recovery process. Higher temperatures are beneficial for shape memory effects. It will reduce recovery time, reduce activation time, and improve the recovery ratio. Higher temperatures allow for more thermal vibrations within the polymer chains. This allows free chains to move with less resistance.

Nozzle temperature, or printing temperature has some effect on part strength as was discussed before. Higher temperatures will increase recovery time and increase activation time. However, higher printing temperatures are also beneficial for the recovery ratio.

Lastly, printing speed, which is the speed at which the nozzle moves over the build plate. Higher speeds result in a lower melt pressure. This draws the plastic out during printing and this in turn results in planar stresses inside the material. Increasing the printing speed will increase recovery time and activation time. The recovery ratio can decrease when layers do not have enough time to fully solidify before a new layer is placed [2], [35], [36].

K.2 Biodegradability of PLA

The European norm EN13432 was created to define which properties a material must have in order to be called biodegradable or compostable. It states that most of the polymer can be decomposed by living organisms within 12 weeks, into CO2, water, minerals and biomass. Furthermore, all residue must be below a certain size limit and be non-toxic. Lastly, compositable materials must be compostable under industrial conditions.

A biodegradable polymer can, under normal environmental conditions, degrade into carbon dioxide and water through microbial action. PLA can degrade under four different mechanisms, hydrolytic, photodegradative, microbial and enzymatic degradation. PLA is often cited as a polymer which can be produces with renewable resources such as corn, and as a biodegradable material. The rate of degradation is influenced by several factors. Some factors are the size of the material, oxygen, humidity, burial time, pH, temperature of hydrolysis and isomer ratio [61].

Hydrolytic degradation

In the presence of water, ester groups of the main chain of PLA are cleaved. These are the parts of a polymer where two monomers were linked together. This causes the molecular weight of PLA to decrease and causes the release of soluble oligomers and monomers. It is for example possible to degrate 80% of a PLA sample under 85°C in 60 weeks [29].

Photodegradation

Polymers which are exposed to UV light can undergo photochemical reactions. Photo ionization initiatives the degradation mechanism, after which the bonds in the polymer backbone will start

to break. The scission of the polymer chain can in turn lead to several reactions like oxidative processes or crosslinking reactions.

Microbial degradation

Microbial degradation uses the natural ability of microbes to degrade plastics into less toxic or useful forms. This can be done in natural environments, or under controlled laboratory setups. Microbes can start with their degradation process after PLA underwent hydrolysis. Microbes are capable of breaking down polymers, by producing enzymes called depolymerases. This is a group of enzymes which can depolymerize polymers. This process requires some amount of stimulation in the form of inducers (silk fibroin, elastin or gelatin), amino acids or peptides.

When ester links of the polymer are broken down by the enzymes, smaller parts are produced in the form of monomers, dimers and oligomers. This process lowers the molecular weight of the material, which allows microbes to further infiltrate the plastic structure. The degradation process reduces PLA to carbon dioxide and water, or methane. Compared to other biodegradable plastics, PLA requires a relatively long time to degrade when placed in soil. This is due to the high resistance of PLA to microbial attacks. However, using a special soil mixture, it is possible to fully decompose PLA samples within 15 days [41].

Enzymatic degradation

PLA can also be hydrolysed by enzymes such as lipase, esterase, and alcalase. Several environmental factors influence the speed of degradation, such as pH values, temperatures, chain stereochemistry and material crystallinity. Creating an environment that is optimal for this type of biodegration, requires the aforementioned parameters to be optimal, and must also be suitable for the microorganisms which create the enzymes. These constraints result in this form of degradation being unapplicable in normal environmental conditions. This process is slow and can take several weeks in laboratory conditions.

PLA is often described as a biodegradable material. Technically this is true, by the definition of European norm EN13432. However, it is however worth remembering that PLA is a very durable material within soil at ambient temperatures. This means that without proper collection, separation and recycle systems, PLA can cause environmental problems similar to those of conventional fossil fuel-based plastics. PLA does not biodegrade in nature on it's own. More research and perhaps practical specialised waste-treatment methods are needed, before waste PLA from non-industrial large scale sources can be considered a true biodegradable material for end users [61].